

University of New Mexico

UNM Digital Repository

Chemical and Biological Engineering ETDs

Engineering ETDs

Fall 12-12-2019

AN INVESTIGATION OF THE CHEMISTRY, THERMODYNAMICS AND CATALYTIC ACTIVITY OF MOLYBDENUM CARBIDES

Shanti Kiran Nayak

University of New Mexico - Main Campus

Follow this and additional works at: https://digitalrepository.unm.edu/cbe_etds



Part of the [Catalysis and Reaction Engineering Commons](#), and the [Thermodynamics Commons](#)

Recommended Citation

Nayak, Shanti Kiran. "AN INVESTIGATION OF THE CHEMISTRY, THERMODYNAMICS AND CATALYTIC ACTIVITY OF MOLYBDENUM CARBIDES." (2019). https://digitalrepository.unm.edu/cbe_etds/84

This Dissertation is brought to you for free and open access by the Engineering ETDs at UNM Digital Repository. It has been accepted for inclusion in Chemical and Biological Engineering ETDs by an authorized administrator of UNM Digital Repository. For more information, please contact amywinter@unm.edu, lsloane@salud.unm.edu, sahrk@unm.edu.

SHANTI KIRAN NAYAK

Candidate

CHEMICAL AND BIOLOGICAL ENGINEERING

Department

This dissertation is approved, and it is acceptable in quality and form for publication:

Approved by the Dissertation Committee:

DR. FERNANDO GARZON , Chairperson

DR. ABHAYA DATYE

DR. ADRIAN BREARLEY

DR. ERIC COKER

DR. IVANA GONZALES

**AN INVESTIGATION OF THE CHEMISTRY, THERMODYNAMICS
AND CATALYTIC ACTIVITY OF MOLYBDENUM CARBIDES**

By

SHANTI KIRAN NAYAK

(B.E. in Chemical Engineering, Birla Institute of Technology & Science Pilani, India)
(M.S in Chemical & Biological Engineering, University of New Mexico, Albuquerque, NM)

DISSERTATION

Submitted in Partial Fulfilment of the
Requirements for the Degree of
Doctor of Philosophy in Engineering
The University of New Mexico
Albuquerque, New Mexico
May, 2020

Dedication

This is for my parents and my sister for always believing in me and having my back.

Acknowledgements

First and foremost, I would like to thank my advisor, **Professor Fernando Garzon**, for his guidance throughout my years of graduate school. His kind leadership, keen insights, attention to detail and encouraging nature have made my graduate school experience a memorable journey. I am grateful for the opportunity to learn from him and to be inspired by him.

I would also like to thank the research professors in our group, **Dr. Ivana Gonzales**, **Dr. Angelica Benavidez** and **Dr. Lok-kun Tsui** for being my mentors for all these years. They've always taken the time to teach, inspire and help me and tirelessly answer my many questions.

I would also like to acknowledge the members of my committee: **Dr. Abhaya Datye**, **Dr. Adrian Brearley**, **Dr. Eric Coker** and **Dr. Ivana Gonzales** for their guidance and mentorship. Dr. Datye and Dr. Brearley taught me the class on Characterization of Nanomaterials and this has been one of my favorite classes in graduate school. Dr. Eric Coker has always lent a helping hand in running many of the experiments. I am grateful to them and all of CBE faculty for their mentorship and my education.

I am very grateful to the **US Department of Energy ARPA-E** and **National Science Foundation CISTAR** for funding my education. A special thanks to ARPA-E program director, **Dr. Grigori Soloveichik**, for supporting us in carrying out this fundamental research.

Thank you to the members of our group: Dr. John Plumley, Tybur Casuse and Andre Spears, for your willingness to help, teach and discuss science stuff.

I would like to acknowledge the invaluable friends I have made on the way, Dr. Raviteja (Ravi) Vangara, Dr. Yechuan Chen, Mounika Kodali, Milan Rede, Andre Spears and many others. Thank you to especially Ravi, for your support during the hard times; I'm very grateful.

A big thank you to my parents, Dr. Nilakantha Nayak and Mrs. Mitanjali Nayak, for supporting and pushing (when necessary) me and my sister, Asha Rashmi Nayak, for always believing in me even when I didn't; my best friends Gokul, Mrudu and Swati for their words of encouragement from across the world and my favorite beings: Aaron Boswell, Zeema and KAH-BOOCE for keeping me relatively sane during the dissertation writing process.

None of this would be possible without any of you. Thank you for being there.

AN INVESTIGATION OF THE CHEMISTRY, THERMODYNAMICS AND CATALYTIC ACTIVITY OF MOLYBDENUM CARBIDES

By

SHANTI KIRAN NAYAK

(B.E. in Chemical Engineering, Birla Institute of Technology & Science Pilani, India; 2015)

(M.S in Chemical & Biological Engineering, University of New Mexico; 2017)

(Ph.D. Engineering, University of New Mexico; 2020)

ABSTRACT

These studies investigate the chemistry and stability of molybdenum carbides as an electrocatalyst. Due to their unique electronic properties, molybdenum carbides are purposed as electrocatalysts for reaction systems such as hydrogen evolution reaction, bifunctional water splitting and CO oxidation.

In this study, various synthesis processes were utilized to produce different types of molybdenum carbide with varying properties of particle size, surface area and excess carbon. The samples characterized by XRD accompanied by Whole Profile Fitting, Electron Microscopy, Gas Adsorption (surface area) and XPS.

These synthesis processes were refined using fundamental thermodynamic analyses. These analyses highlight regions of stability of different phases of the carbide under differing conditions of temperature, partial pressures and hydrocarbons.

The phase stabilities of the molybdenum carbides in aqueous electrolytes were investigated as well in this study. Using thermodynamic modeling, the dependence of oxide formation potentials on pH at different temperatures is established. This was then used to guide the CV studies of the different molybdenum carbide samples. It was observed that the surface chemistry of the carbide species influences the electrochemical activity for hydrogen evolution reaction.

The results in this dissertation provide a comprehensive guide for the refinement of synthesis procedures as well as a roadmap for development of molybdenum carbide as an electrocatalyst.

The exploration of electrochemical stabilities leads to a better understanding of the applicability of molybdenum carbide not only in the hydrogen evolution reaction but also important systems such as fuel cells and CO₂ and N₂ reduction.

TABLE OF CONTENTS

LIST OF FIGURES.....	viii
LIST OF TABLES.....	xv
GLOSSARY.....	xvi
Chapter 1: Introduction and Literature Review.....	1
1.1 Statement of Research Problem.....	1
1.2 Ceramics: Transition Metal Carbides.....	2
1.3 Hydrogen Evolution Reaction.....	3
1.4 Phases, Structures, Morphologies and Thermodynamic Properties.....	4
1.5 Synthesis.....	13
1.6 Electrochemical Activity and Stability.....	38
1.7 A Note about Heterogeneous Catalytic Activity: Ammonia Synthesis.....	44
1.8 Summary and Objectives.....	44
References.....	47
Chapter 2: Methods.....	60
2.1 Thermodynamic Calculations.....	60
2.1.1 Ellingham Diagrams.....	60
2.1.2 Gas Phase Equilibrium Diagrams.....	64
2.2 Significant Experimental Procedures.....	64
2.2.1 Characterization Technique: X-ray Diffraction.....	64
2.2.2 Characterization Technique: Surface Area by Gas Adsorption.....	66
2.2.3 Additional Characterization Techniques: Specifications.....	68
2.2.4 Electrochemical Measurements.....	69
References.....	71
Chapter 3: Thermochemical Modeling.....	72
3.1 Ellingham Diagrams.....	73
3.2 Gas Phase Equilibrium Diagrams.....	80
3.3 Summary.....	84
References.....	86
Chapter 4: Synthesis.....	87
4.1 Ion Exchange Synthesis.....	87
4.2 Ammonolysis and Methane Treatment of Molybdenum Oxide.....	103
4.3 Other Characterization Studies.....	111
4.4 Attempts to use Molybdenum Carbide as a Support for Precious Metals.....	115
4.5 Summary.....	122
References.....	124
Chapter 5: Investigation of Electrochemical Properties.....	125
5.1 Cyclic Voltammetry Experiments (Molybdenum Carbide from oxide precursor).....	130
5.2 Cyclic Voltammetry Experiments (Molybdenum Carbides from Ion Exchange Protocol).....	136
5.3 Cyclic Voltammetry Experiments : Ru and Pt.....	144
5.4 Summary.....	145
References.....	147
Chapter 6: Conclusions and Future Work.....	149
Appendix A: List of Accomplishments.....	152

LIST OF FIGURES

Chapter 1

- Figure 1-1: Hydrogen evolution rate over electrocatalyst/TiO₂. One of the earliest studies involving ceramics powders carried out by Oosawa (58)
- Figure 1-2. Typical structures of transition metal carbides and nitrides as shown by Chen (44).
- Figure 1-3. Four phases of molybdenum carbide postulated by Wan et al. (11, 36).
- Figure 1-4. Phases of molybdenum carbide synthesized by Guzman et al. (48).
- Figure 1-5. Energy of formation of different phases of molybdenum carbide studied by Hugosson et al. (49).
- Figure 1-6. Scanning Electron Microscopy images of molybdenum carbide synthesized via different methods outlined by Wan et al. (36).
- Figure 1-7. High-resolution transmission electron microscopy (HRTEM) morphologies of molybdenum carbide formed during carburization using ethane/hydrogen at different temperatures.
- Figure 1-8. SEM (a) and TEM (b) images of 1D nanowires of molybdenum carbide synthesized by Liao et al. (35).
- Figure 1-9. Schematic of processes to synthesize different phases of molybdenum carbide by Lee *et al.* (14).
- Figure 1-10. Effect of synthesis parameters on properties of molybdenum nitride as shown by Choi *et al.* (17).
- Figure 1-11. XRD patterns after pyrolysis at 1200 °C at different concentrations of C/MoO₃ (a: the stoichiometric concentration, 0.77; b: 1.5 times and c: 2 times the stoichiometric concentration) as reported by Patel *et al.* (10).
- Figure 1-12. XRD patterns of sonochemically produced Mo₂C where the upper curve is after the heat treatment at 450 °C under He as reported by Hyeon *et al.* (28).
- Figure 1-13. The series of catalysts prepared by Gomez-Marín *et al.* (29): synthesis conditions and information obtained from XRD.
- Figure 1-14. Molybdenum to carbon ratios obtained from EDS analysis by Gomez-Marín *et al.* (29).
- Figure 1-15. Low-angle (inset) and wide-angle XRD patterns of (a) Ordered Mesoporous Carbon (OMC), (b) MoC–OMC and (c) Mo₂C/OMC as shown by Wang *et al.* (30).

Figure 1-16. TEM images of (a) MoC–OMC, (b) Mo₂C/OMC and (c) HRTEM images of MoC–OMC as shown by Wang *et al.* (30).

Figure 1-17. Schematic for synthesis of molybdenum carbides as shown by He *et al.* (31).

Figure 1-18. XRD patterns for synthesized molybdenum carbide samples in He *et al.* (5).

Figure 1-19. Schematic illustration of synthesis pathways by Wu *et al.* (32).

Figure 1-20. XRD pattern of synthesized molybdenum carbide by Wu *et al.* (32).

Figure 1-21. XRD patterns of Chen *et al.*'s (33) synthesized molybdenum carbides.

Figure 1-22. Schematic for synthesizing molybdenum carbides reported by Pan *et al.* (34).

Figure 1-23. XRD patterns for of the hydrothermal product (down) and the carburized (up) Mo₂C–RGO hybrid as synthesized by Pan *et al.* (34).

Figure 1-24. Raman spectra for molybdenum carbides by Pan *et al.* (34).

Figure 1-25. Raman spectra of molybdenum oxide subjected to different carburization protocols developed by Xiao *et al.* (24).

Figure 1-26. Diffraction data for molybdenum carbides synthesized by Liao *et al.* (35)

Figure 1-27. X-ray diffraction patterns of multiple phases of molybdenum carbide synthesized by Wan *et al.* (11).

Figure 1-28. XRD pattern of carbides synthesized by Guil-Lopez *et al.* (37)

Figure 1-29. XRD patterns of different molybdenum carbide samples synthesized by Elbaz *et al.* (38).

Figure 1-30. In situ XRD characterization of the MoO₂–MoO_xH_y mixture during methane carburization reported by Bouchy *et al.* (40).

Figure 1-31. Proposed mechanism for the oxycarbide phase formation in the absence of platinum as shown by Bouchy *et al.* (41).

Figure 1-32. Electrochemical performance of Mo based catalysts designed by Xiong *et al.* (60). Lin *et al.* synthesized heteronanowires of MoC – Mo₂C which displayed promising HER activity as well with low overpotential, small Tafel slope and low onset overpotential (61).

Figure 1-33. Polarization curves and (b) Tafel plots for the HER on modified GCEs comprising (I) MoC–Mo₂C-31.4, (II) Mo₂C, (III) MoC–Mo₂C-68.1, (IV) MoC–Mo₂C-30 (mixed), (V) MoC, and (VI) commercial Pt/C as reported by Lin *et al.* (61).

Figure 1-34. Cyclic voltammetry curves of Mo₂C and Pt/Mo₂C surfaces reported by Weigert *et al.* (64).

Figure 1-35. Cyclic Voltammetry curves for Pt/C and molybdenum-based materials showing an oxidation peak at 0.45 V (vs RHE) in figures corresponding to Pt/Mo₂C/C, Pt/Mo/C and PtMo/Mo₂C/C.

Figure 1-36. Cyclic voltammetry curves for molybdenum-based materials synthesized by Valk *et al.* (66)

Figure 1-37. Irreversible peak observed at 0.47 V (vs RHE) in the cyclic voltammetry of molybdenum-based materials reported by Saha *et al.* (66)

Figure 1-38. Stability mapping of Mo₂C obtained by CP titration experiments carried out by Weidman *et al.* (68)

Figure 1-39. Possible reactions involved with the corrosion of transition metal carbides reported by Weidman *et al.* (68).

Chapter 2

Figure 2-1. An example of Ellingham diagram from (1).

Figure 2-2. A Langmuir model plot (3)

Figure 2-3. Theories to describe adsorption behavior: BET and Langmuir models

Chapter 3

Figure 3-1. (a) Hexagonal Mo₂C and (b) cubic MoC molybdenum carbide structures.

Figure 3-2. Ellingham diagram showing the formation of MoC (left, a) and Mo₂C (right, b) with respect to CH₄. The solid lines correspond to the free energy of formation of methane with respect to temperature. The numbers mentioned on the solid lines represent the equilibrium constant, K.

Figure 3-3. Ellingham diagram showing the formation of Mo₂C with respect to C₂H₄. The solid lines correspond to free energy of formation of ethylene with respect to temperature. The numbers mentioned on the solid lines represent the equilibrium constant, K.

Figure 3-4. Ellingham diagram showing the formation of Mo₂C with respect to C₂H₂. The solid lines correspond to free energy of formation of acetylene with respect to temperature. The numbers mentioned on the solid lines represent the equilibrium constant, K.

Figure 3-5. Ellingham diagram showing the formation of MoC with respect to C₂H₄. The solid lines correspond to free energy of formation of ethylene with respect to temperature. The numbers mentioned on the solid lines represent the equilibrium constant, K.

Figure 3-6. Ellingham diagram showing the formation of MoC with respect to C₂H₂. The solid lines correspond to free energy of formation of acetylene with respect to temperature. The numbers mentioned on the solid lines represent the equilibrium constant, K.

Figure 3-7. DFT calculated phase diagrams of a) hexagonal Mo₂C and b) MoC in the cubic (black) and hexagonal phase (red). Dotted data on the left figure correspond to the experimental data for the Mo₂C heat and free energy of formation taken from (4). Figure taken from (3).

Figure 3-8. Gas phase equilibrium studies for the Mo-Mo₂C-MoC system with respect to hydrogen and methane relative partial pressures pertaining to temperatures of 700 °C (a), 800 °C (b), 900 °C (c), 1000 °C (d) and 1100 °C (e).

Figure 3-9. Appropriate methane to hydrogen ratios in order for the hydrogen methanization treatment at 800 °C.

Chapter 4

Figure 4-1: Synthesis of molybdenum carbide via ion exchange followed by pyrolysis and decarburization via hydrogen methanization.

Figure 4-2. Thermogravimetric Analysis of Amberlite IRA 67 Resin.

Figure 4-3. Thermogravimetric Analysis of ion-exchanged resin.

Figure 4-4. Scanning Electron Microscopy images of samples before (a) and after (b) pyrolysis (800°C, 1 hour in nitrogen).

Figure 4-5. Scanning Electron Microscopy images of samples after pyrolysis at 800°C for 1 hour in nitrogen.

Figure 4-6. X-Ray Diffraction of samples under different pyrolysis condition.

Figure 4-7 X-Ray Diffraction pattern of molybdenum carbide (pyrolyzed at 800 °C for 1 hour in nitrogen) (top) and whole profile fitting refinement fit (R = 1.61%), (bottom).

Figure 4-8. TEM images of molybdenum carbide: a & b) molybdenum carbide prepared at 800°C in nitrogen; c & d) molybdenum carbide prepared at 800 °C in argon; e & f) molybdenum carbide prepared at 800 °C in nitrogen with 6 hour hold.

Figure 4-9. Adsorption Isotherm of molybdenum carbide after pyrolysis at 800 °C in nitrogen.

Figure 4-10. Thermogravimetric Analysis of molybdenum carbide in forming gas.

Figure 4-11. X-Ray Diffraction of post-TGA sample after forming gas treatment

Figure 4-12. Scanning Electron Microscopy of molybdenum carbide after forming gas treatment

Figure 4-13. Mass spectroscopy on methanized molybdenum carbide sample.

Figure 4-14. Surface area analysis of molybdenum carbide using argon as an adsorbate.

Figure 4-15. X-Ray Diffraction pattern and Whole Profile Fitting refinement of molybdenum carbide after methanization treatment.

Figure 4-16. HRTEM images of molybdenum carbide post methanization treatment and fourier transform of indicated region.

Figure 4-17. XPS analyses of molybdenum carbide samples before (a) and after (b) methanization

Figure 4-18. XPS analysis showing N 1s fit.

Figure 4-19. X-Ray Diffraction of molybdenum carbide materials after methanization at $\text{CH}_4 : \text{H}_2 = 1:5$.

Figure 4-20. Surface areas of carbide materials obtained via different decarburization protocols.

Figure 4-21. Schematic for synthesis process using molybdenum oxide as precursor.

Figure 4-22. The X-Ray diffraction pattern of molybdenum oxide.

Figure 4-23. Point of zero charge measurements done on molybdenum oxide.

Figure 4-24. Adsorption isotherm for molybdenum oxide.

Figure 4-25. X-ray diffraction pattern of samples post-ammonolysis (a) treatment.

Figure 4-26. (Left) X-ray diffraction pattern of samples after ammonolysis protocol (a) and methane treatment (a). (Right) The WPF fit showing crystallite sizes of Mo_4O_{11} , Mo_3N_2 and MoO_2

Figure 4-27. X-ray diffraction pattern of samples after ammonolysis protocol (b) and methane treatment (b).

Figure 4-28. SEM image of sample after ammonolysis protocol (b) and methane treatment (b).

Figure 4-29. Adsorption studies of sample after ammonolysis protocol (b) and methane treatment (b).

Figure 4-30. (Top) XPS analysis (Mo spectra) of molybdenum carbide samples (a) pyrolysis of exchanged resin (b) decarburized sample post-pyrolysis of exchanged resin and (c) molybdenum carbide from oxide precursor. (Bottom) Comparison of C 1s spectra for three carbide samples prepared: Sample M1: pyrolysis of exchanged resin. Sample M2: decarburized sample post-pyrolysis of exchanged resin. Sample M3: molybdenum carbide from oxide precursor

Figure 4-31. TEM micrograph of sample after ammonolysis protocol (b) and methane treatment (b).

Figure 4-32. Raman Spectroscopy of IRA 67 resin.

Figure 4-33. Raman Spectroscopy of sample after hydrogen treatment at 600 °C done on molybdenum carbide prepared in (top) Ar (800 °C, 1 hr) (bottom) Ar (800 °C, 6 hrs).

Figure 4-34. Raman Spectroscopy of molybdenum oxide (precursor for Synthesis Protocol II).

Figure 4-35. FTIR analyses done on molybdenum carbide samples prepared via various synthesis routes as well as Vulcan carbon.

Figure 4-36. 4-probe conductivity measurement setup consisting of a copper foil and nickel rod.

Figure 4-37. XRD pattern of Ru/C prepared via incipient wetness (10 depositions), ‘*’ represents hexagonal Ru.

Figure 4-38. HRTEM micrograph of Ru/C prepared via incipient wetness (10 depositions).

Figure 4-39. XRD pattern of Ru/C prepared via incipient wetness (30 depositions).

Figure 4-40. SEM images of Ru/C prepared via incipient wetness (30 depositions).

Figure 4-41. XRD pattern of Ru/C synthesized via wet impregnation method.

Figure 4-42. XRD pattern of Ru/C prepared via polyol method.

Figure 4-43. XRD pattern of Ru/MoC prepared via incipient wetness method.

Figure 4-44. (Left) XRD pattern of Ru/MoC prepared via wet impregnation (‘Δ’ indicates MoC and ‘O’ indicates Ru). (Right) WPF of diffraction pattern showing 2.6 nm of MoC and 40 nm Ru.

Figure 4-45. XRD pattern of Pt/MoC.

Figure 4-46. SEM micrograph of Pt/MoC.

Chapter 5

Figure 5-1. Stability regions of cubic MoC in water as a function of applied potential and pH at 25 °C. The lines correspond to the dependence of formation potential (vs SHE) on pH as listed in the Table 6-2. (1)

Figure 5-2. Cyclic Voltammetry scans (20 cycles) of Molybdenum carbide (from oxide precursor). Inset: Magnified figure of sweeps in negative direction.

Figure 5-3. Cyclic Voltammetry scans (20 cycles) of Molybdenum carbide (from oxide precursor) after being held at -0.1 V for 1 hour. Inset: Magnified figure of sweeps in negative direction.

Figure 5-4. Cyclic Voltammetry scans (20 cycles) of Molybdenum carbide (from oxide precursor) after being held at 0.4 V for 1 hour. Inset: Magnified figure of sweeps in negative direction (arrow indicates direction of cycles from 1st to last).

Figure 5-5. 1st cycles of CVs of MoC without any holds, MoC held at 0.1 V for 1 hour and MoC held at 0.4 V for 1 hour.

Figure 5-6. XPS analysis of (a) fresh molybdenum carbide sample mixed in Nafion before electrochemical measurements, (b) carbide sample post-mortem after being held at -0.1 V for 1 hour and (c) carbide sample post-mortem after being held at 0.4 V for 1 hour.

Figure 5-7. XPS analysis of Nafion.

Figure 5-8. Cyclic Voltammetry scans (20 cycles) of Molybdenum carbide (carbonized) Inset: Magnified figure of sweeps in negative direction.

Figure 5-9. 1st and 20th cycles of CV done on molybdenum carbide (carbonized).

Figure 5-10. 1st cycle of CV scans of MoC (carbonized) and CV scan of MoC (carbonized) when swept from positive potentials.

Figure 5-11. Cyclic Voltammetry scans (20 cycles) of Molybdenum carbide (methanized) Inset: Magnified figure of sweeps in negative direction.

Figure 5-12. 1st and 20th (last) cycles of CV scans done on molybdenum carbide (methanized).

Figure 5-13. Cyclic voltammetry scans of carburized resin.

Figure 5-14. A comparison of last cycles of CV runs of the carburized resin, MoC methanized and MoC carbonized samples.

Figure 5-15. Cyclic Voltammetry on Ru/carbon in 0.5M H₂SO₄ electrolyte.

Figure 5-16. CV run of Pt ring in 0.5M H₂SO₄ electrolyte.

Chapter 6

Figure 6-1. Known phases of Mo-O-C-N system.

LIST OF TABLES

Table 3-1. Calculated enthalpy, entropy and heat capacity values of reactions used in Ellingham and gas phase equilibrium figures (in Section 3.2 of this chapter). Thermochemical data for each substance was obtained from (1,2).

Table 4-1. Surface Area of MoC post-methanization (CH₄:H₂=2:1 at 800 °C) using different adsorbates and surface area models.

Table 4-2. EDS analyses of molybdenum carbide materials before and after the decarburization via hydrogen methanization treatments.

Table 4-3. Relative molybdenum compositions from XPS analysis of synthesized MoC powders before and after the methanization treatment.

Table 4-4. Elemental compositions from XPS analyses.

Table 4-5. EDS analysis of sample after ammonolysis protocol (b) and methane treatment (b).

Table 4-6. Conductivity measurements of all molybdenum carbide samples.

Table 4-7. EDS analysis of Ru/C prepared via incipient wetness (10 depositions).

Table 4-8. EDS analysis of Ru/C prepared via incipient wetness (30 depositions).

Table 4-9. EDS analysis of Ru/MoC prepared via incipient wetness method.

Table 5-1. Samples and their corresponding synthesis routes and properties for cyclic voltammetry measurements.

Table 5-2. Stability regions of hexagonal and cubic MoC in water at 25 °C. (1)

Table 5-3. Relative molybdenum compositions obtained from XPS analysis of fresh and post-mortem molybdenum carbide (from oxide precursor) sample.

GLOSSARY

TMC Transition Metal Carbide

XRD X-ray Diffraction

XPS X-ray Photoelectron Spectroscopy

TEM Transmission Electron Microscopy

HRTEM High Resolution Transmission Electron
Microscopy

SEM Scanning Electron Microscopy

EDS Energy Dispersive Spectroscopy

FTIR Fourier Transform Infrared Spectroscopy

CV Cyclic Voltammetry

HER Hydrogen Evolution Reaction

Chapter 1: Introduction and Literature Review

1.1 Statement of Research Problem

This research is aimed at understanding the surface properties of as-synthesized molybdenum carbides. It is also unknown how different synthesis pathways affect the chemistry, stability and the activity of the carbide. The study of transition metal carbides is of great interest to the community of electrochemists, chemical engineers, and materials scientists. The electronic properties they exhibit are similar to precious noble metals such as platinum and ruthenium making them excellent substitutes for the expensive noble metals that are scarce but critical to the catalyst industry. The transition metal carbides and molybdenum carbide in particular have an immense potential as active electrocatalysts for hydrogen evolution, bifunctional water splitting, CO oxidation, anion material for Li ion batteries and excellent supports for precious metals for electrochemical reaction systems. Molybdenum carbide has also found use in heterogenous reaction systems such as synthesis of ammonia and hydrogenation reactions. However, successful implementation of molybdenum carbide as an electrocatalyst or support is hindered by the fact that the current synthesis processes produce low surface area materials, which often contain contaminants such as excess carbon and surface and chemisorbed oxygen. Moreover, attempts to refine the synthesis pathways are usually not supported by any thermochemical modeling. Hence, there is a need for an investigation into molybdenum carbide's phase stability, synthesis and thermodynamics in order to develop it as a viable catalyst for commercial applications. Additionally, there are contradictory reports in literature regarding synthesis methods to produce pure molybdenum carbide, analysis of phases and their stoichiometries and activities for different reactions.

1.2 Ceramics: Transition Metal Carbides

The art of using ceramics for engineering purposes has existed since the 1700s when coke was first used to improve the yield of the smelting process. Over the years, developing and utilizing these materials has expanded greatly and because of their unique properties they have been applied as catalysts, sensors, and refractory materials to name a few. As a result, they have and are still replacing precious, expensive and rare materials such as platinum and palladium. One of the first studies to utilize ceramics as an electrocatalyst was by Oosawa in 1983 where titanium oxide was loaded into various transition metal carbides and their subsequent activities for photocatalytic hydrogen evolution were investigated and shown in Figure 1-1. (58). Over the years, countless ceramics of differing compositions consisting of carbides, nitrides, sulfides, silicides and borides to name a few have been utilized as heterogeneous and electrochemical catalysts and supports.

Transition metal carbides (TMCs) have been in the limelight since the pioneering works of Levy and Boudart in 1973 which showed the platinum like behavior of tungsten carbide (1). TMCs combine the physical properties of transition metals, ionic and covalent solids. They retain the conductivity of transition metals while exhibiting the structural coordination and high melting points of ionic solids and hardness of the covalent solids. Additionally, their band structures and electronic conductivities are governed by extent of metallic, covalent and ionic bonding character of the metal–metal and metal–carbon bonds. Many of the transition metals such as molybdenum are earth abundant in addition to being stable, selective and exhibiting a variety of oxidation states. As a result, compounds of these transition metals (including carbides) are known for their profound catalytic activity and are replacing precious metals such as Pt, Pa and Ru.

Despite their advantages of being active, low cost and earth abundant, there are many gaps in literature regarding controlled synthesis of such materials, scientifically sound characterization

techniques to accurately analyze phase compositions and thermochemical modelling to understand the stability of these materials under conditions of synthesis and application. This review goes into detail regarding such gaps in the case of transition metal carbides with particular emphasis on molybdenum carbides in the areas of phases and structures, morphologies, thermodynamic properties, synthesis, characterization and electrochemical stabilities.

Borides	rate	Nitrides & Phosphide	rate	Carbides	rate	Others	rate
TiB ₂	0.16	TiN	0.060	ZrC	0.037	none ^{d)}	< 0.001
ZrB ₂	0.14	ZrN	0.034	VC	0.050		
NbB	0.17	VN	< 0.001	NbC	0.097	Pt black ^{e)}	10.6
TaB	0.019	TaN	0.061	Cr ₃ C ₂	0.28	Ru black ^{f)}	1.5
CrB	0.96	Mo ₂ N	< 0.001	Mo ₂ C	0.32	RuO ₂ ^{g)}	2.5
Mo ₂ B ₅	0.016			WC(1) ^{b)}	3.0		
Ni ₂ B	0.96	Co ₂ P	0.75	WC(2) ^{c)}	3.3	Pt/TiO ₂ ^{h)}	16.2

Figure 1-1. Hydrogen evolution rate over electrocatalyst/TiO₂. One of the earliest studies involving ceramics powders carried out by Oosawa (58)

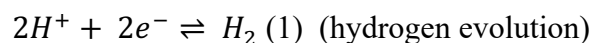
1.3 Hydrogen Evolution Reaction

Sustainable hydrogen production has been of great interest to researchers as that would be the pathway to a carbon free energy economy (104). Hydrogen evolution from electrochemical water splitting is being extensively investigated in order to develop clean energy technologies. Precious noble metals such as platinum are state-of-the-art electrocatalysts for hydrogen evolution reaction (HER) as they demonstrate exceptional behavior with zero overpotential in acidic media (105-106). However, their high cost and scarcity hinders their use in large scale hydrogen evolution reaction systems. Therefore, the scale of global energy demand calls for HER catalysts to be

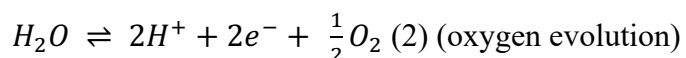
designed from non-precious materials such as transition metal carbides. The use of molybdenum carbide as a HER catalyst has been reviewed in a later section in this chapter.

Electrochemical water splitting in acidic media consists of the following reactions:

At the cathode:



At the anode:



1.4 Phases and Structures, Morphologies and Thermodynamic Properties

The center of the periodic table *i.e.* the transition metals have been of much interest to the communities of chemical engineers, materials scientists, nanotechnologists and ceramics engineers. The addition of carbon to transition metals such as Mo and W gives them catalytically active properties like that of precious metals such as Pd and Pt. (1) Transition metal carbides are also widely known for the useful properties such as exceptional hardness, resistance to corrosion and high temperatures and high electronic conductivity ranging from semiconductor to almost metallic behavior. (2) As a result, they have been purposed as structural supports, wear resistant components, industrial cutting tools, optical coatings, diffusion barriers and electrical contacts.

Nowotny et al. (16) was one of the first studies to develop a composite phase diagram with molybdenum and carbon and it consisted of three major regions – Mo₂C, MoC, and Mo₂C and C. It also has been long hypothesized that Mo₂C is the only stable phase at room temperature however, later studies have shown that Mo₂C is the thermodynamically stable phase and MoC is a metastable phase thereby existing at room temperature as well.

However, Nowotny *et al.* characterized the MoC phase as hexagonal and by then there were reports of co-existence of a hexagonal and cubic phase for both Mo₂C and MoC.

It is interesting to note that despite the first phase diagram being published in the 1940s, there are still contradictory reports of molybdenum-carbon phase behavior with reports of orthorhombic, cubic and hexagonal structures of varying stoichiometries. (7, 9, 10). Chen's (44) review into the transition metal carbides states the existence of three phases of carbides: hexagonal close packed (Mo_2C), simple hexagonal (MoC) and face centered cubic (MoC) and is shown in Figure 1-2.

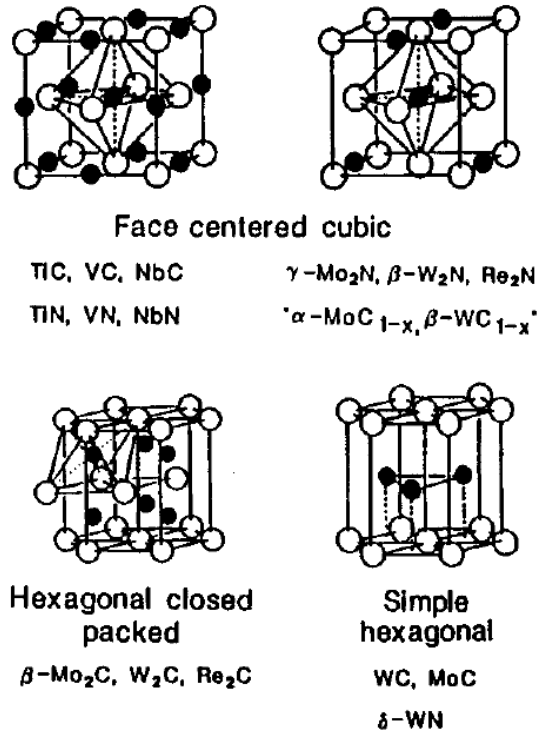


Figure 1-2. Typical structures of transition metal carbides and nitrides as shown by Chen (44).

One of the interesting reports however is that of existence of four different phases of the carbide discussed by Wan *et al.* (11, 36) and shown in Figure 1-3. The authors reported the existence of two additional hexagonal structures of MoC in addition to the hexagonal Mo_2C and cubic MoC. According to Wan *et al.*, the stacking sequences of the hexagonal phases of MoC are different from that of Mo_2C . The MoC hexagonal phases are of WC (ABCABC) and MoC (AAAA) types as opposed to the ABAB packing in hexagonal Mo_2C . The cubic MoC has been correctly characterized as isostructural to NaCl.

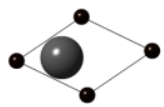
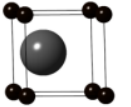
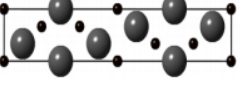
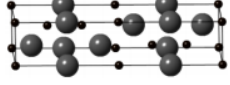
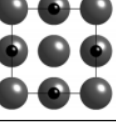
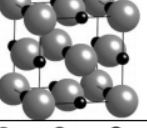
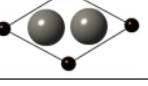
Name	Structure	
γ -MoC (WC type)		
η -MoC (MoC type)		
α -MoC _{1-x} (NaCl type)		
β -Mo ₂ C (Fe ₂ N type)		

Figure 1-3. Four phases of molybdenum carbide postulated by Wan et al. (11, 36).

As reported by a majority of literature, most reports of molybdenum carbide phases are either cubic or hexagonal. However, there have been mentions of an orthorhombic phase of Mo₂C in Posada-Perez *et al.* (7, 45). The authors claim the presence of hexagonal Mo₂C and cubic MoC as well. Liu *et al.* (46) analyzed the surface of MoC and deduced it to be polycrystalline. Similarly, Anjum *et al.* (79) have observed five phases: Mo₂C in orthorhombic and two hexagonal phases and MoC in both hexagonal and cubic phases.

There are reports of cubic structure of the carbide being analyzed as Mo₂C. Sullivan *et al.* (47) assign the cubic metastable phase of the carbide to Mo₂C. The authors further discuss the hexagonal close packed phase of Mo₂C. According to their study, the experimentally deduced hcp phase of Mo₂C is often misconstrued as hexagonal and it is truly orthorhombic as concluded by Parthe *et al.* (69). Parthe *et al.* (69) after having conducted neutron diffraction stated that the Mo₂C has an orthorhombic structure, composed of slightly distorted hexagonally packed layers of Mo. This is not the only study to declare a cubic Mo₂C phase. The existence of such a phase was discussed by both Hyeon *et al.* (28) and Patel *et al.* (10). However, the authors do not go into detail

about cubic MoC and what sets the two cubic phases apart. Gu *et al.* (50) claimed to synthesize hexagonal Mo₂C with slight amounts of cubic Mo₂C but made no efforts to distinguish between the cubic phases of Mo₂C and MoC. Similarly Jujuri *et al.* (52) talk about the existence of fcc MoC however, they characterize their synthesized fcc phase of the carbide as Mo₂C.

Guzman *et al.* (48) have devised synthesis methods that can produce different phases of the carbide as detected by in-situ X-ray diffraction. The authors discussed the presence of six phases of the carbide as mentioned in literature including hexagonal Mo₂C, orthorhombic Mo₂C and cubic MoC. However, their detailed synthesis methods with varying conditions only produce hexagonal Mo₂C and cubic MoC as shown in Figure 1-4.

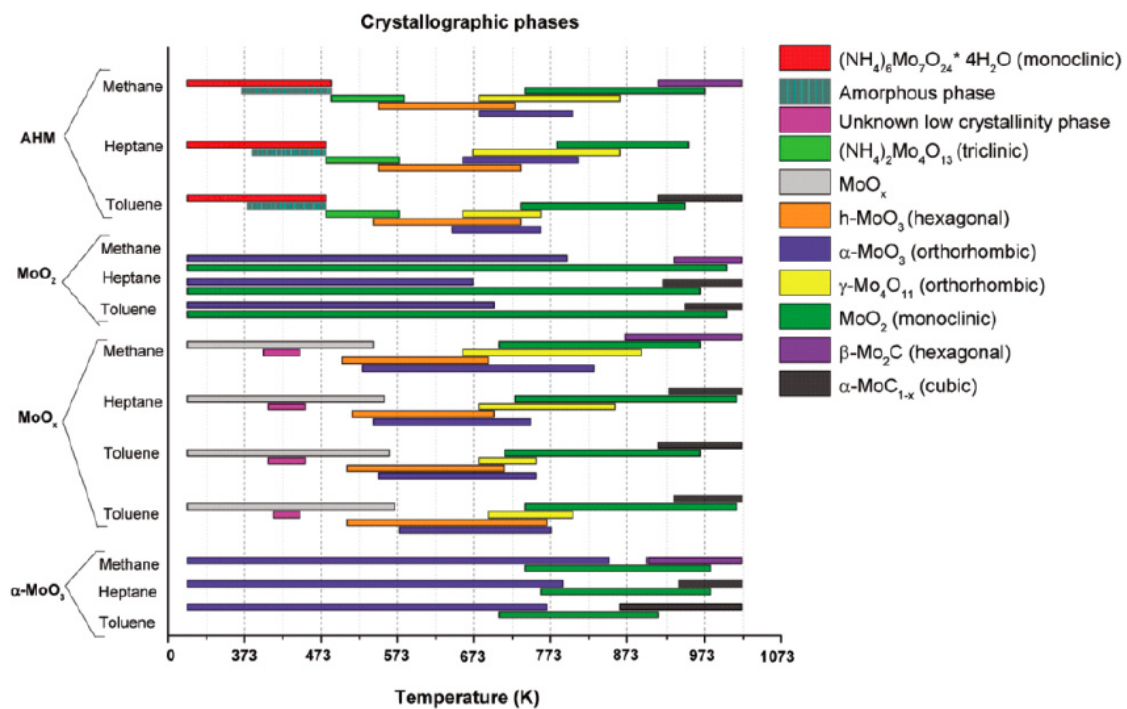


Figure 1-4. Phases of molybdenum carbide synthesized by Guzman *et al.* (48).

A theoretical study by Hugosson *et al.* (49) provides detailed phase analysis conducted with transition metal carbides over the years and according to their investigation, there are three phases of the MoC: a cubic NaCl type, a hexagonal WC type and a hexagonal TiAs type alongside three

phases of the Mo_2C : two hexagonal and one orthorhombic as in Figure 1-5. The authors in a different study (43, 51) have determined that the orthorhombic Mo_2C is more stable than its hexagonal counterpart and the cubic MoC .

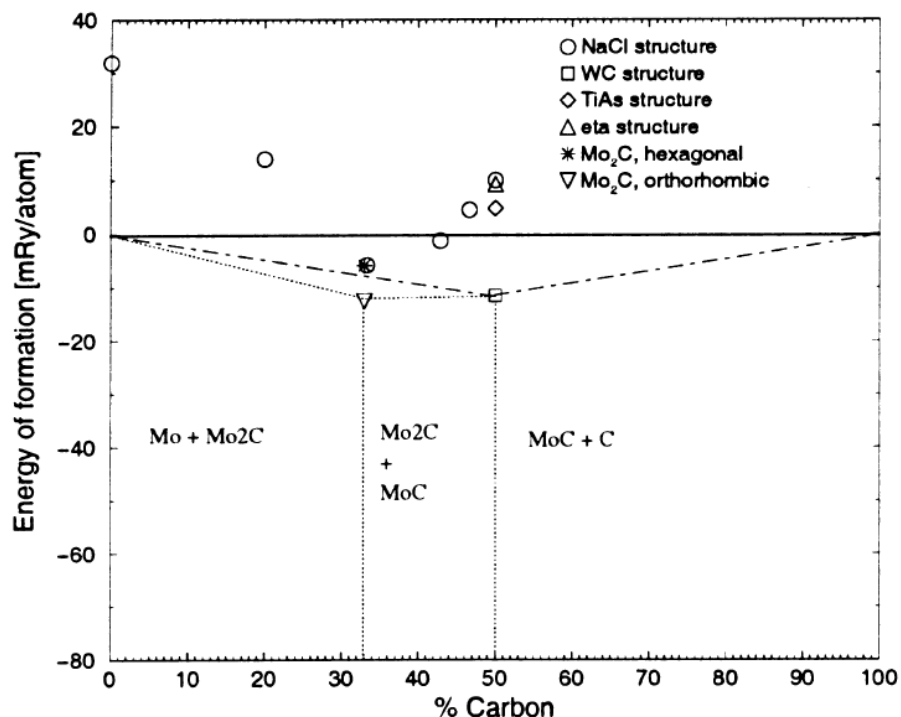


Figure 1-5. Energy of formation of different phases of molybdenum carbide studied by Hugosson et al. (49)

Therefore, multiple phases of molybdenum carbide exist and they exhibit different catalytic activity and stability. (1) However most experimental studies with sound characterization techniques and analysis have proposed the existence of only two phases: a thermodynamically stable hexagonal Mo_2C and a metastable cubic MoC as seen in Bouchy *et al.* (40) and Lee *et al.* (13, 14). The existence of a theoretical hexagonal MoC phase was proposed; however, there is no clear evidence of the experimental synthesis of such a phase exclusively. Tang *et al.* (80) report the existence of hexagonal MoC ; however, little was done to distinguish it from the hexagonal Mo_2C phase.

The morphologies of the molybdenum carbide synthesized are varied: rods, cubes, wires, flowers, flakes, layers and spheres. Wan *et al.* (36) tuned their synthesis parameters to produce all the different morphologies: the hexagonal Mo_2C exists in rod, wire, sphere and flower shapes whereas the cubic MoC exists as cubes, flakes and layers. They are shown in Figure 1-6.

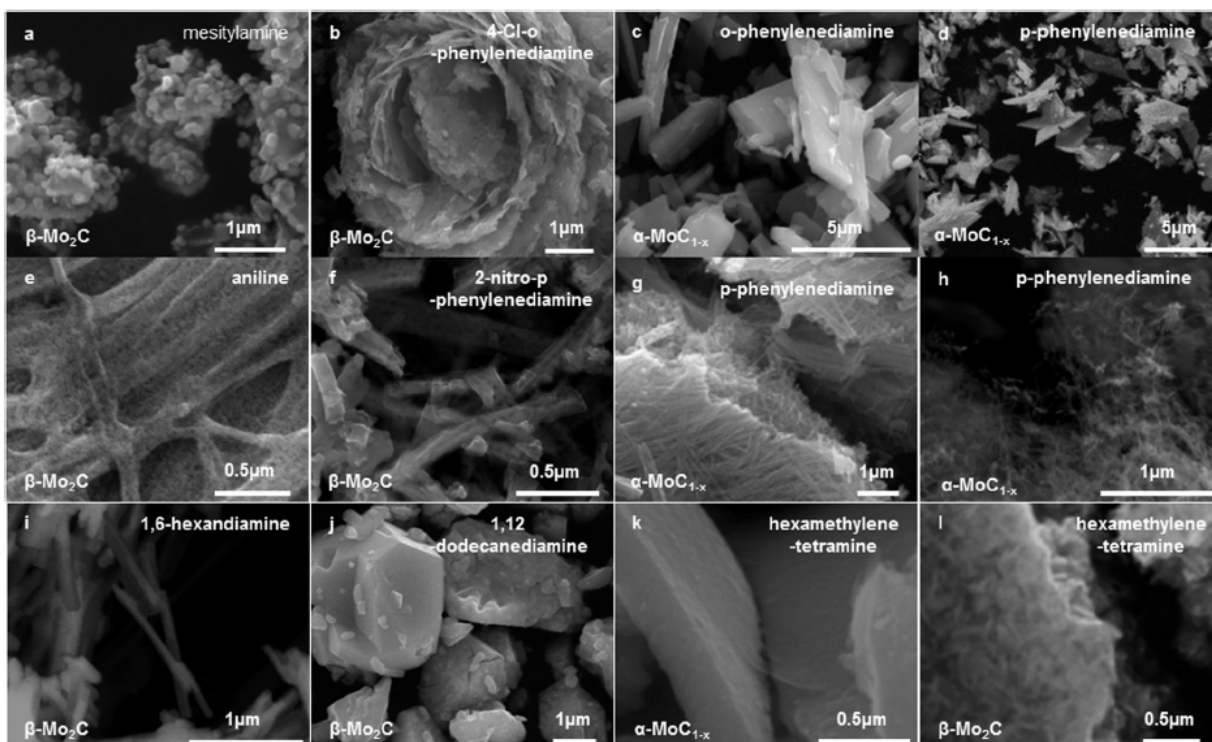


Figure 1-6. Scanning Electron Microscopy images of molybdenum carbide synthesized via different methods outlined by Wan *et al.* (36)

Hanif *et al.* (27) discussed the change in the morphology during the process of carburizing the oxide. The molybdenum oxide has a needlelike shape, which disappears after the carburization protocol, and the particles get rougher indicating an increase in surface area. The morphologies of their carburized products were studied using high-resolution transmission electron microscopy and are shown in Figure 1-7. Researchers carried out controlled synthesis of the carbides in order to yield certain morphologies such as 1D nanowires of Mo_2C as in Liao *et al.* (35) (Figure 1-8) and heteronanowires composed of both MoC and Mo_2C nanoparticles as in Lin *et al.* (53).

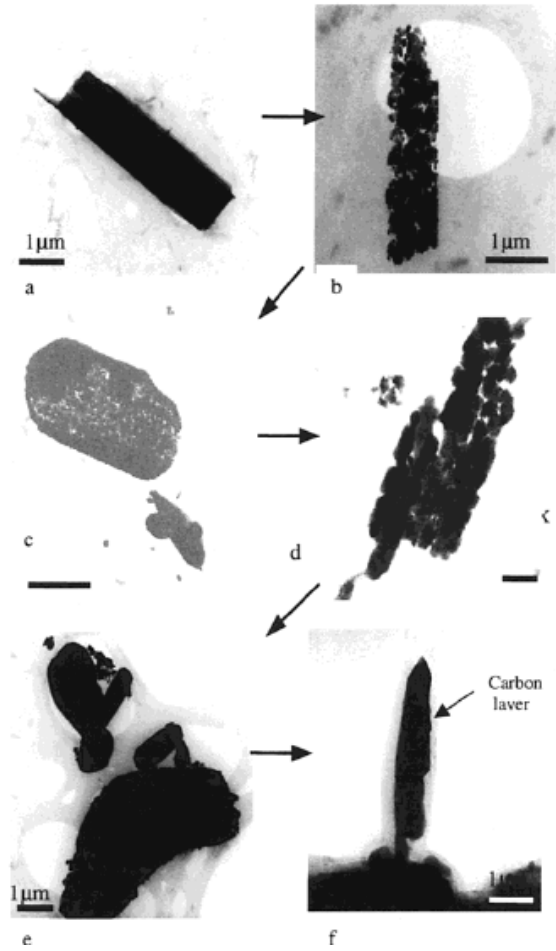


Figure 1-7. High-resolution transmission electron microscopy (HRTEM) morphologies of molybdenum carbide formed during carburization using ethane/hydrogen at different temperatures.

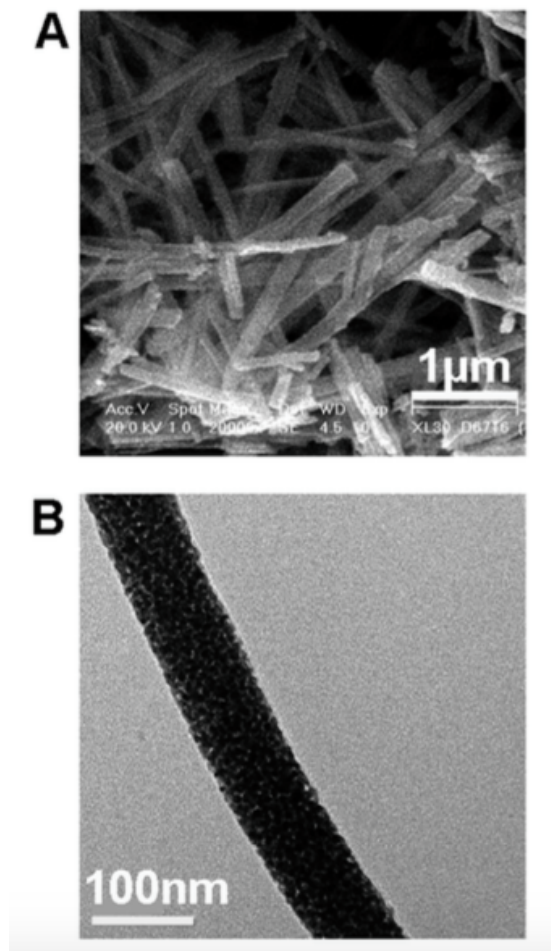


Figure 1-8. SEM (a) and TEM (b) images of 1D nanowires of molybdenum carbide synthesized by Liao et al. (35)

Nanobelts were reported by Li *et al.* (81) where the authors state that they have achieved simultaneous control of shape, size, and phase of the carbide synthesized. The shape of the final product is due to the belt shape of the precursor material, MoO_3 , as developed by the authors in a different study (82). The authors synthesized nanobelts of both hexagonal Mo_2C and cubic MoC with a width of around 60 nm. A discussion about the synthesis process is mentioned in the next section.

N-doped carbon nanotubes embedded with molybdenum carbide nanoparticles were developed by Zhang *et al.* (83), which possess the morphology of nanorods. Great attention was given to the tubular morphology and the small size to design efficient catalysts for hydrogen evolution reaction. Interesting structures and arrangements such as micro islands of Mo₂C on carbon, microflowers of MoC on N-doped carbonaceous support, origami-like carbide nanoflakes and necklace like MoC embedded in carbon nanofibers were reported by Fan *et al.* (84) Chen *et al.*(75), Koizumi *et al.* (85) and Shi *et al.* (86) respectively.

The stable phase of the carbide: hexagonal Mo₂C was experimentally synthesized and studied since the 1940s, therefore there is accurate thermodynamic information such as heat of formation, heat capacity and entropy. The heat of formation of Mo₂C was measured by Mah (54) in 1963. However, the ‘MoC’ sample used for the measurement decomposed to form Mo₂C and C upon cooling thereby giving an inaccurate value. Various authors have attempted the investigation into free energy of formation of MoC; however, they were often rife with inaccuracies due to contamination from carbon, other phases of the carbide and even oxygen. Kouvetakis *et al.* (55) however investigated the temperature stability of the binary MoC phase and found values for enthalpy and entropy of formation, but the authors deduced the MoC to be of hexagonal phase while it may have been a cubic structure. Shatynski (56) comments on the irregularities in thermodynamic data regarding molybdenum carbide as a whole due to the confusion regarding the phase composition and structure of the carbides in literature. Browning and Emmett (57) attempted to measure the properties of MoC but the resultant free energy was similar to that of Mo₂C and C.

1.5 Synthesis

Molybdenum carbide has been emerging as an efficient catalyst and support material because of the unique combination of its structural and electronic properties. (3-7) However, there have been difficulties in synthesizing phase pure carbide owing to chemisorption and insertion of oxygen atoms, formation of surface oxides and oxycarbides (8) and deposition of amorphous and graphitic carbon.

There exists a myriad of methods to synthesize the various phases of molybdenum carbide. The traditional methods to synthesize transition metal carbides include directly sintering the metal/metal precursor with carbon and reacting metal oxide with excess carbon, metal with carburizing gas and metal halide or carbonyl vapor with carburizing gas/hydrogen. (2, 3) However, these methods require high synthesis temperatures and volatile reactants and often produce toxic by-products. An exception is a synthesis process reported by Alhajri *et al.* (92) where the chloride form (MoCl_5) is used as the molybdenum precursor. The synthesis took place within a carbon matrix at temperatures as high as $1300\text{ }^\circ\text{C}$ leading to large crystallites of Mo_2C (ranging from 12 to 50 nm). The surface areas reported are as high as $300\text{ m}^2/\text{g}$ however a back of the envelope calculation reveals that a particle size of around 30 nm molybdenum carbide nanoparticles would yield a much lower surface area of around $12\text{ m}^2/\text{g}$ leading to the observation that most of the high surface area is due to the carbon. A similar paper which utilizes the halide is reported by Ma *et al.* (91). In this study, the authors have used urea as the carbon precursor and reported the synthesis of both pure Mo_2C and Mo_2N by simply changing the ratio of urea to metal precursor.

The synthesis routes that are widely used today often use similar oxide based precursors but try to bypass the other drawbacks of the traditional methods *i.e.* high synthesis temperatures and toxic byproducts.

They comprise of a reaction between molybdenum and carbon precursors (usually oxide and carburizing gas respectively) under a variety of conditions such as temperature, pressure and atmosphere.

One of the widely known, well-referenced and breakthrough methods was detailed by Lee *et al.* (4, 5) and involves a two part reaction to synthesize the cubic phase of molybdenum carbide, MoC:

- a. Ammonolysis of the oxide, MoO₃ at 700 °C to produce the cubic phase of nitride, Mo₂N.
- b. Carburization of the nitride under methane and hydrogen to synthesize cubic MoC.

Another reaction pathway discussed by the authors involves the direct carburization of the oxide, which yields the thermodynamically stable phase of the carbide, hexagonal Mo₂C. The schematic of the process is shown in Figure 1-9. The crystallite size and surface area of the synthesized MoC is around 6 nm and 180 m²/g, respectively.

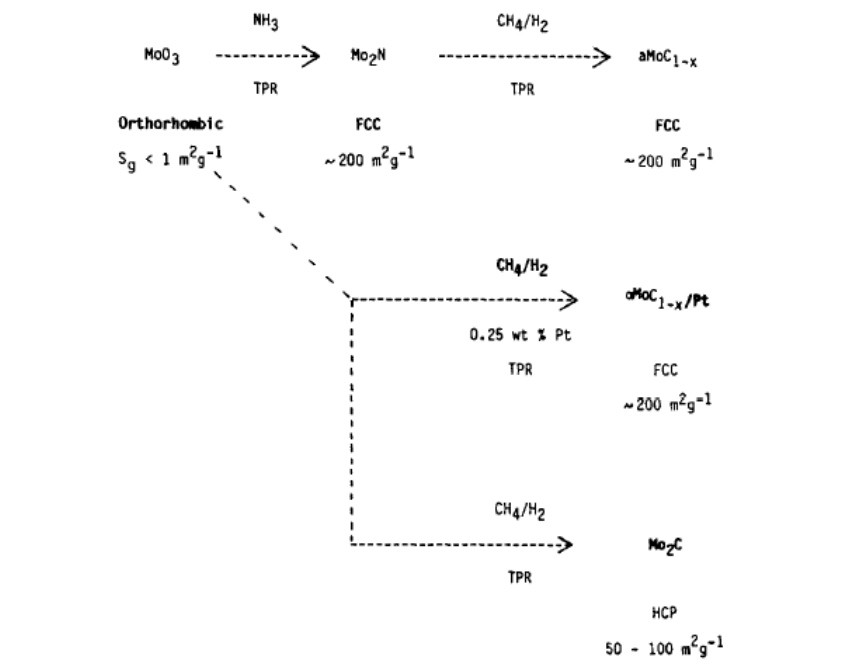


Figure 1-9. Schematic of processes to synthesize different phases of molybdenum carbide by Lee *et. al* (14).

Lee *et al.* demonstrated that the phase of carbide synthesized not only depends on the temperature, pressure and precursors but also the type of synthesis route taken. The first reaction pathway produces the cubic phase of the carbide because the final product, MoC and the by-product, Mo₂N are isostructural (fcc). However, it has been reported that a range of oxycarbides have fcc lattices and are therefore, isostructural with Mo₂N as well.(6) That combined with the fact that transition metal carbides can dissolve considerable amounts of oxygen by substitution of carbon (7) indicates that Lee *et al.*'s choice of precursor increases the probability of synthesizing oxycarbides and oxynitrides and extensive characterization of the carbide powders is required to ensure that these undesirable products have not been formed. It was also long concluded by Huttig *et al.* (42) that a solid solution between the carbide and oxide of molybdenum exists and the reaction is promoted by the presence of hydrogen. Therefore, it is advisable not to use an oxide precursor unless the product is purified in high vacuum. (16)

Choi *et al.* (8) and Volpe *et al.* (39) examined in detail the first step of Lee *et al.*'s method to synthesize MoC: the reaction between MoO₃ and NH₃ to produce molybdenum nitride and conclude that the nitridation of the oxide occurs in two steps. Choi *et al.*'s observations have been summarized in Figure 1-10. Products of this reaction often involve oxides such as MoO₂ and oxynitrides such as Mo₂O_yN_{1-y}.

Catalyst code	Heating rate (K/hr)		Space velocity (hr ⁻¹)	Preparation code	Surface area (m ² /g)	Particle size ^a (nm)	O ₂ uptake (μmole/g)
	β ₁	β ₂					
MoN-1	100	200	17	+++	24	27	67
MoN-2	40	200	17	-++	116	6	112
MoN-3	100	100	17	+--+	44	15	85
MoN-4	40	100	17	--+	52	12	93
MoN-5	100	200	8.5	++-	12	53	24
MoN-6	40	200	8.5	-+-	28	23	54
MoN-7	100	100	8.5	+--	39	14	58
MoN-8	40	100	8.5	---	4	160	7

^a Estimated from the surface areas assuming spherical particles.

Figure 1-10. Effect of synthesis parameters on properties of molybdenum nitride as shown by Choi *et al.* (17).

Lee *et al.*'s temperature programmed reaction mechanism has been optimized and utilized to synthesize a variety of molybdenum carbide samples for applications such as heterogeneous ammonia synthesis (9, 10). Zheng *et al.* (10) slightly altered the original TPR parameters of temperature and dwell time. As a result, the authors synthesized hexagonal Mo₂C with surface areas around 40 m²/g, which is considerably lower than that reported by Lee *et al.*

Kojima *et al.* (9) similarly prepared hexagonal Mo₂C with lower surface areas. However, the synthesized cubic MoC had surface areas close to 140 m²/g which is similar to that of Lee *et al.* Monjardin *et al.* (11) also carried out the TPR experiments where they have varied the heating ramp schedule as well as composition of the feed gas. The oxide precursor was carburized in both 20% and 40% CH₄/H₂ at temperatures ranging from 750 °C to 900 °C. These synthesis conditions yielded a series of samples consisting of mixed carbides, hexagonal Mo₂C and cubic MoC, with surface areas ranging from 9 to 30 m²/g.

Oshikawa *et al.*'s (12) play on Lee *et al.*'s method involved alteration of the carburization temperature to 600 °C – 900 °C in the two-step process. This resulted in the formation of various

samples of molybdenum carbide with surface areas ranging from 3 to 150 m²/g. The lower surface areas are attributed to the formation of carbonaceous carbon, which blocks the active sites or pores. Mo *et al.* (13) attempted a series of synthesis processes by changing the temperature, hydrocarbon and feed gas composition. Their synthesis conditions involve the use of methane, ethane, butane and carbon monoxide as the carburizing agent in various ratios in combination with hydrogen and temperatures ranging from 550 °C to 800 °C and these yield a variety of products mixed alongside each other: MoO₂, Mo₄O₁₁ and hexagonal and cubic phases of molybdenum carbide.

Wang *et al.* (14) tackled the issue of oxycarbides formation on direct carburization of MoO₃ with a hydrocarbon, in this case propane. It is their observation that simply carburizing the oxide leads to the formation of cubic MoC or MoO_xC_y and further treatment with pure hydrogen transforms it to phase-pure hexagonal Mo₂C.

The synthesis of the carbide using butane as the carburizing gas was studied by Xiao *et al.* (15) where they concluded that the carburization of molybdenum oxide, MoO₃, goes through four phases transitions before transforming to pure phase hexagonal Mo₂C. Reduction of the oxide with a combination of butane and hydrogen leads to the formation of monoclinic MoO₂ followed by cubic MoC (which could also be an oxycarbide as oxygen was detected). By increasing the temperature further to 750 °C, single carbide phase hexagonal Mo₂C is formed. Temperatures higher than 750 °C lead to formation of coke as observed by the authors. Similar observations were noted by the authors in (16) where they studied the synthesis of molybdenum carbides using ethylene.

York *et al.* (17) analyzed the influence of ethane versus methane as the carbon source for the synthesis of high surface area transition metal carbides. Hanif *et al.* (18) studied this in much greater detail with respect to only molybdenum carbide.

Another study which used the “20% methane in hydrogen” feature was reported by Li *et al* (81) where the authors have not only controlled the shape but the size and phase of the carbide formed by carefully choosing reaction conditions such as carburizing and reducing agent and temperatures. The hexagonal Mo₂C phase was synthesized using Lee *et al.*'s method of carburizing molybdenum oxide using 20% methane in hydrogen. The cubic MoC phase was synthesized using 5% butane in hydrogen mix, however there is no reasoning provided for choice of carburizing agent and molar ratio chosen.

It is clear that Lee *et al.*'s detailed study and analysis of the molybdenum carbide phases has influenced researchers everywhere to pursue the development of TMCs as catalysts and has also provided a fundamental building block for others to base their synthesis methods on. However, later researchers of the topic have not carried out the detailed analysis as was carried out by Lee *et al.* Their studies are often devoid of sensible thermodynamic calculations, which are vital when changing the reaction conditions such as temperature, hydrocarbon and feed gas composition, or detailed characterization of the materials to understand its properties thoroughly.

A counter to the different TPR experiments was conducted by Wang *et al.* (93) who reported the superiority of the hydrogen thermal treatment to synthesize molybdenum carbide. According to the authors, this is due to the dispersion of the carbide and lower quantities of polymeric carbon due to the small amount of carbon source used. This study is of great interest as it shown that different molar ratios of molybdenum to carbon precursors and gases for thermal treatment lead to formation of materials with varying stoichiometries of molybdenum, carbon and nitrogen. For instance, the authors deduce that a lower molar ratio of carbon precursor and under hydrogen thermal treatment, a carbo-nitride is formed. This is one of the very few studies to report an existence of a molybdenum carbon nitrogen compound. However, when the thermal treatment is

done in argon, only the formation of molybdenum nitride is reported. Higher ratios of the carbon precursor and hydrogen treatment lead to the formation of single carbide phase hexagonal molybdenum carbide, Mo_2C . Given the variety of products formed by changing reaction conditions and XRD being the significant tool of characterization to distinguish between the products, it would have been a good idea if the authors had attempted Rietveld refinement of the diffraction patterns instead of mere peak identification. The authors in a different study (94) go into detail the synthesis process of molybdenum carbide using the precursors of ammonium molybdate- hexamethylenetetramine (Mo-HMT) and HMT and the formations of Mo_2C , Mo_2N or a mixture of both when changing the reaction conditions. The authors postulate that the molybdenum precursor decomposes to form Mo_2N whereas the HMT at high temperatures forms carbon. The reaction between the two yields Mo_2C however, there is not much reasoning provided for the molar ratios of precursors chosen. Similar processes using HMT have been reported by Huo *et al.* (95) to synthesize both bulk as well as Ni supported on molybdenum carbides.

A similar synthesis route but with different precursors has been reported by Patel *et al.* (19). This method uses ammonium molybdate and sucrose as molybdenum and carbon precursors respectively. They are pyrolyzed at temperatures of around 800 °C and 1200 °C to yield Mo_2C . The authors conducted thermogravimetric analyses on the precursors and concluded that ammonium molybdate and sucrose decompose to form molybdenum oxide and carbon and therefore, Mo_2C is formed from the carbothermic reduction of MoO_3 . From X-ray diffraction, the crystallite size was determined to be close to 3.2 nm but the surface areas were not reported. However, the X-ray diffraction pattern clearly shows a cubic pattern akin to 'MoC' but the authors have analyzed the same as cubic Mo_2C as seen in Figure 1-11. The authors further stipulate that

the crystal structure of Mo_2C formed with stoichiometric composition is orthorhombic whereas the same formed with excess carbon is cubic.

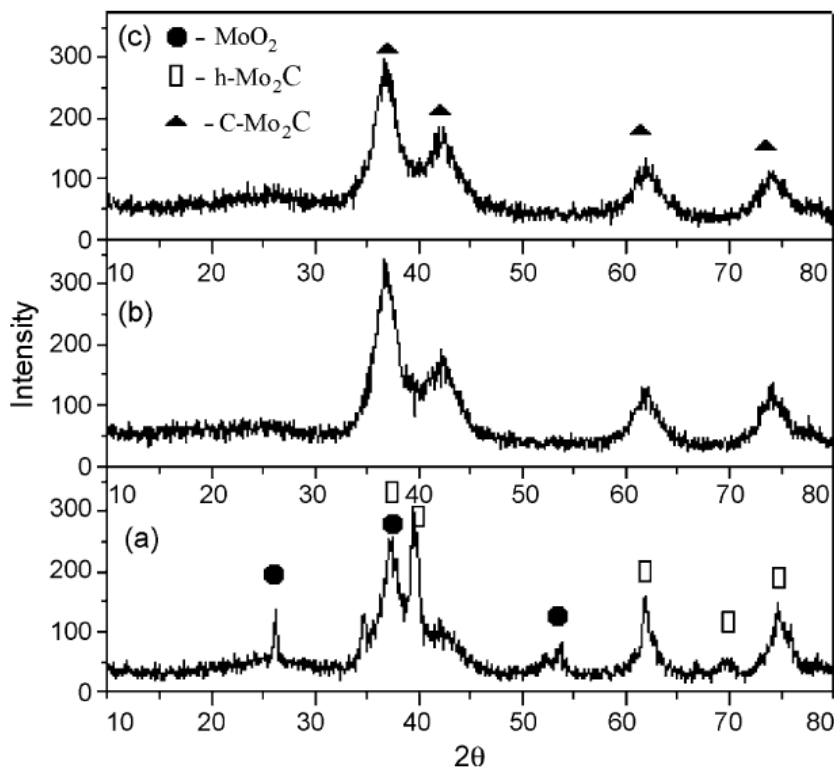


Figure 1-11. XRD patterns after pyrolysis at 1200 °C at different concentrations of C/ MoO_3 (a: the stoichiometric concentration, 0.77; b: 1.5 times and c: 2 times the stoichiometric concentration) as reported by Patel *et al.* (10)

The existence of a cubic Mo_2C has been also reported by Hyeon *et al.* (20) where the authors developed a synthesis method involving the irradiation of a slurry of molybdenum hexacarbonyl followed by a heat treatment at 450 °C under He and carburization in methane and hydrogen. The authors have not utilized thermodynamic information regarding the phases of molybdenum carbide to refine the synthesis pathways, thereby exerting little or no control over the phase of the carbide formed. Moreover, the X-ray diffraction pattern only shows regions of 2θ higher than 30 ° and hence, is incomplete since information regarding the presence of carbon which is critical to

synthesis of carbides lies in the region below 30° as in Figure 1-12. It is also interesting to note that the X-ray diffraction patterns reported by Patel *et al.* do not correspond to that by Hyeon *et al.* despite their statement that they have synthesized the same phase of the carbide.

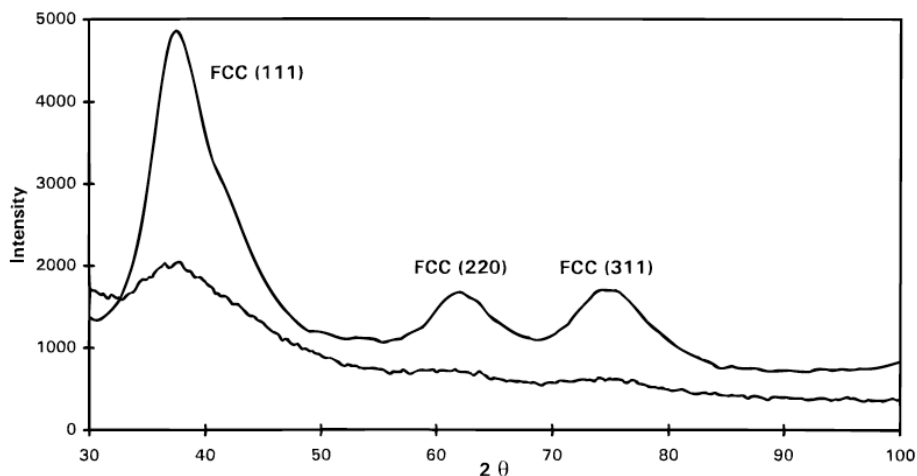


Figure 1-12. XRD patterns of sonochemically produced Mo_2C where the upper curve is after the heat treatment at 450°C under He as reported by Hyeon *et al.* (28).

Gomez-Marin *et al.* (21) reported a different method of synthesis which involved the oxide, MoO_3 and carbon. Their method comprises of wet impregnation of MoO_3 on carbon black using isopropanol as a solvent and pyrolysis of the slurry at 900°C in either argon or hydrogen atmospheres. The synthesis conditions have been reported to produce hexagonal Mo_2C or a mixture of Mo_2C and MoO_2 as shown in Figure 1-13. The crystallite sizes have been reported to be in range of 30-40 nm. Carbon to molybdenum ratios were analyzed by EDS and reported to be around 5 to 6 (Figure 1-14). Despite the reports of formation of mixed oxides and carbides, oxygen ratios have not been mentioned. The catalysts prepared have excess carbon as reported in the surface analysis studies.

Catalysts	wt.% MoO ₃	wt.% Carbon black	Carburization gas	T _{carb} (°C)	Holding time, t _h (min)	Mo-Crystalline phases	Crystallite size (nm) *
A	77.3	22.7	Ar	750	20	α-Mo ₂ C	35
B	77.2	22.8	10% H ₂ -Ar	725	30	α-Mo ₂ C	29
C	81.3	18.7	Ar	800	45	α-Mo ₂ C	40
D	81.3	18.7	Ar	900	30	α-Mo ₂ C	42
E	81.3	18.7	Ar	700	720	α-Mo ₂ C	41
F	81.3	18.7	Ar	700	0	MoO ₂ and α-Mo ₂ C	42/35
G	77.2	22.8	10% H ₂ -Ar	625	30	MoO ₂	39

* Calculated from XRD data.

Figure 1-13. The series of catalysts prepared by Gomez-Marín *et al.* (29): synthesis conditions and information obtained from XRD.

EDX compositions for different catalysts (wt.%).

Catalyst	Determined by EDX		
	Mo	C	C/Mo*
A	62.3 ± 4.8	37.7 ± 4.8	4.9 ± 1.0
B	57.9 ± 4.8	42.1 ± 4.8	5.8 ± 1.0
C	87.9 ± 0.5	12.1 ± 0.5	1.1 ± 0.1
D	85.4 ± 1.6	14.9 ± 1.6	1.4 ± 0.2
E	83.9 ± 0.2	16.1 ± 0.0	1.5 ± 0.9

* Molar fraction.

Figure 1-14. Molybdenum to carbon ratios obtained from EDS analysis by Gomez-Marín *et al.* (29).

A study reporting a different carbon source (dimethyl ether) was carried out by Zhao *et al.* (96). The authors state that they have synthesized a variety of phases over the carburization process ranging from oxides, MoO₃, Mo₄O₁₁ and MoO₂ to oxycarbides, MoO_xC_y and carbides, MoC and Mo₂C. The XPS analysis conducted by the authors accounts for a peak at ~229.5 eV for the oxycarbide however, the oxycarbide and the cubic MoC phases are indistinguishable in the XRD pattern. Gao *et al.* (97) report a peak at ~229 eV which they assign to the oxycarbide.

Another unique method to synthesize the carbide from the oxide is through solid–state metathesis developed by Nartowski *et al.* (98) Here, the authors used both MoO₃ and Li₂MoO₄ as molybdenum precursors and CaC₂ as the carbon source. It was their observation that reaction conditions of 1000 °C and 6 hours produces the thermodynamically stable carbide. This is true in

the case of molybdenum as Mo_2C is the thermodynamically stable phase, however, further characterization would have shed more light to the efficacy of the process.

Wang *et al.* (22) detailed a one-pot synthesis process that yielded molybdenum carbide with high surface areas of around $700 \text{ m}^2/\text{g}$. The synthesis process involves a lengthy step of letting a solution of molybdenum and carbon precursors and formaldehyde stand for about a week at room temperature before pyrolyzing it. XRD patterns indicate MoC is poorly crystallized as shown in Figure 1-15 and hence, it can be concluded that the high surface area ($\sim 700 \text{ m}^2/\text{g}$) is due to carbon and not the carbide nanoparticles. Moreover, back-of-the-envelope calculations show that the surface area of $700 \text{ m}^2/\text{g}$ corresponds to a MoC particle size of 1 nm, which is improbable. The authors observe in their TEM images in Figure 1-16 the presence of ordered mesoporous carbon with pore sizes of $\sim 6 \text{ nm}$ and also, highly dispersed MoC nanoparticles embedded within the walls of the carbon with sizes of 3 – 5 nm.

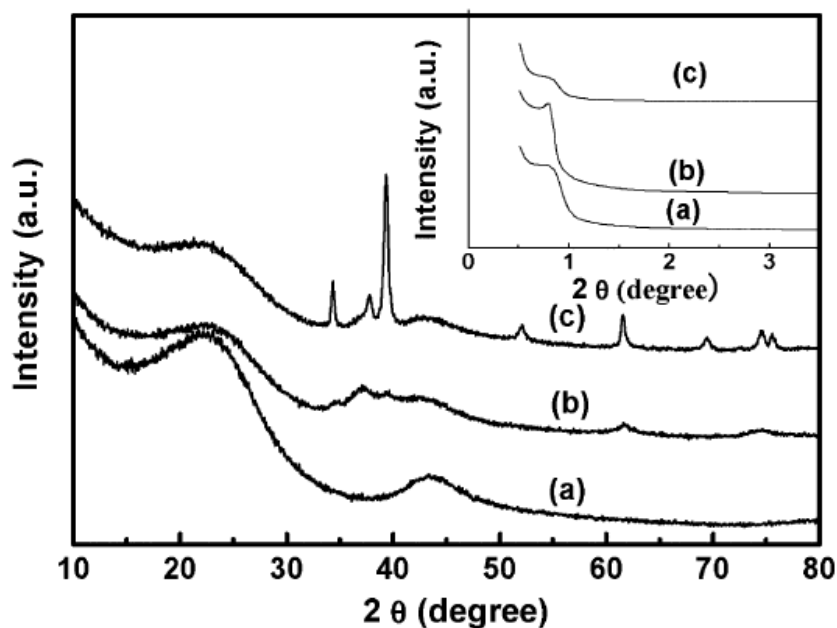


Figure 1-15. Low-angle (inset) and wide-angle XRD patterns of (a) Ordered Mesoporous Carbon (OMC), (b) MoC-OMC and (c) Mo₂C/OMC as shown by Wang *et al.* (30)

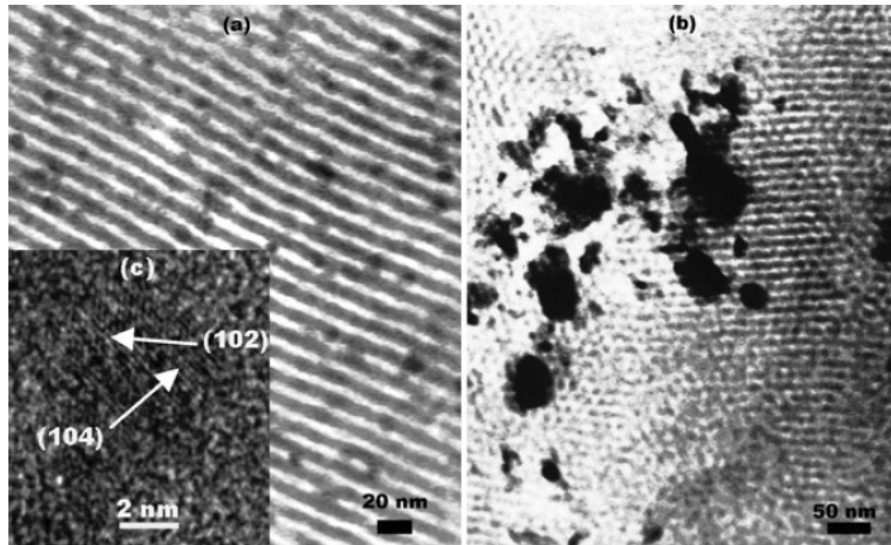


Figure 1-16. TEM images of (a) MoC-OMC, (b) Mo₂C/OMC and (c) HRTEM images of MoC-OMC as shown by Wang *et al.* (30).

He *et al.* (23, 24) developed a method to synthesize multiple phases of ultra-small molybdenum carbides with surface areas as high as 278 m²/g to 344 m²/g. The process involves freeze-drying a solution of graphene oxide and ammonium molybdate prior to pyrolyzing it at different temperatures to synthesize MoC and Mo₂C (Figure 1-17). This process like that of Wang *et al.* is time-consuming owing to the freeze-drying step. X-Ray diffraction patterns of the synthesized MoC-G show peaks corresponding to both graphite and cubic MoC. However, those of Mo₂C-G appear to have a cubic pattern along with peaks of the hexagonal Mo₂C phase indicating that both phases are formed as shown in Figure 1-18.

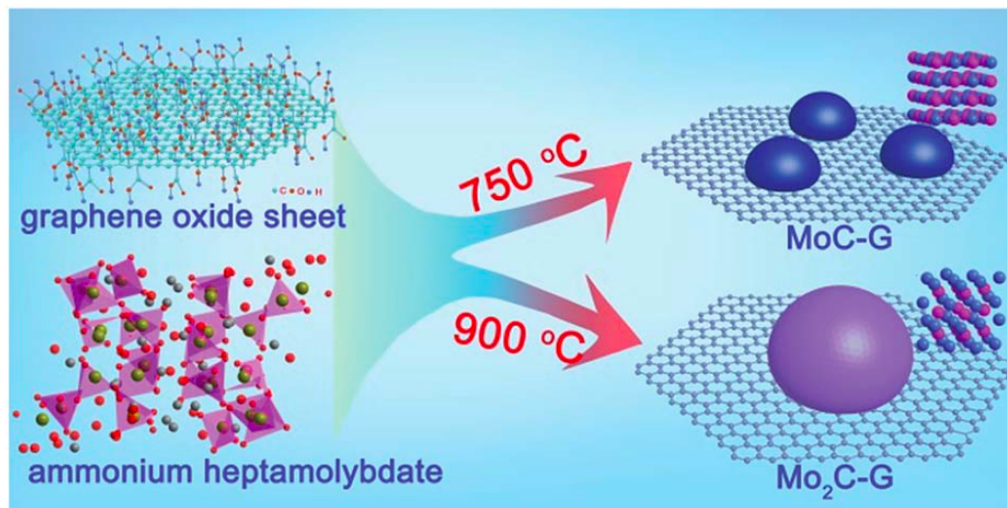


Figure 1-17. Schematic for synthesis of molybdenum carbides as shown by He *et al.* (31)

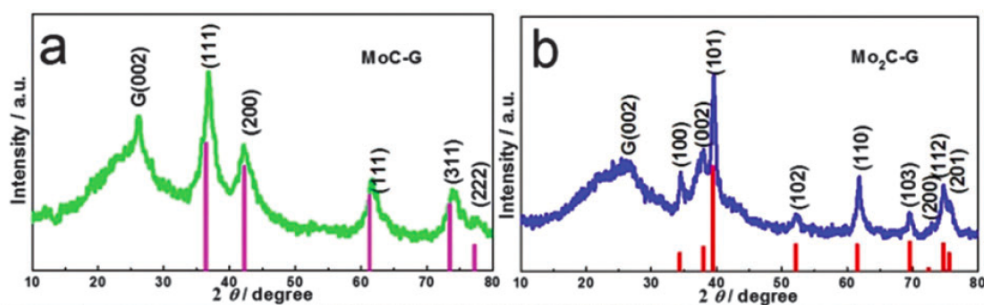


Figure 1-18. XRD patterns for synthesized molybdenum carbide samples in He *et al.* (5).

Metal organic frameworks (MOFs) have been used for synthesizing nanoparticles (9). Wu *et al.* (25) developed a metal organic framework assisted method to synthesize porous molybdenum carbide octahedral nanoparticles. Their synthesis pathway involves the co-precipitation of MOFs-based compound and molybdenum precursor, pyrolysis at 800 °C in N₂, and etching with FeCl₃ to remove Cu contamination as shown in Figure 1-19. The authors state that the diffraction pattern of their samples is atypical compared to those corresponding to similar synthesis processes, which also involve annealing of molybdenum salts and organic compounds at similar temperatures. According to their reports, hexagonal MoC is formed unlike an orthorhombic Mo₂C phase, which is generally reported for similar synthesis processes. As mentioned earlier, this once again shows

that the synthesis pathway influences the phase of carbide formed along with other factors such as precursors, temperature, pressure, and atmosphere. However, it is worthwhile to note that the reported X-Ray diffraction pattern (Figure 1-20) upon examination appears cubic with some hexagonal phase contamination. The authors stipulate that the nano-octahedrons of MoC_x have particle sizes of around 5 nm and that amorphous carbon stabilizes the carbide nanoparticles and prevents their agglomeration. The surface area reported for these molybdenum carbide samples is around $150 \text{ m}^2/\text{g}$.

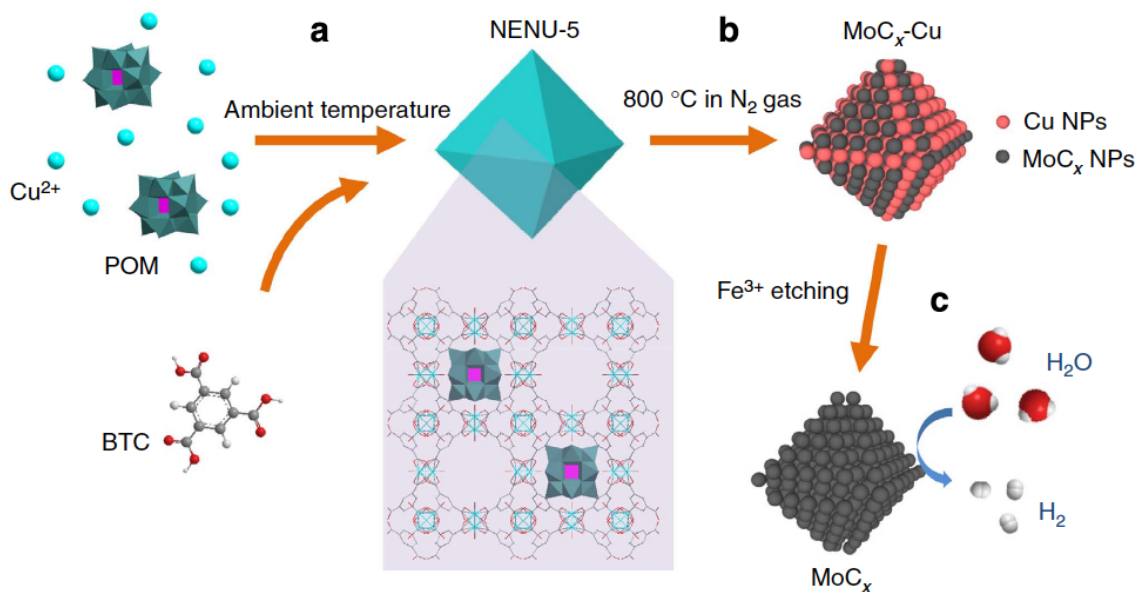


Figure 1-19. Schematic illustration of synthesis pathways by Wu *et al.* (32)

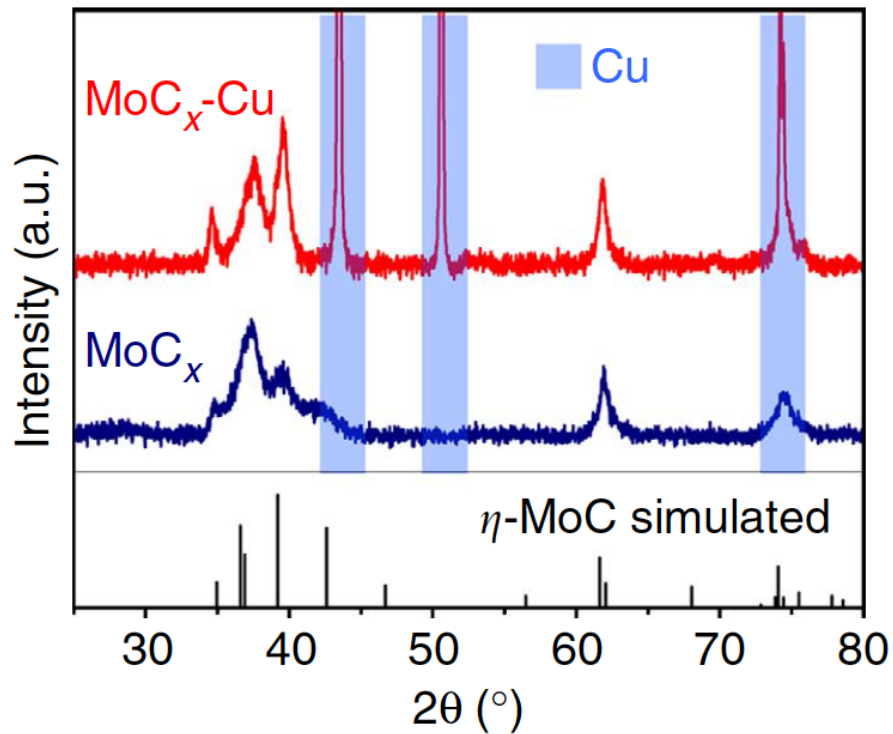


Figure 1-20. XRD pattern of synthesized molybdenum carbide by Wu *et al.* (32).

Chen *et al.* (26) report the synthesis of orthorhombic Mo_2C as mentioned in (25) and their process involves in-situ carburization of ammonium molybdate on carbon nanotubes and Vulcan XC-72. The standout feature of this process is the absence of a carburizing gas which, according to the authors, prevents the formation of chars formed from pyrolysis of carbonaceous gases. The authors further stipulate that their X-Ray diffraction pattern indicates the formation of pure orthorhombic phase of Mo_2C (Figure 1-21). However, the pattern corresponds to a hexagonal Mo_2C phase as corroborated by Pan *et al.* (27) and Liao *et al.* (28).

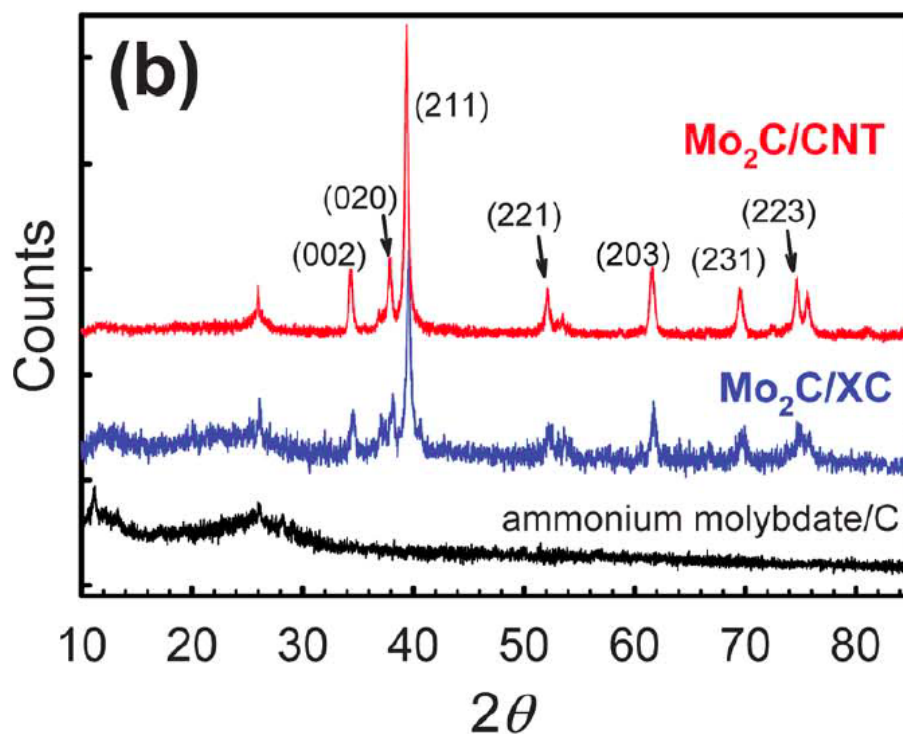


Figure 1-21. XRD patterns of Chen *et al.*'s (33) synthesized molybdenum carbides.

Pan *et al.* (27) detail a synthesis process that involves the hydrothermal carbonization of ammonium molybdate and glucose followed by carburization in argon to produce a Mo₂C – reduced graphene oxide hybrid (Figure 1-22). The authors have correctly analyzed the primary phase of the carbide to be hexagonal Mo₂C and stipulated that the absence of other peaks indicates that the complete reaction to desired product has occurred as shown in the XRD pattern in Figure 1-23. However, Rietveld analysis is required to successfully conclude that there are no contributions from other phases of carbide that may have been formed as well as unreacted by-products. The Raman spectra show pronounced peaks at around 700 cm⁻¹, 800 cm⁻¹ and 1000 cm⁻¹ in addition to the D and G peaks (Figure 1-24). These were assigned to the hexagonal phase of molybdenum carbide. However, Xiao *et al.* (15) observed that the peaks 666 cm⁻¹, 819 cm⁻¹ and 995 cm⁻¹ correspond to MoO₃ and the carburization of the oxide over a range of temperatures to form the carbide leads to the eventual disappearance of the peaks as shown in Figure 1-25. Hence,

detailed whole profile fitting of the X-ray diffraction pattern would have shed light on the possible presence of oxides or oxycarbides.



Figure 1-22. Schematic for synthesizing molybdenum carbides reported by Pan *et al.* (34).

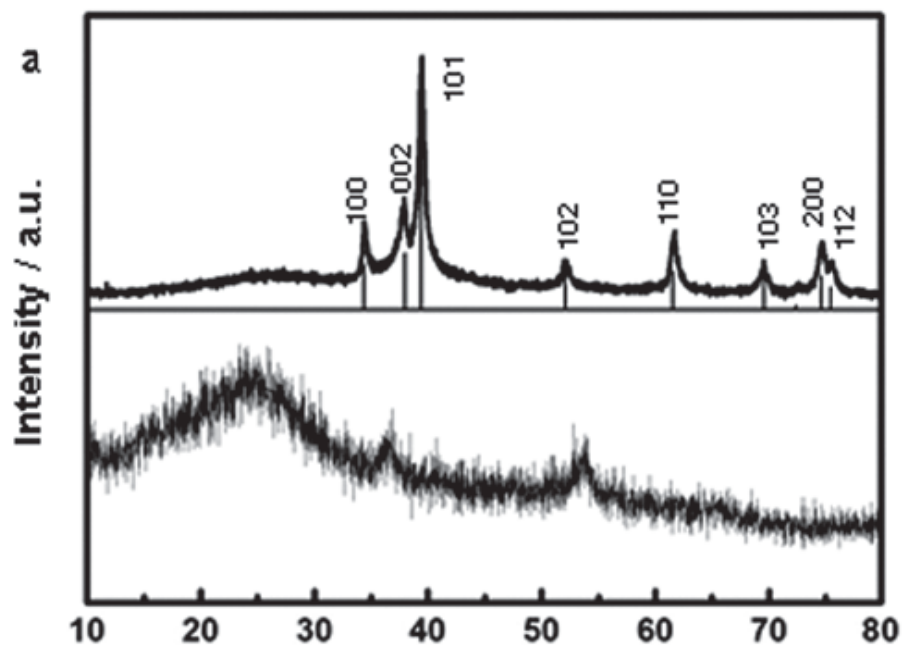


Figure 1-23. XRD patterns of the hydrothermal product (down) and the carburized (up) Mo₂C-RGO hybrid as synthesized by Pan *et al.* (34).

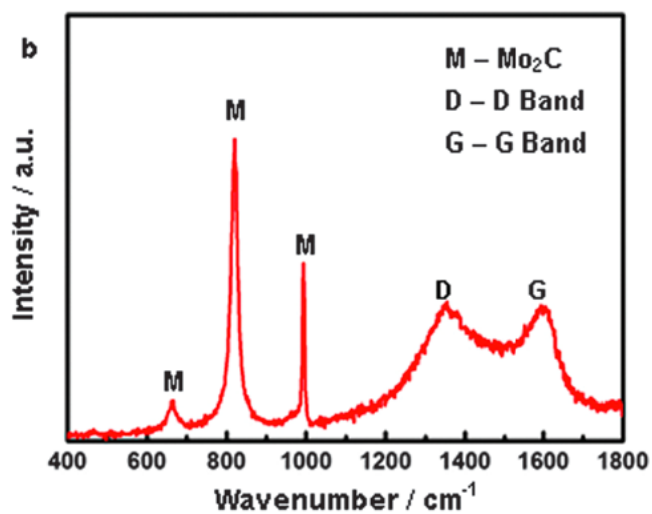


Figure 1-24. Raman spectra of molybdenum carbides by Pan *et al.* (34).

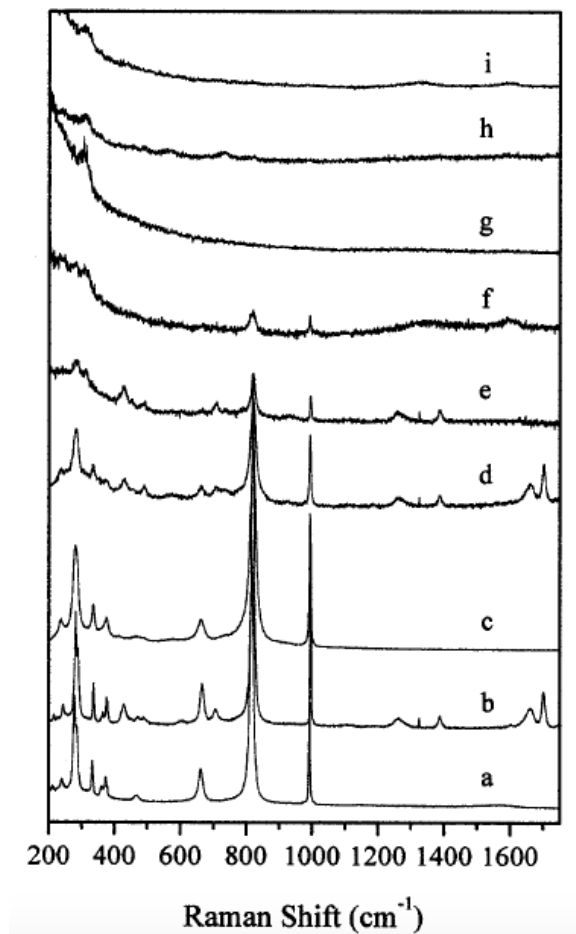


Figure 1-25. Raman spectra of molybdenum oxide subjected to different carburization protocols developed by Xiao et al. (24)

Liao *et al.* (28) developed a method to synthesize nanowires of molybdenum carbide by calcination of ammonium molybdate and aniline at 725 °C. The authors carried out X-ray diffraction of the samples and concluded that they synthesized the hexagonal phase of Mo₂C (Figure 1-26). However, there is no diffraction data between 20° and 30° which would indicate the presence of carbon.

Vengust et al. (99) have also synthesized nanowires initially comprising of both MoC and Mo₂C, and the authors have carried out controlled reduction to achieve single carbide phase nanowires. Their ability to synthesize nanowires comes from the unique use of their precursor, Mo₆S₂I₈.

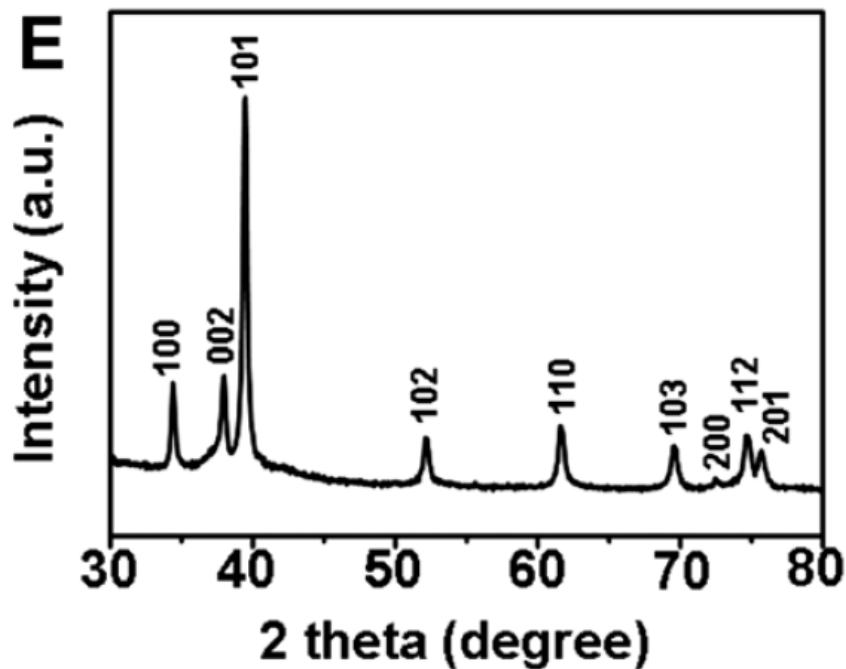


Figure 1-26. Diffraction data for molybdenum carbides synthesized by Liao *et al.* (35)

Multiple phases of the carbide have been stipulated and analyzed by Wan *et al.* (1, 29). They have concluded the formation of hexagonal Mo_2C , cubic MoC , and two hexagonal phases of MoC . The authors have utilized ammonium molybdate and 4-Cl-o-phenylenediamine (4Cl-oPDA) as molybdenum and carbon sources thereby forming an amine metal oxide hybrid precipitate. Different phases have been synthesized at temperatures of 850°C and 1050°C with differing hold times of 12 and 24 hrs. The diffraction patterns for the hexagonal phases of MoC consist of closely spaced peaks at 2θ angles lower than 20° , which could belong to unreacted oxide or excess carbon rather than a different phase of the carbide as shown in Figure 1-27.

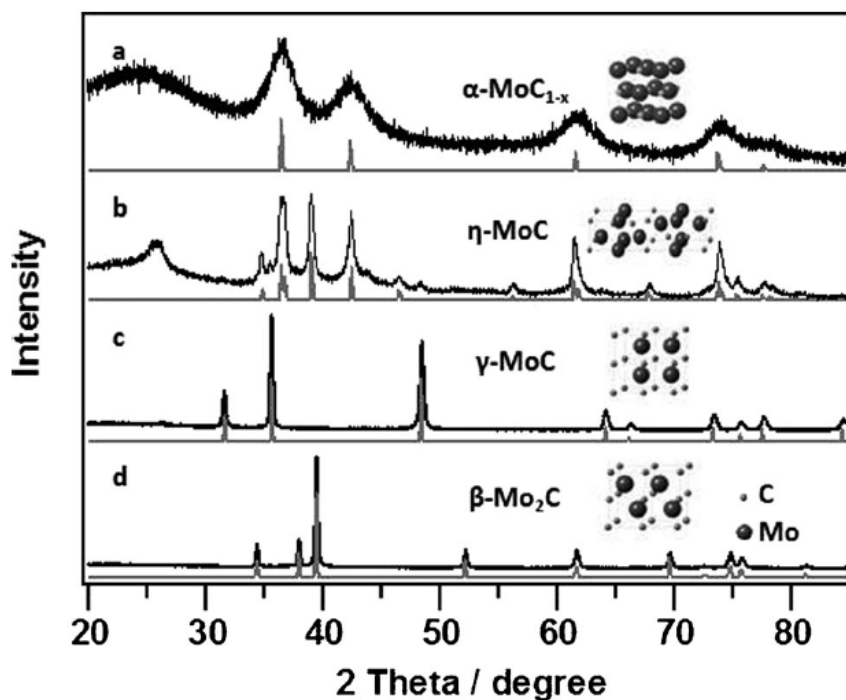


Figure 1-27. X-ray diffraction patterns of multiple phases of molybdenum carbide synthesized by Wan *et al.* (11).

Microwave heating is another process that has gained popularity in the field of synthesis of nanostructures owing to the controlled and efficient heating provided by this kind of irradiation (100). Vallance *et al.* (101) utilize this method to synthesize the hexagonal Mo_2C . The superior characteristics of this study are the use of Rietveld refinement to analyze the diffraction data, which showed only the hexagonal Mo_2C phase and no excess carbon or oxide precursor. Their results were backed up by XRF and EDS analysis and this is a well-characterized method to synthesize pure phase hexagonal Mo_2C . However, the diffraction data shows sharp peaks suggesting large crystallites of molybdenum carbide being formed.

Similarly, spray pyrolysis has been utilized to synthesize molybdenum carbide nanoparticles and has been reported by Lv *et al.*(102). Here too, molybdenum chloride has been used as a precursor

to produce reasonably high surface area ($\sim 149 \text{ m}^2/\text{g}$) 3.5 nm MoC/C with more than 3 layers of carbon as observed via TEM.

Guil-Lopez *et al.* (30) have synthesized a series of carbide samples by the deposition of the molybdenum precursor on the Vulcan XC 72 carbon substrate followed by carburization in a 10% H_2/N_2 atmosphere at various temperatures of 600 °C, 840 °C and 975 °C. The X-ray diffraction patterns of carbides obtained from all three synthesis pathways show prominent peaks corresponding to the Vulcan XC 72 carbon; however, the molybdenum-based material appears to be poorly crystallized (Figure 1-28). Moreover, the authors concluded that their samples were comprised of around 4 wt% Mo which implies that their synthesized materials are primarily carbon with very little molybdenum which may or may not be the carbide.

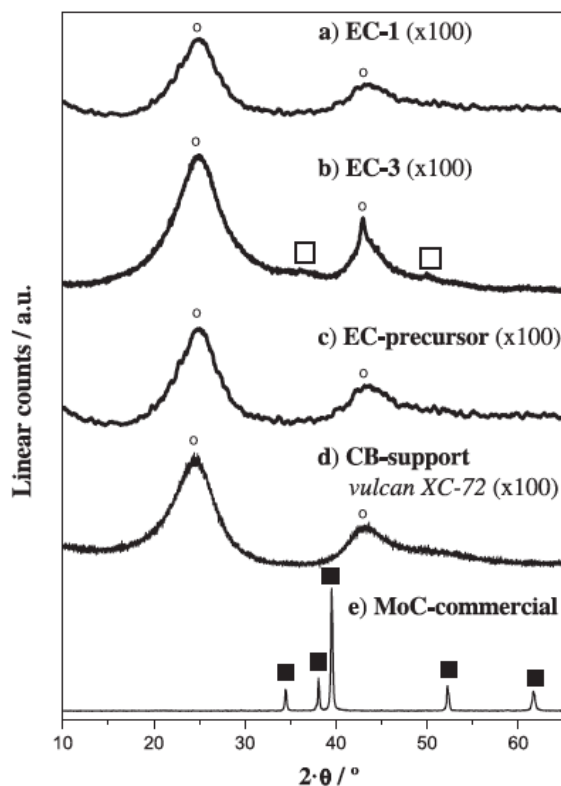


Figure 1-28. XRD pattern of carbides synthesized by Guil-Lopez *et al.* (37)

Elbaz *et al.*'s (31) method of synthesis included the blending of urea and ammonium molybdate (carbon and molybdenum sources respectively) followed by carburization at 800°C in nitrogen. One of the superior points regarding this method is the use of whole profile fitting for the diffraction patterns (Figure 1-29). The analyses indicate the formation of single carbide phase however it has been identified as Mo₂C while the cubic nature of the pattern indicates the possible presence of MoC.

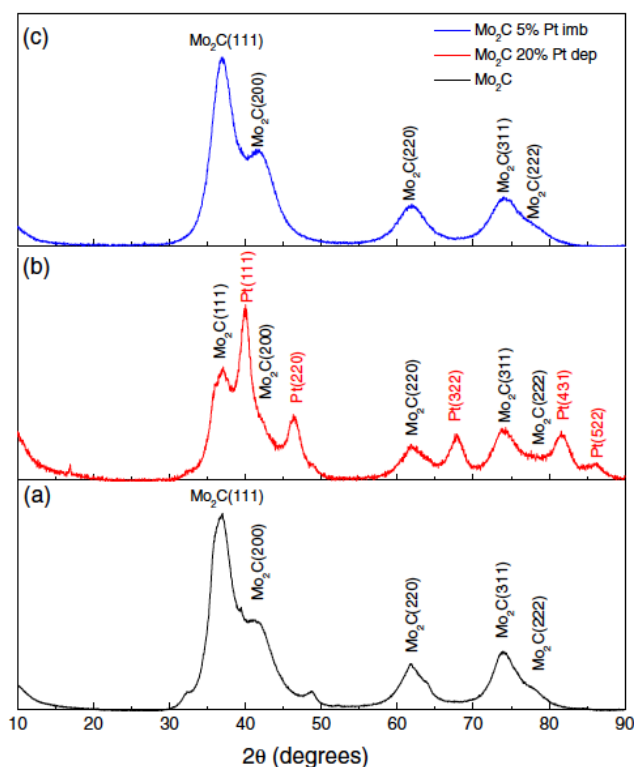


Figure 1-29. XRD patterns of different molybdenum carbide samples synthesized by Elbaz *et al.* (38).

Another method worthy of mention owing to their use of the superior Rietveld refinement of the diffraction data is reported by Kumar *et al.* (103) where the authors have synthesized a molybdenum catalyst composed of both hexagonal Mo₂C and cubic Mo₂N

Bouchy *et al.* (40) proposed a new method to synthesize the metastable FCC phase of molybdenum carbide, MoC as compared to the usual temperature programmed reaction route involving the carburization of MoO₃ using methane. The new step implemented by the authors here is the reduction of the oxide in pure hydrogen at 350°C for 24 hours. Over the course of the reduction process the oxide is converted to a suboxide, MoO₂ and then an oxyhydride, MoO_xH_y. The feed gas is switched to methane and heated to 710 °C while constantly studying the composition of the product via in-situ X-ray diffraction. At temperatures around 680 °C, pure phase metastable MoC is formed with slight traces of thermodynamically stable hexagonal Mo₂C. Scherrer line broadening analysis indicates a crystallite size of 3.4 nm and lattice parameters show that it is the carbide and not the oxycarbide that was synthesized. This is one of the few studies that has correctly characterized the cubic phase of MoC as metastable. A point of interest is the presence of a peak (between 20°-30) at lower temperatures (560 °C - 650 °C), which disappears as the molybdenum carbide peaks become more pronounced. It has been assigned to MoO₂; however, it could also belong to graphitic carbon. Also, according to their surface chemistry studies, the C/Mo ratio is lower than that of Lee *et al.*'s synthesized molybdenum carbide indicating that the coke formation is much lesser here. It is however interesting to note Lee *et al.*'s method is not as time consuming as the Bouchy *et al.*'s route and does indeed produce single carbide phase pure MoC.

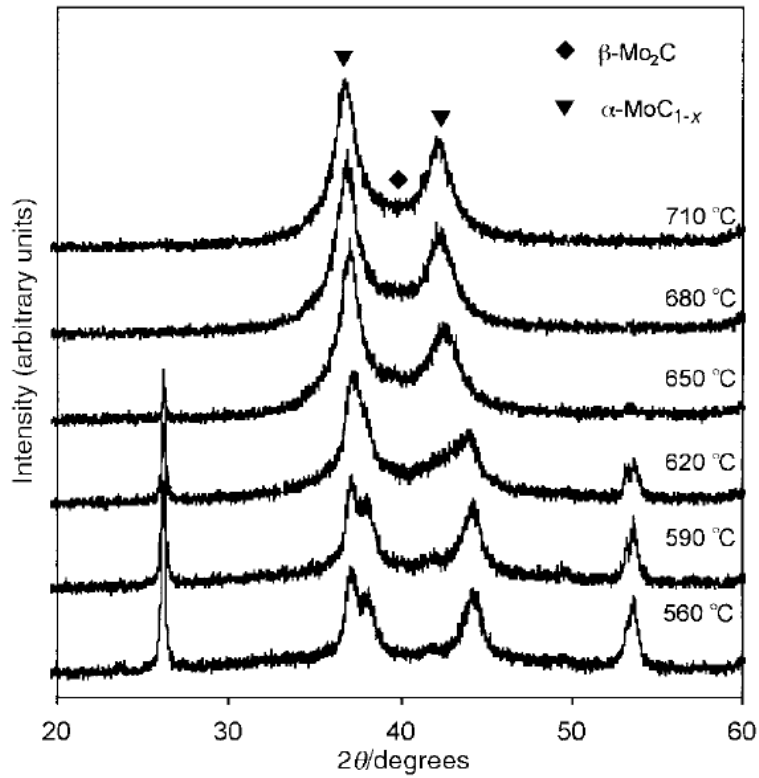


Figure 1-30. In situ XRD characterization of the $\text{MoO}_2\text{-MoO}_x\text{H}_y$ mixture during methane carburization reported by Bouchy *et al.* (40).

Bouchy *et al.* (41) has also studied in detail the insertion of carbon to the molybdenum oxyhydride.

They concluded that the diffusion of hydrogen is essential for the formation of oxycarbide.

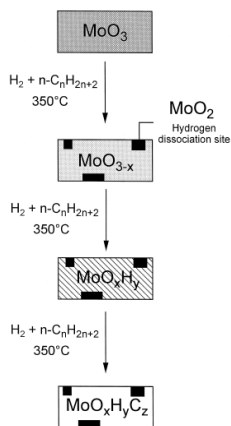


Figure 1-31. Proposed mechanism for the oxycarbide phase formation in the absence of platinum as shown by Bouchy *et al.* (41)

1.6 Electrochemical Activity and Stability

Esposito *et al.* explored the use of transition metal carbides including Mo_2C as low cost substrates for precious metal catalysts such as Pt, Pd, and Au to carry out HER (59). Xiong *et al.* designed two dimensional Mo/ Mo_2C nanosheets which they determined leads to an increase in the number of catalytically active sites and it showed HER performance with an overpotential of 89 mV and current density of 10 mA/cm^2 in an acidic environment as shown in Figure 1-32 (60).

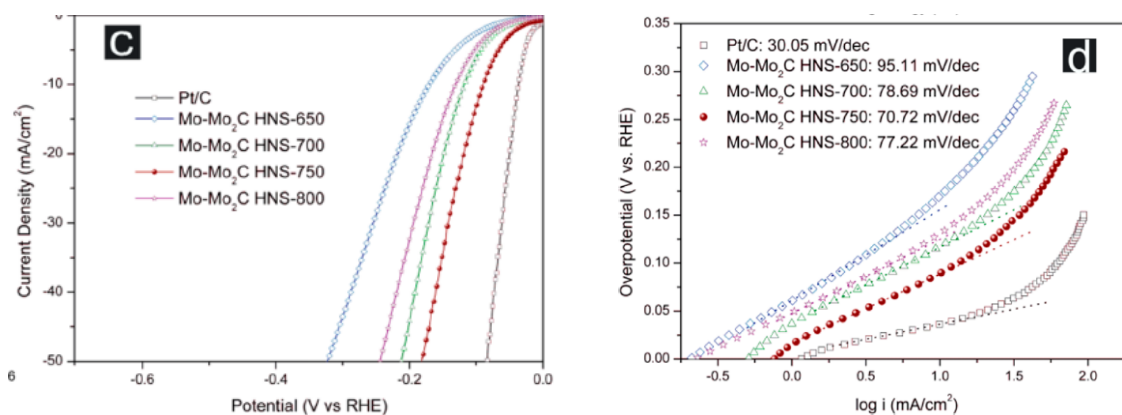


Figure 1-32. Electrochemical performance of Mo based catalysts designed by Xiong *et al.* (60).

Lin *et al.* synthesized heteronanowires of $\text{MoC} - \text{Mo}_2\text{C}$ that displayed promising HER activity with low overpotential, small Tafel slope and low onset overpotential (61).

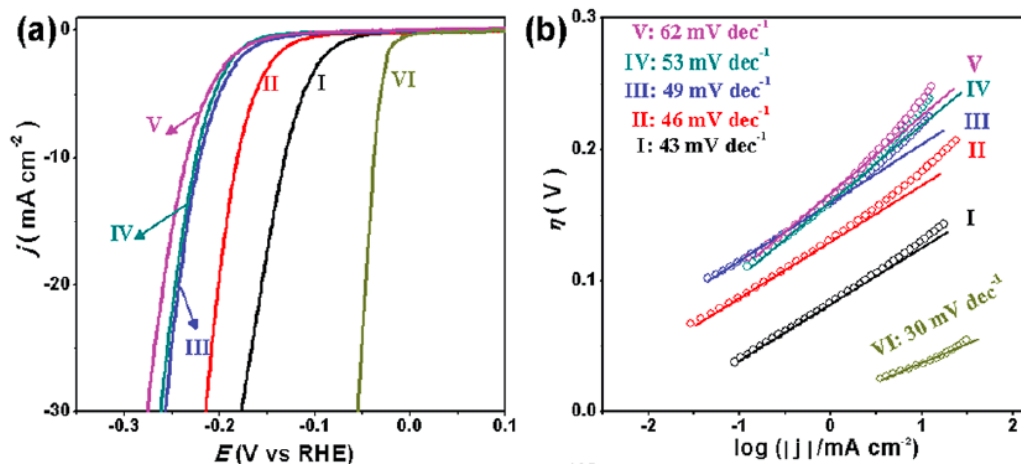


Figure 1-33. Polarization curves and (b) Tafel plots for the HER on modified GCEs comprising (I) MoC–Mo₂C-31.4, (II) Mo₂C, (III) MoC–Mo₂C-68.1, (IV) MoC–Mo₂C-30 (mixed), (V) MoC, and (VI) commercial Pt/C as reported by Lin *et al.* (61).

Xing *et al.* purposed single carbide phase Mo₂C embedded in a carbon matrix as an electrocatalyst for bifunctional water splitting (62). Yan *et al.* developed a bimetallic carbide (FeMo₂C) promoted Pd electrocatalyst for oxygen reduction reaction in acidic media and concluded that its performance was superior to Pt/C (63). Guil-Lopez *et al.* found that molybdenum carbide, Mo_xC, supported on Vulcan XC 72 carbon serves as a potential electrocatalyst for CO oxidation (37).

Gao *et al.* (73) have synthesized molybdenum carbide quantum dots dispersed in ultra-thin carbon films to be a photocatalyst for hydrogen evolution. The carbide has been utilized widely as anode materials for Li ion batteries (74-76). In addition to being a conventional electrocatalyst, molybdenum carbide has been designed to be a nanocarrier for an electrochemical reporting probe (thionin) for label-free immunosensing of α -fetoprotein (77). Cho *et al.* (78) developed solid-state gas sensors using the carbide and found them to possess high sensitivity for ammonia and nitrogen dioxide detection, high electrical conductivity and good corrosion resistance.

Despite its vast applications in electrochemical systems there is no comprehensive study regarding the chemistries and stabilities of various phases of molybdenum carbides under different conditions such as pH and potential. Current studies often contain incorrectly analyzed characterization results and little or no fundamental theoretical analyses to back their experimental results. This leads to use of synthesis processes with oxygen, nitrogen and carbon impurities, confusion regarding the phase of carbide synthesized and further formation of contaminants such as surface oxides that negatively impact electrocatalytic activity. There have been mentions of oxide formation under positive potentials in literature. Weigert *et al.* comment on the stability

regions of Mo_2C and its irreversible oxidation at potentials greater than 0.4 V (RHE) shown in Figure 1-34 (64).

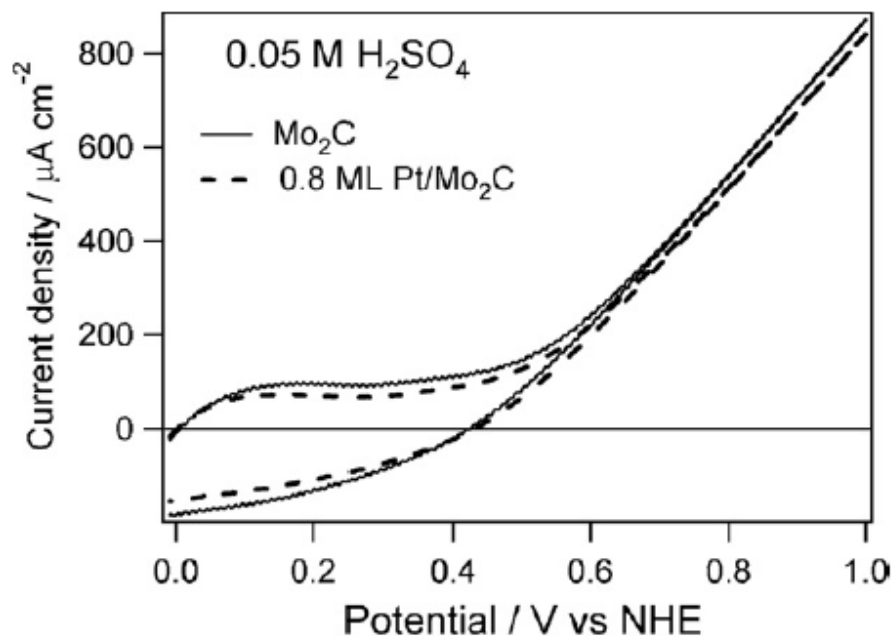


Figure 1-34. Cyclic voltammetry curves of Mo_2C and $\text{Pt}/\text{Mo}_2\text{C}$ surfaces reported by Weigert *et al.* (64).

Hassan *et al.* have also observed an oxidation peak at positive potentials in the voltammetric profiles of the Mo-based electrocatalysts and attribute it to oxidation of Mo^{+4} into Mo^{+6} (Figure 1-35) (65).

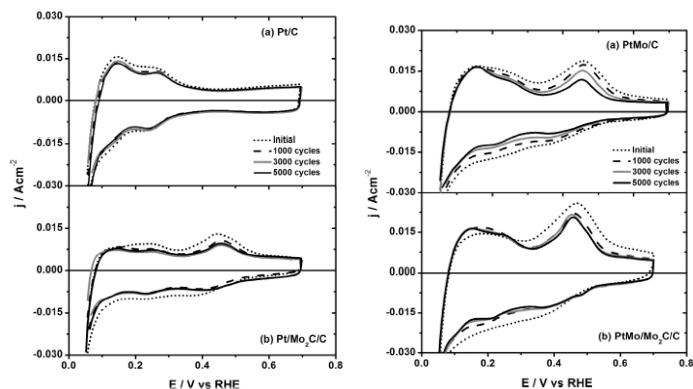


Figure 1-35. Cyclic Voltammetry curves for Pt/C and molybdenum-based materials showing an oxidation peak at 0.45 V (vs RHE) in figures corresponding to Pt/Mo₂C/C, Pt/Mo/C and PtMo/Mo₂C/C.

Valk *et al.* document the oxidation peaks of Mo₂C at potentials of -0.1 V and -0.3 V vs MSE and mention that they are probably caused by the redox equilibria between various molybdenum compounds (Figure 1-36) (66). Gomez-Marin *et al.* clearly state that while carrying out oxygen reduction on molybdenum carbides, the catalyst is oxidized at potentials higher than 0.5 V (RHE) (29). They also observe that improved catalyst performances of Pt supported on molybdenum carbides should be attributed to a favorable interaction between Pt and Mo_xO_y species. Xing *et al.* also observed the formation of surface oxides in their electrocatalyst comprising of Mo₂C a carbon matrix and stipulated that the Mo-oxides play a vital role in the OER process (62). Saha *et al.* observed a peak near 0.47 V in CV profiles of a Pt/Mo₂C catalyst, which they attribute to likely molybdenum oxide species (67) as shown in Figure 1-37.

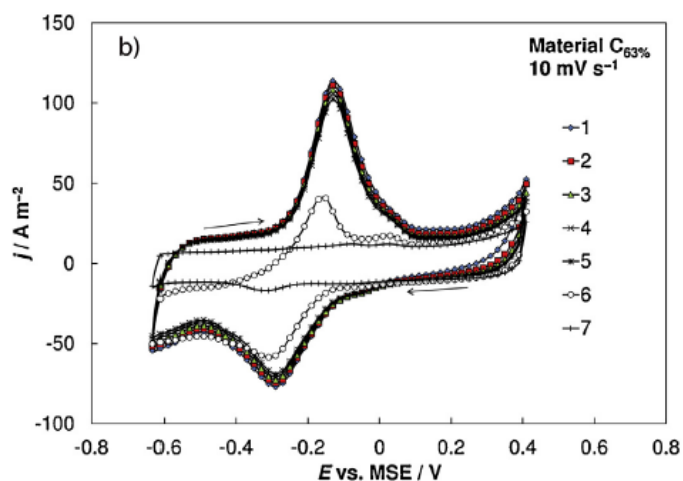


Figure 1-36. Cyclic voltammetry curves for molybdenum-based materials synthesized by Valk *et al.* (66)

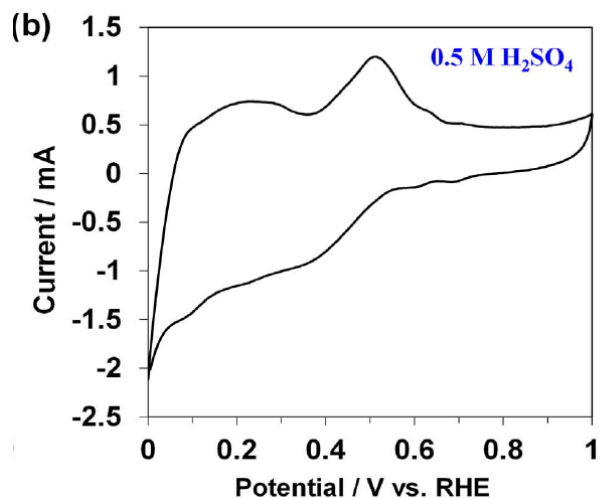


Figure 1-37. Irreversible peak observed at 0.47 V (vs RHE) in the cyclic voltammetry of molybdenum-based materials reported by Saha *et al.* (66)

A fundamental study by Weidman *et al.* examined Pourbaix diagrams of various transition metal carbides (including that of molybdenum) and established regions of immunity, passivation and surface oxidation as shown in Figures 1-38 and 1-39 (68). However, information contradictory to that reported by Weidman *et al.* is reported in (87-91). It is also worthwhile to note that while some research has been done on experimental and theoretical fronts to explore molybdenum carbides as electrochemical catalysts and supports, almost all of these studies revolve only around the hexagonal Mo₂C phase.

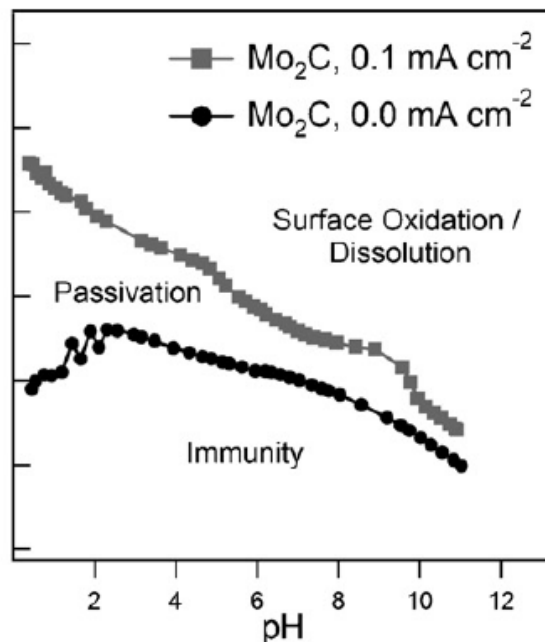


Figure 1-38. Stability mapping of Mo₂C obtained by CP titration experiments carried out by Weidman *et al.* (68)

Reaction No.	Type	Electrode	Overall reaction	(ν_{H^+}/n)	$d(E)/d(\text{pH})$ [mV/pH unit ⁻¹]
1	i	W	$\text{W} + 3\text{H}_2\text{O} \rightarrow \text{WO}_3(\text{s}) + 6\text{H}^+ + 6\text{e}^-$	1.00	-59.1
2	i		$\text{W} + 2\text{H}_2\text{O} \rightarrow \text{WO}_2(\text{s}) + 4\text{H}^+ + 4\text{e}^-$	1.00	-59.1
3	ii		$\text{W} + 4\text{H}_2\text{O} \rightarrow \text{WO}_4^{2-}(\text{aq}) + 8\text{H}^+ + 6\text{e}^-$	1.33	-78.8
4	i	WC	$\text{WC} + 5\text{H}_2\text{O} \rightarrow \text{WO}_3 + \text{CO}_2 + 10\text{H}^+ + 10\text{e}^-$	1.00	-59.1
5	i		$\text{WC} + 4\text{H}_2\text{O} \rightarrow \text{WO}_2(\text{s}) + \text{CO}_2 + 8\text{H}^+ + 8\text{e}^-$	1.00	-59.1
6	ii		$\text{WC} + 14\text{OH}^- \rightarrow \text{WO}_4^{2-} + \text{CO}_3^{2-} + 7\text{H}_2\text{O} + 10\text{e}^-$	1.40	-82.7
7	i	W ₂ C	$\text{W}_2\text{C} + 8\text{H}_2\text{O} \rightarrow 2\text{WO}_3 + \text{CO}_2 + 16\text{H}^+ + 16\text{e}^-$	1.00	-59.1
8	i		$\text{WC} + 4\text{H}_2\text{O} \rightarrow \text{WO}_2(\text{s}) + \text{CO}_2 + 8\text{H}^+ + 8\text{e}^-$	1.00	-59.1
9	ii		$\text{W}_2\text{C} + 22\text{OH}^- \rightarrow 2\text{WO}_4^{2-} + \text{CO}_3^{2-} + 11\text{H}_2\text{O} + 16\text{e}^-$	1.38	-81.3
10	iii	W, WC, or W ₂ C	$\text{WO}_3(\text{s}) + \text{OH}^- \rightarrow \text{WO}_4^{2-} + \text{H}^+$	∞	$-\infty$
11	i		$\text{WO}_2(\text{s}) + \text{H}_2\text{O} \rightarrow \text{WO}_3(\text{s}) + 2\text{H}^+ + 2\text{e}^-$	1.00	-59.1
12	ii		$\text{WO}_2(\text{s}) + 2\text{H}_2\text{O} \rightarrow \text{WO}_4^{2-}(\text{aq}) + 4\text{H}^+ + 2\text{e}^-$	2.00	-118.2
13	i	Mo ₂ C	$\text{Mo}_2\text{C} + 8\text{H}_2\text{O} \rightarrow 2\text{MoO}_3(\text{s}) + \text{CO}_2 + 16\text{H}^+ + 16\text{e}^-$	1.00	-59.1
14	iv		$\text{Mo}_2\text{C} \rightarrow 2\text{Mo}^{3+} + \text{CO}_2 + 6\text{e}^-$	0.00	0.0
15	i		$\text{Mo}_2\text{C} + 6\text{H}_2\text{O} \rightarrow \text{MoO}_2(\text{s}) + \text{CO}_2 + 12\text{H}^+ + 12\text{e}^-$	1.00	-59.1
16	ii		$\text{Mo}_2\text{C} + 10\text{H}_2\text{O} \rightarrow 2\text{MoO}_4^{2-}(\text{aq}) + \text{CO}_2 + 20\text{H}^+ + 16\text{e}^-$	1.25	-73.9
17	iii		$\text{MoO}_3(\text{s}) + \text{OH}^- \rightarrow \text{MoO}_4^{2-}(\text{aq}) + \text{H}^+$	∞	$-\infty$
18	ii		$\text{MoO}_2(\text{s}) + 2\text{H}_2\text{O} \rightarrow \text{MoO}_4^{2-}(\text{aq}) + 4\text{H}^+ + 2\text{e}^-$	2.00	-118.2

Figure 1-39. Possible reactions involved in the corrosion of transition metal carbides reported by Weidman *et al.* (68)

Therefore, substantial work has been done to understand the stability and activity of the hexagonal phase of molybdenum carbide, Mo₂C (59, 64, 68), however there is very little to no information regarding the cubic phase of MoC.

1.7 A Note about Heterogeneous Catalytic Activity: Ammonia Synthesis

Molybdenum has been shown to be active towards ammonia synthesis in a variety of studies as established in (70, 71, 72). However, these are different variations of molybdenum from the carbide form. For instance, in (70) Jacobsen establishes a novel class of ammonia synthesis catalysts composed of combinations of Fe, Mo, Co and N and concluded that the promotion of $\text{Co}_3\text{Mo}_3\text{N}$ with caesium shows higher catalytic activity than any commercial iron-based catalyst. Similarly, in (71), Arashiba *et al.* show that a dimolybdenum dinitrogen complex can carry out ammonia synthesis under ambient reaction conditions thereby providing a method to fix nitrogen under mild conditions. Similarly, Yandulov *et al.* (72) introduce a molybdenum catalyst containing tetradentate triamidoamine ligands that can reduce nitrogen to ammonia at room temperature and 1 atmosphere. Kojima *et al.* (18) utilize molybdenum carbide as catalysts to carry out synthesis of ammonia. They found that that the hexagonal Mo_2C is most active towards ammonia synthesis followed by cubic Mo_2N . Cubic MoC was found to be unstable when exposed to reactant gases. The addition of caesium improved the activities of the cubic nitride and carbide.

1.8 Summary and Objectives

This chapter establishes the state of current literature surrounding the chemistry, synthesis and application of molybdenum carbide. As evidenced by the various reports reviewed in this chapter, there are contradictory reports regarding the phases and structure of molybdenum carbides. There have been reports of cubic, hexagonal and orthorhombic structures of varying stoichiometries. Moreover, crystal structures are often misidentified, and this is a result of poor characterization techniques and data analysis. The synthesis of molybdenum carbides is in a state of disarray in literature. There are very few reports that truly synthesize the cubic phase of the carbide and even fewer who correctly recognize the phase once synthesized. A majority of the synthesis processes

use molybdenum oxide as the precursor which often leads to the formation of oxycarbides especially since oxygen occupies the same vacancies in fcc lattice as carbon, which makes oxycarbides isostructural to carbide. This combined with the absence of whole profile fitting of XRD patterns, among other incorrectly analyzed characterization data, is the reason for the contradictory reports in literature. The Lee *et al.* method published in the 80s was a breakthrough in the synthesis of molybdenum carbides. The study carefully separated the phases of molybdenum carbide into a cubic ‘MoC’ phase and a hexagonal ‘Mo₂C’ phase. The authors established scientifically sound protocols to synthesize both phases, characterized them thoroughly and also, carried out thermochemical modeling to limit the formation of polymeric carbon. This method has been recycled since then with few changes made to the synthesis protocols usually without any scientific reason. As a result, there is an imminent need for the following:

- Correct recognition of the different phases of molybdenum carbide and establishing their crystal structures.
- Thermochemical modeling of the molybdenum carbon system accounting for the documented phases.
- Development of synthesis processes to produce single carbide phase of the material and careful characterization of the same to ensure that the right phase has been synthesized.
- Understanding the stability of molybdenum carbides under reaction conditions before application as an electrocatalyst.

The subsequent chapters describe attempts made to answer at least parts of the above questions and fill the gaps in the literature. The objectives of this study are as follows:

- ✓ Thermochemical modelling of Mo-C-H system
- ✓ Synthesis of different types of molybdenum carbide with differing properties.

- ✓ Detailed characterization studies to understand and discern different carbide materials.
- ✓ Exploration of the stability and activity of molybdenum carbide as an electrocatalyst

REFERENCES

1. Levy RB, Boudart M. Platinum-Like Behavior of Tungsten Carbide in Surface Catalysis. *Science*. 1973;181(4409):547-9.
2. Oyama ST. Preparation and catalytic properties of transition metal carbides and nitrides *Catalysis Today*. 1992.
3. Oyama ST. *The chemistry of transition metal carbides and nitrides*. Glasgow, UK: Blackie Academic and Professional; 1996.
4. Tang C, Sun A, Xu Y, Wu Z, Wang D. High specific surface area Mo₂C nanoparticles as an efficient electrocatalyst for hydrogen evolution. *Journal of Power Sources*. 2015;296:18-22.
5. He C, Tao J. Synthesis of nanostructured clean surface molybdenum carbides on graphene sheets as efficient and stable hydrogen evolution reaction catalysts. *Chemical communications*. 2015;51(39):8323-5.
6. Sarno M, Cirillo C, Ponticorvo E, Ciambelli P. Synthesis and Characterization of Mo₂C/MoO₃ Nanohybrid as Electrocatalyst for Hydrogen Evolution Reaction. *Chemical Engineering Transactions*. 2015;43:943-8.
7. Posada-Perez S, Ramirez PJ, Evans J, Vines F, Liu P, Illas F, et al. Highly Active Au/delta-MoC and Cu/delta-MoC Catalysts for the Conversion of CO₂: The Metal/C Ratio as a Key Factor Defining Activity, Selectivity, and Stability. *Journal of the American Chemical Society*. 2016;138(26):8269-78.
8. Ledoux MJ, Huu CP, Guille J, Dunlop H. Compared activities of platinum and high specific surface area Mo₂C and WC catalysts for reforming reactions. I. Catalyst

- Activation and Stabilization: Reaction of n-Hexane. *Journal of Catalysis*. 1992;134:383-98.
9. David Farrusseng Metal-Organic Frameworks: Applications from Catalysis to Gas Storage
 10. Patel M, Subrahmanyam J. Synthesis of nanocrystalline molybdenum carbide (Mo₂C) by solution route. *Materials Research Bulletin*. 2008;43(8-9):2036-41.
 11. Wan C, Regmi YN, Leonard BM. Multiple phases of molybdenum carbide as electrocatalysts for the hydrogen evolution reaction. *Angewandte Chemie*. 2014;53(25):6407-10.
 12. Toth LE. *Transition Metal Carbides and Nitrides*. New York: Academic Press; 1971.
 13. Lee JS, Oyama ST, Boudart M. Molybdenum Carbide Catalysts I. Synthesis of Unsupported Powders. *Journal of Catalysis*. 1987;106:125-33.
 14. Lee JS, Volpe L, Ribeiro FH, Boudart M. Molybdenum carbide catalysts. II. Topotactic synthesis of unsupported powders *Journal of Catalysis*. 1988;112:44-53.
 15. Leclercq L, Imura K, Yoshida S, Barbee T, Boudart M. Synthesis of new catalytic materials: metal carbides of the group VI B elements. In: Delmon B, Grange P, Jacobs PA, Poncelet G, editors. *Preparation of Catalysts II*. Amsterdam: Elsevier; 1978.
 16. Storms EK. *The Refractory Carbides*. New York and London: Academic Press; 1967.
 17. Choi J-G, Curl RL, Thompson LT. Molybdenum Nitride Catalysts: I. Influence of the Synthesis Factors on Structural Properties. *Journal of Catalysis*. 1994;146:218-27.
 18. Kojima R, Aika K-i. Molybdenum nitride and carbide catalysts for ammonia synthesis. *Applied Catalysis A: General*. 2001;219(1-2):141-7.

19. Zheng W, Cotter TP, Kaghazchi P, Jacob T, Frank B, Schlichte K, et al. Experimental and theoretical investigation of molybdenum carbide and nitride as catalysts for ammonia decomposition. *Journal of the American Chemical Society*. 2013;135(9):3458-64.
20. Espinoza M, Cruz-Reyes J, Del Valle-Granados M, Flores-Aquino E, Avalos-Borja M, Fuentes-Moyado S. Synthesis, Characterization and Catalytic Activity in the Hydrogenation of Cyclohexene with Molybdenum Carbide. *Catalysis Letters*. 2007;120(1-2):137-42.
21. Oshikawa K, Nagai M, Omi S. Characterization of Molybdenum Carbides for Methane Reforming by TPR, XRD, and XPS. *The Journal of Physical Chemistry B*. 2001;105(38):9124-31.
22. Mo T, Xu J, Yang Y, Li Y. Effect of carburization protocols on molybdenum carbide synthesis and study on its performance in CO hydrogenation. *Catalysis Today*. 2016;261:101-15.
23. Wang X-H, Hao H-L, Zhang M-H, Li W, Tao K-Y. Synthesis and characterization of molybdenum carbides using propane as carbon source. *Journal of Solid State Chemistry*. 2006;179(2):538-43.
24. Xiao T-c, York APE, Williams VC, Al-Megren H, Hanif A, Zhou X-y, et al. Preparation of molybdenum carbides using butane and their catalytic performance. *Chem Mater*. 2000;12:3896-905.
25. Xiao T, Wang H, Da J, Coleman K, Green M. Study of the Preparation and Catalytic Performance of Molybdenum Carbide Catalysts Prepared with CH/H Carburizing Mixture. *Journal of Catalysis*. 2002;211(1):183-91.

26. York APE, J.B. C, Williams VC, A.J B, Sloan J, Hanif A, et al. Synthesis of high surface area transition metal carbide catalysts. In: A. C, F.V. M, Mendioroz S, Fierro JLG, editors. *Studies in Surface Science and Catalysis*. 130: Elsevier Science B.V; 2000.
27. Hanif A, Xiao T, York APE, Sloan J, Green MLH. Study on the Structure and Formation Mechanism of Molybdenum Carbides. *Chemistry of Materials*. 2002;14(3):1009-15.
28. Hyeon T, Fang M, Suslick KS. Nanostructured Molybdenum Carbide: Sonochemical Synthesis and Catalytic Properties. *Journal of the American Chemical Society*. 1996;118(23):5492-3.
29. Gómez-Marín AM, Ticianelli EA. Analysis of the electrocatalytic activity of α -molybdenum carbide thin porous electrodes toward the hydrogen evolution reaction. *Electrochimica Acta*. 2016;220:363-72.
30. Wang H, Wang A, Wang X, Zhang T. One-pot synthesized MoC imbedded in ordered mesoporous carbon as a catalyst for N₂H₄ decomposition. *Chemical communications*. 2008(22):2565-7.
31. He C, Tao J. Exploration of the electrochemical mechanism of ultrasmall multiple phases molybdenum carbides nanocrystals for hydrogen evolution reaction. *RSC Advances*. 2016;6(11):9240-6.
32. Wu HB, Xia BY, Yu L, Yu XY, Lou XW. Porous molybdenum carbide nano-octahedrons synthesized via confined carburization in metal-organic frameworks for efficient hydrogen production. *Nature communications*. 2015;6:6512.
33. Chen WF, Wang CH, Sasaki K, Marinkovic N, Xu W, Muckerman JT, et al. Highly active and durable nanostructured molybdenum carbide electrocatalysts for hydrogen production. *Energy & Environmental Science*. 2013;6(3).

34. Pan LF, Li YH, Yang S, Liu PF, Yu MQ, Yang HG. Molybdenum carbide stabilized on graphene with high electrocatalytic activity for hydrogen evolution reaction. *Chemical communications*. 2014;50(86):13135-7.
35. Liao L, Wang S, Xiao J, Bian X, Zhang Y, Scanlon MD, et al. A nanoporous molybdenum carbide nanowire as an electrocatalyst for hydrogen evolution reaction. *Energy Environ Sci*. 2014;7(1):387-92.
36. Wan C, Knight NA, Leonard BM. Crystal structure and morphology control of molybdenum carbide nanomaterials synthesized from an amine-metal oxide composite. *Chemical communications*. 2013;49(88):10409-11.
37. Guil-López R, Martínez-Huerta MV, Guillén-Villafuerte O, Peña MA, Fierro JLG, Pastor E. Highly dispersed molybdenum carbide as non-noble electrocatalyst for PEM fuel cells: Performance for CO electrooxidation. *International Journal of Hydrogen Energy*. 2010;35(15):7881-8.
38. Elbaz L, Phillips J, Artyushkova K, More K, Brosha EL. Evidence of High Electrocatalytic Activity of Molybdenum Carbide Supported Platinum Nanorrafts. *Journal of The Electrochemical Society*. 2015;162(9):H681-H5.
39. Volpe. Compounds of molybdenum and tungsten with high specific surface area. I. Nitrides. *Journal of Solid State Chemistry* 59, 332-347 (1985).
40. Bouchy C, Hamid SBD, Derouane EG. A new route to the metastable FCC molybdenum carbide $\alpha\text{-MoC}_{1-x}$ *Chem. Commun.*, 2000, 125–126
41. Bouchy C, Pham-huu C, Ledoux MJ. On the role of hydrogen during the reduction–carburation of MoO_3 into molybdenum oxycarbide. *Journal of Molecular Catalysis A: Chemical* 162 2000. 317–334.

42. Huttig et al. Powder Met. Bull. 5, 307 (1950)
43. Lu J, Hugosson H, Eriksson O, Nordstrom L, Jansson U. Chemical vapour deposition of molybdenum carbides: aspects of phase stability. Thin Solid Films.,2000, 370 203-212
44. Chen JG. Carbide and Nitride Overlayers on Early Transition Metal Surfaces: Preparation, Characterization, and Reactivities. Chem. Rev. 1996, 96, 1477-1498
45. Posada Perez S, Vines F, Ramirez PJ, Vidal AB, Rodriguez JA, Illas F. The bending machine: CO₂ activation and hydrogenation on d-MoC(001) and b-Mo₂C(001) surfaces. Phys. Chem. Chem. Phys., 2014, 16, 14912-14921
46. Liu P, Rodriguez J, Asakura T, Gomes J, Nakamura K. Desulfurization Reactions on Ni₂P(001) and r-Mo₂C(001) Surfaces: Complex Role of P and C Sites. J. Phys. Chem. B 2005, 109, 4575-4583
47. Sullivan M, Held JT, Bhan A. Structure and site evolution of molybdenum carbide catalysts upon exposure to oxygen. Journal of Catalysis 326 (2015) 82–91
48. Guzman HJ, Xu W, Stacchiola D, Vitale G, Scott CE, Rodriguez JA, Pereira-Almao P. In situ time-resolved X-ray diffraction study of the synthesis of Mo₂C with different carburization agents. Can. J. Chem. 91: 573–582 (2013)
49. Hugosson HW, Jansson U, Johansson B, Eriksson O. Phase stability diagrams of transition metal carbides, a theoretical study. Chemical Physics Letters 333 (2001) 444-450
50. Gu Y, Li Z, Chen L, Ying Y, Qian Y. Synthesis of nanocrystalline Mo₂C via sodium co-reduction of MoCl₅ and CBr₄ in benzene. Materials Research Bulletin 38 (2003) 1119–1122.
51. Hugosson HW, Eriksson O, Jansson U, Borje J. Phase stabilities and homogeneity ranges in 4d-transition-metal carbides: A theoretical study. Physical Review B, 63, 134108 (2001).

52. Jujjuri S, Cardenas-Lizana F, Keane MA. Synthesis of group VI carbides and nitrides: application in catalytic hydrodechlorination. *J Mater Sci* (2014) 49:5406–5417
53. Lin H, Shi Z, He S, Yu X, Wang S, Gao Q, Tang Y. Heteronanowires of MoC–Mo₂C as efficient electrocatalysts for hydrogen evolution reaction. *Chem. Sci.*, 2016, 7, 3399–3405
54. Mah (1963) Bureau of Mines (Reports of Investigation)
55. Kouvetdkis J, Brewer L. Temperature stability range of the binary MoC phase. *J Phase Equilibria*. 1992;13(6):601–4.
56. Shatynski. The Thermochemistry of Transition Metal Carbides. *Oxidation of Metals*, Vol. 13, No. 2, 1979
57. Browning LC and Emmett PH. Equilibrium Measurements in Molybdenum-Carbon-Hydrogen System. *J Am. Ceramic Society*, 1952, 74, 4773-4.
58. Oosawa Y. Photocatalytic hydrogen evolution from an aqueous methanol solution over ceramics-electrocatalyst/TiO₂. *CHEMISTRY LETTERS*, pp. 577-580, 1983.
59. Esposito D V, Hunt ST, Kimmel YC, Chen JG. A New Class of Electrocatalysts for Hydrogen Production from Water Electrolysis : Metal Monolayers Supported on Low-Cost Transition Metal Carbides. 2012;
60. Xiong J, Li J, Shi J, Zhang X, Suen N, Liu Z, et al. In Situ Engineering of Double-Phase Interface in Mo/Mo₂C Heteronanosheets for Boosted Hydrogen Evolution Reaction. 2018;3:341–8.
61. Lin H, Shi Z, He S, Yu X, Wang S. Heteronanowires of MoC – Mo₂C as efficient electrocatalysts for hydrogen evolution reaction. 2016;7:3399–405.

62. Xing J, Li Y, Guo S, Jin T, Li H, Wang Y, et al. Molybdenum carbide in-situ embedded into carbon nanosheets as efficient bifunctional electrocatalysts for overall water splitting. 2019;298:305–12.
63. Yan Z, Zhang M, Xie J, Zhu J, Kang P. A bimetallic carbide Fe₂MoC promoted Pd electrocatalyst with performance superior to Pt / C towards the oxygen reduction reaction in acidic media. 2015;165:636–41.
64. Weigert EC, Esposito D V, Chen JG. Cyclic voltammetry and X-ray photoelectron spectroscopy studies of electrochemical stability of clean and Pt-modified tungsten and molybdenum carbide (WC and Mo₂C) electrocatalysts. 2009;193:501–6.
65. Hassan A, Antonio V, Carreras A, Antonio E. Molybdenum carbide based electrocatalysts for CO tolerance in proton exchange membrane fuel cell anodes. *Electrochimica Acta* 2014;142:307–16.
66. Valk P, Nerut J, Tallo I, Tee E, Vaarmets K, Romann T, et al. Structure and stability of partially chlorinated molybdenum carbide composite materials synthesised via high temperature chlorination. *Electrochimica Acta* 2016;191:337–45.
67. Saha S, Rodas JAC, Tan S, Li D. Performance evaluation of platinum-molybdenum carbide nanocatalysts with ultralow platinum loading on anode and cathode catalyst layers of proton exchange membrane fuel cells. *Journal of Power Sources*, 2018, 378, 742-749.
68. Weidman MC, Esposito D V, Hsu Y, Chen JG. Comparison of electrochemical stability of transition metal carbides (WC , W₂C , Mo₂C) over a wide pH range. *Journal of Power Sources*. 2012;202:11–7.
69. E. Parthé, V. Sadagopan. The structure of dimolybdenum carbide by neutron diffraction technique. *Acta Crystallogr.*1963, 16, 202.

70. Jacobsen CJH. Novel class of ammonia synthesis catalysts. *Chem. Commun.*, 2000, 1057–1058
71. Arashiba K, Miyake Y, Nishibayashi Y. A molybdenum complex bearing PNP-type pincer ligands leads to the catalytic reduction of dinitrogen into ammonia. *Nature Chemistry*, 2011, 3, pages 120–125
72. Yandulov DV, Schrock RR. Catalytic Reduction of Dinitrogen to Ammonia at a Single Molybdenum Center. *Science*, 2003, Vol 301.
73. Gao F, Zhao Y, Zhang L, Wang B, Wang Y, Huang X, Wang K, Feng W, Liu P. Well dispersed MoC quantum dots in ultrathin carbon films as efficient co-catalysts for photocatalytic H₂ evolution. *J. Mater. Chem. A*, 2018, 6, 18979–18986
74. Wang B, Wang G, Wang H. Hybrids of Mo₂C nanoparticles anchored on graphene sheets as anode materials for high performance lithium-ion batteries. *J. Mater. Chem. A*, 2015, 3, 17403–17411
75. Chen J, Huang Y, Zhao F, Ye F, Wang Y, Zhou J, Liu Y, Li Y. A hierarchical a-MoC_{1-x} hybrid nanostructure for lithium-ion storage. *J. Mater. Chem. A*, 2017, 5, 8125–8132
76. Yu H, Fan H, Wang J, Zheng Y, Dai Z, Lu Y, Kong J, Wang X, Kim YJ, Yan Q, Lee J. 3D ordered porous Mo_xC (x = 1 or 2) for advanced hydrogen evolution and Li storage. *Nanoscale*, 2017, 9, 7260–7267
77. Zhai Q, Zhang X, Li J, Wang E. Molybdenum carbide nanotubes: a novel multifunctional material for label-free electrochemical immunosensing. *Nanoscale*, 2016, 8, 15303–15308
78. Cho S, Kim JY, Kwon O, Kim J, Tung H. Molybdenum carbide chemical sensors with ultrahigh signal-to-noise ratios and ambient stability. *J. Mater. Chem. A*, 2018, 6, 23408–23416

79. Anjum M, Lee M, Lee J, BCN network-encapsulated multiple phases of molybdenum carbide for efficient hydrogen evolution reactions in acidic and alkaline media. *J. Mater. Chem. A*, 2017, 5, 13122–13129
80. Tang C, Zhang H, Xu K, Zhang Q, Liu J, He C, Fan L, Asefa T. Unconventional molybdenum carbide phases with high electrocatalytic activity for hydrogen evolution reaction. *J. Mater. Chem. A*, 2019, 7, 18030–18038
81. Li Z, Chen C, Zhan E, Ta N, Li Y, Shen W. Crystal-phase control of molybdenum carbide nanobelts for dehydrogenation of benzyl alcohol. *Chem. Commun.*, 2014, 50, 4469--4471
82. Li Z, Li Y, Zhan E, Ta N, Shen W. Morphology-controlled synthesis of α -MoO₃ nanomaterials for ethanol oxidation. *J. Mater. Chem. A*, 2013, 1, 15370
83. Zhang K, Zhao Y, Fu D, Chen Y. Molybdenum carbide nanocrystal embedded Ndoped carbon nanotubes as electrocatalysts for hydrogen generation. *J. Mater. Chem. A*, 2015, 3, 5783–5788
84. Fan M, Chen H, Wu Y, Feng L, Liu Y, Li G, Zou X. Growth of molybdenum carbide micro-islands on carbon cloth toward binder-free cathodes for efficient hydrogen evolution reaction. *J. Mater. Chem. A*, 2015, 3, 16320–16326
85. Koizumi R, Ozden S, Samanta A, Alves APP, Mishra A, Ye G, Silva GG, Vatjai R, Singh AK, Tiwari CS, Ajayan PM. Origami-Inspired 3D Interconnected Molybdenum Carbide Nanoflakes. *Adv. Mater. Interfaces*, 2018, 5,
86. Shi H, Sun Z, Lv W, Wang S, Shi Y, Zhang Y, Xiao S, Yang H, Yang Q, Li F. Necklace-like MoC sulfiphilic sites embedded in interconnected carbon networks for Li–S batteries with high sulfur loading. *J. Mater. Chem. A*, 2019, 7, 11298–11304

87. Luo et al. In situ preparation of hollow Mo₂C–C hybrid microspheres as bifunctional electrocatalysts for oxygen reduction and evolution reactions. *J. Mater. Chem. A*, 2016, 4, 12583–12590
88. Qamar et al. Metal–organic framework-guided growth of Mo₂C embedded in mesoporous carbon as a high performance and stable electrocatalyst for the hydrogen evolution reaction. *J. Mater. Chem. A*, 2016, 4, 16225–16232
89. Ji et al. In situ O₂-emission assisted synthesis of molybdenum carbide nanomaterials as an efficient electrocatalyst for hydrogen production in both acidic and alkaline media. *J. Mater. Chem. A*, 2017, 5, 5178–5186
90. Guo et al. Controllable synthesis of molybdenum-based electrocatalysts for a hydrogen evolution reaction. *J. Mater. Chem. A*, 2017, 5, 4879–4885
91. Ma et al. Efficient hydrogen evolution reaction catalyzed by molybdenum carbide and molybdenum nitride nanocatalysts synthesized via the urea glass route. *J. Mater. Chem. A*, 2015, 3, 8361–8368
92. Alhajri NS, Anjum DH, Takanabe K. Molybdenum carbide–carbon nanocomposites synthesized from a reactive template for electrochemical hydrogen evolution. *J. Mater. Chem. A*, 2014, 2, 10548–10556
93. Wang Z, Zhang Z, Zhang M. The efficient synthesis of a molybdenum carbide catalyst via H₂-thermal treatment of a Mo(VI)–hexamethylenetetramine complex. *Dalton Trans.*, 2011, 40, 1098
94. Wang et al. Synthesis of Bulk and Supported Molybdenum Carbide by a Single-Step Thermal Carburization Method. *Chem. Mater.* 2007, 19, 1801-1807

95. Huo et al. One-step synthesis of bulk Mo and Ni–Mo carbides for methanation. *RSC Adv.*, 2016, 6, 24353–24360
96. Zhao et al. A novel approach to the synthesis of bulk and supported b-Mo₂C using dimethyl ether as a carbon source. *New J. Chem.*, 2015, 39, 4901--4908
97. Gao et al. Simple and large-scale synthesis of β -phase molybdenum carbides as highly stable catalysts for dry reforming of methane. *Inorg. Chem. Front.*, 2018, 5, 90–99
98. Nartowski et al. Solid state metathesis: synthesis of metal carbides from metal oxides. *J. Mater. Chem.*, 2001, 11, 3116–3119
99. Vengust D et al. Molybdenum carbide nanowires: facile synthesis, a new hybrid phase and their use as transparent electrodes. *RSC Adv.*, 2016, 6, 90806–90812
100. Bilecka I, Niederberger M. Microwave chemistry for inorganic nanomaterials synthesis. *Nanoscale*, 2010, 2, 1358–1374
101. Vallance SR, Kingman S, Gregory DH. Ultra-rapid processing of refractory carbides; 20 s synthesis of molybdenum carbide, Mo₂C.
102. Lv et al. Ultrafast synthesis of molybdenum carbide nanoparticles for efficient hydrogen generation. *J. Mater. Chem. A*, 2017, 5, 22805–22812
103. Kumar et al. Nano-structured hybrid molybdenum carbides/ nitrides generated in situ for HER applications. *J. Mater. Chem. A*, 2017, 5, 7764–7768
104. Turner J. Sustainable Hydrogen Evolution. *Science*, 2004, 305, 972
105. Kong D, Cha J, Wang H, Lee H and Cui Y. First-row transition metal dichalcogenide catalysts for hydrogen evolution reaction. : *Energy Environ. Sci.*, 2013, 6, 3553.

106. Xiao P, Sk MA, Thia L, Ge X, Lim R J, Wang J, Lim KH and Wang X.
Molybdenum phosphide as an efficient electrocatalyst for the hydrogen evolution reaction.
Energy Environ. Sci., 2014, 7, 2624-2629.

Chapter 2

2.1 Thermodynamic calculations

Theoretical thermochemical modeling using Ellingham and Gas Phase Equilibrium diagrams has been done in Chapter 3. The following fundamental equations were used to calculate the thermodynamic parameters, enthalpy, entropy and free energy of reactions:

$$\Delta H_T^\circ = \Delta H_{298K}^\circ + \int_{298K}^T \Delta C_p dT \quad (1)$$

$$\Delta S_T^\circ = \Delta S_{298K}^\circ + \int_{298K}^T \frac{\Delta C_p}{T} dT \quad (2)$$

$$\Delta G^\circ = \Delta H^\circ - T\Delta S^\circ \quad (3)$$

$$\Delta G_T = \Delta G_T^\circ + RT \ln K \quad (4)$$

Where ΔH is the enthalpy, ΔS is the entropy, ΔC_p is the change in heat capacity in the reaction, ΔG is the Gibbs free energy of formation/reaction, R is the molar gas constant, T is the temperature, and K is the thermodynamic equilibrium constant.

Free energy of reactions can therefore be related to temperature and partial pressures of gases.

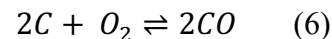
These relationships at relevant temperatures and pressures were plotted using MATLAB programming.

Two types of thermodynamic studies were done in Chapter 3: Ellingham and gas phase equilibrium figures. The theory behind both is explained here.

2.1.1 Ellingham Diagrams

Ellingham diagrams show the thermodynamic stability of various compounds such as oxides, chlorides and sulfides with respect to temperature and partial pressure of gases in the system. These diagrams are constructed by analyzing the Gibbs free energy of formation of the materials in the

multicomponent system under study. The free energy of the reaction is a measure of the thermodynamic driving force for the reaction to take place. Equation (3) shows the relationship between the free energy, ΔG , and the enthalpy, ΔH and the entropy, ΔS . An Ellingham diagram is essentially the plot of ΔG vs temperature, T . Since the standard enthalpy and entropy of the reactions are fixed quantities unless there is a phase change (which is not observed in the temperatures under study here as seen in Chapter 3), the plot usually is a straight line with ΔH as the intercept and $-\Delta S$ as the slope. Most Ellingham diagrams in textbooks and literature involve the formation of oxides from different metals as seen in Figure 2-1. In such analyses, the reactions are normalized to consume 1 mol of oxygen and the oxygen partial pressure is taken as 1 atmosphere. Two reactions usually accompany such calculations to understand the reduction of the metallic oxides to form the metal:



Additionally, in multicomponent systems (such as shown in Figure 2-1 and those under study here), these parameters are involved in the analysis:

- a. The temperature is the independent thermodynamic variable, which is varied in the construction of the Ellingham diagram.
- b. The ratio of partial pressures of the gases in the system is taken as the other thermodynamic variable, which may be changed in the analysis.

A three-dimensional diagram can be constructed by varying both temperature and partial pressures of gases and the same can be projected in two-dimensional space.

There are three pieces of key information that can be obtained from Ellingham diagrams:

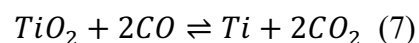
1. Relative ease of reducing oxides to form the metal.

2. Partial pressure of oxygen in equilibrium with the oxide at a given temperature.
3. The ratio of partial pressures of gases involved (CO, CO₂ in this case) in order to reduce the oxide to metal.

For instance, in Figure 2-1, the free energies of reactions involving the formation of oxides are displayed. Hence, the reactions closer to the top of the diagram indicate that the oxides are unstable (higher Gibbs energy of formation for the oxides) and hence can be easily reduced to form the metal. Similarly, metals occupying the bottom of the diagram (such as Ca, Mg and Ti, *etc.*) are more reactive and their oxides are more stable and harder to reduce. The figure also gives information regarding metal's ability to reduce another oxide: the MgO line is below the Al₂O₃ line at temperatures around 800 K implying that the formation of MgO is more favorable than that of Al₂O₃ at a given temperature. Thus, Mg would be able to reduce Al₂O₃ to form Al metal and MgO.

The right side of Figure 2-1 is denoted by P_{O_2} and indicates the partial pressure of oxygen and can show its value when in equilibrium with metal and metal oxide at a particular temperature. For example, at temperatures ~1500 K, the partial pressure of oxygen when in equilibrium with Ti/TiO₂ is $\sim 10^{-18}$. When the oxygen partial pressure is higher than the equilibrium value, it can oxidize the metal and similarly, pressures lower than the equilibrium value implies the oxide will be reduced.

When C is used as the reducing agent there is a minimum ratio of CO/CO₂ required to reduce the oxide to the metal. The reaction under analysis in the case of Ti/TiO₂ is:



If the oxide is harder to reduce, a higher partial pressure of CO will be required to form the metal.

Similar analysis can be done using carbides, which are under study (explained in detail in Chapter 3). The gases under consideration are a hydrocarbon (such as methane, ethylene or acetylene) and hydrogen. The reactions are normalized to 1 mole of carbon and the ratio of partial pressures of hydrocarbon to hydrogen is used to analyze the formation of the carbides, Mo_2C and MoC . More details about the calculations, results, observations and conclusions are explained in Chapter 3.

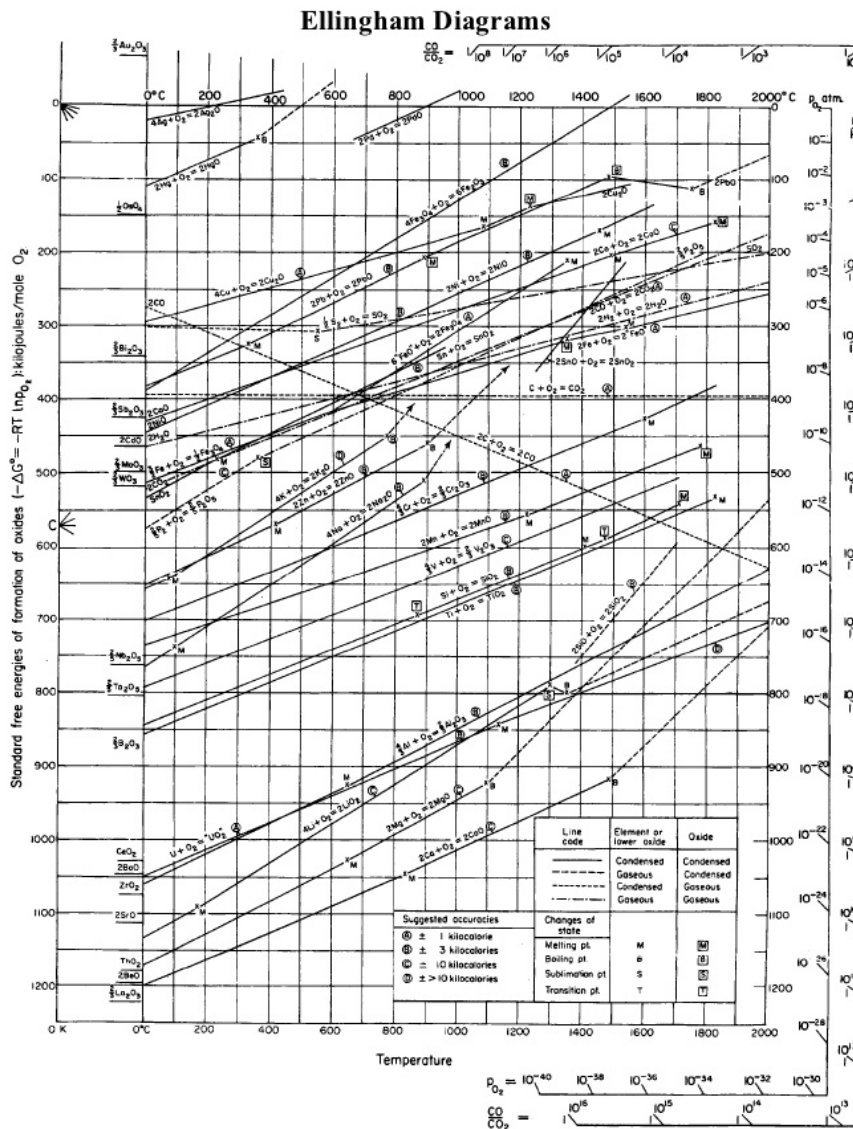


Figure 2-1. An example of Ellingham diagram from (1)

2.1.2 Gas Phase Equilibrium Diagrams

Gas phase equilibrium diagrams or phase diagrams are constructed to provide similar information as the Ellingham diagrams which is the stabilities of various materials in a multicomponent system. However, it is often difficult to deduce experimental parameters of temperature and partial pressures from the Ellingham Diagrams due to the sheer volume of information displayed in one figure. It is also important to note that these figures only provide information regarding the thermodynamic favorability of a certain reaction to occur and do not discuss the kinetics of the reaction. For instance, at lower temperatures, a reaction might be thermodynamically favorable but kinetically slow to occur. Gas phase equilibrium figures are usually constructed at a constant temperature and show the stabilities of various phases/components when the partial pressures/mole fractions are varied.

2.2 Significant Experimental Procedures

2.2.1 Characterization Techniques: X-Ray Diffraction

X-Ray diffraction (XRD) was carried out on samples in a PANalytical Xpert Pro using CuK α radiation and at 40 kV and 40 mA on a zero background holder. The 2θ angular region ranged from 10 to 100° with differing scan rates (as low as 1°/min) and a step size of 0.04°. MDI Jade (version 9) Whole Profile Fitting (WPF) was used to analyze the diffraction patterns. XRD analyses are significant as they shed light on important properties such as phase composition, crystallite sizes, lattice parameters, stress broadening to name a few. Extremely small crystallites (relevant to this study) produce incoherent scattering from edges of the crystal structures. The incoherent scatter can result in broadening of the resultant peak, described by the Scherrer equation:

$$\tau = K \lambda / B_{\tau} \cos\theta$$

Where τ is the mean crystallite size, K is the shape factor (~ 0.9), λ is the wavelength and B_τ is the crystallite size broadening ($B - b$ where B is the width of the diffraction line at half intensity maximum and b is the instrument broadening).

There is plenty of information that can be obtained from diffraction data: lattice parameters (thereby shedding light on presence of interstitial atoms), crystallite size, phase composition, contaminants, etc. This is also a bulk technique, which implies information is received from the scattering of millions of atoms as opposed to electron microscopy where relatively few regions are observed at a time. In this study (especially in Chapter 4), information regarding phase composition and crystallite size is of utmost relevance and significance. Peak positions are used to provide information regarding unit cell lattice parameters; peak shapes are analyzed to understand microstrain in a sample, and peak intensities are used to calculate weight fractions of phases in a sample.

Whole pattern/profile fitting (WPF) is a superior technique to simple peak identification, which is often carried out in literature as seen in Chapter 1. When carrying out WPF, an ideal diffraction pattern is calculated from a model of the sample and is fitted to the experimental pattern. The model is refined till the difference between the fit and the experimental data is minimized. The goodness of the fit is determined by the difference between the two and has been displayed in the plots in Chapter 4. Rietveld refinement technique was utilized for the analysis of diffraction data here. In this technique, the position and intensity of diffraction peaks are calculated from the crystal structure.

Also, as is the norm, pseudo-Voigt function (a combination of Gaussian and Lorentzian components) was used in the WPF analysis as the materials synthesized have a crystallite size < 20 nm.

2.2.2 Characterization Techniques: Surface Area by Gas Adsorption

Surface area is an important parameter to be determined for materials that are being designed for catalytic applications. There are various ways to measure surface area: particle size distribution (from dynamic light scattering), microscopy (shape analysis), small angle X-ray scattering and as is carried out here in this study, gas adsorption.

The surface area obtained from gas adsorption follows this equation:

$$S = A_x N_m \quad (8)$$

Where S is the surface area of the material, A_x is the cross-sectional area of the adsorbed molecule (usually nitrogen or argon) and N_m is the number of adsorbate molecules required to cover the solid with a single monolayer. There are two types of models that are widely used to fit adsorption data (both have been used in Chapter 4): Langmuir and BET models.

The Langmuir model usually follows these assumptions: monolayer adsorption, energetically uniform surface, and absence of interactions between adsorbed species. A typical Langmuir adsorption is shown in Figure 2-2 (3). The Langmuir model requires the pressure (P) and volume adsorbed (V) as known parameters. The Langmuir equation is given by this equation relating P/V and P :

$$\frac{P}{V} = \frac{1}{KV_m} + \frac{P}{V_m} \quad (9)$$

The slope of the line plotted would be $1/V_m$ and the intercept would be $1/KV_m$. The number of adsorbate molecules, N_m is found by the following equation:

$$N_m = \frac{V_m \times 6.023 \times 10^{23}}{22400} \text{ molecules} \quad (10)$$

Thus the specific surface area using the Langmuir model can be calculated from equation 8.

The BET model on the other hand assumes multilayer adsorption and that the first layer follows Langmuir adsorption. Beyond the first layer the condensation of gas into liquid needs to be considered. The BET model takes into account the relative pressure (P/P_o) and volume adsorbed (V). The BET equation establishes a linear relationship between $1/(V(P_o/P - 1))$ and P/P_o as follows:

$$\frac{1}{V(P_o - P)} = \frac{1}{V_m C} + \frac{P}{P_o} \frac{(C-1)}{V_m C} \quad (11)$$

The slope is given by $(C-1)/V_m C$ and the intercept is $1/V_m C$. As a result, $V_m = 1/(\text{slope} + \text{intercept})$ which gives the number of adsorbed molecules using equation 10. This in turn gives the specific surface area established by equation 8. The differences between the Langmuir and BET model are displayed in Figure 2-3 (3). Additionally, for the BET model, only relative pressures between 0.05 and 0.3 are considered to account for monolayer adsorption.

Here in this study, argon has been primarily used as the adsorbate for surface area measurements of molybdenum carbides. Argon gas adsorption was performed at 77 K in a Micromeritics Tristar Surface Area and Porosity Analyzer. Both Langmuir and BET models have been used to fit the adsorption behavior and to obtain specific surface area. This has been explained in detail in Chapter 4. It is also important to note that since 77 K is below the triple point of Argon, adsorption cannot be measured in the highest P/P_o region.

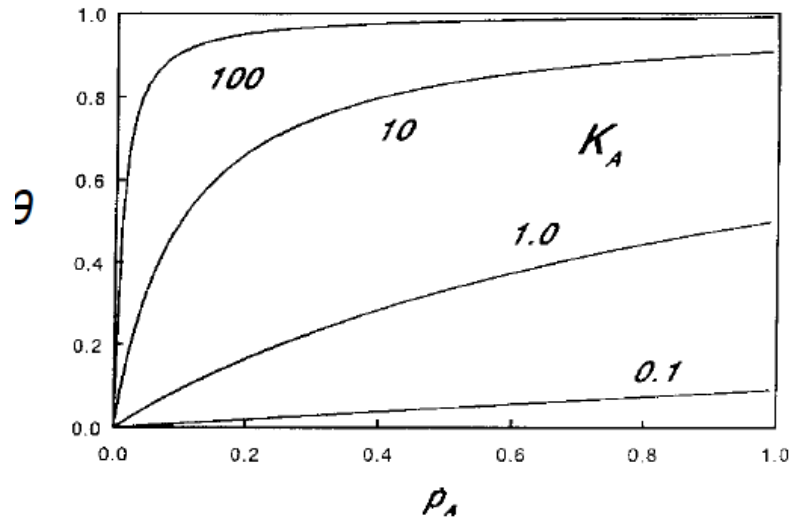


Figure 2-2. A Langmuir model plot (3)

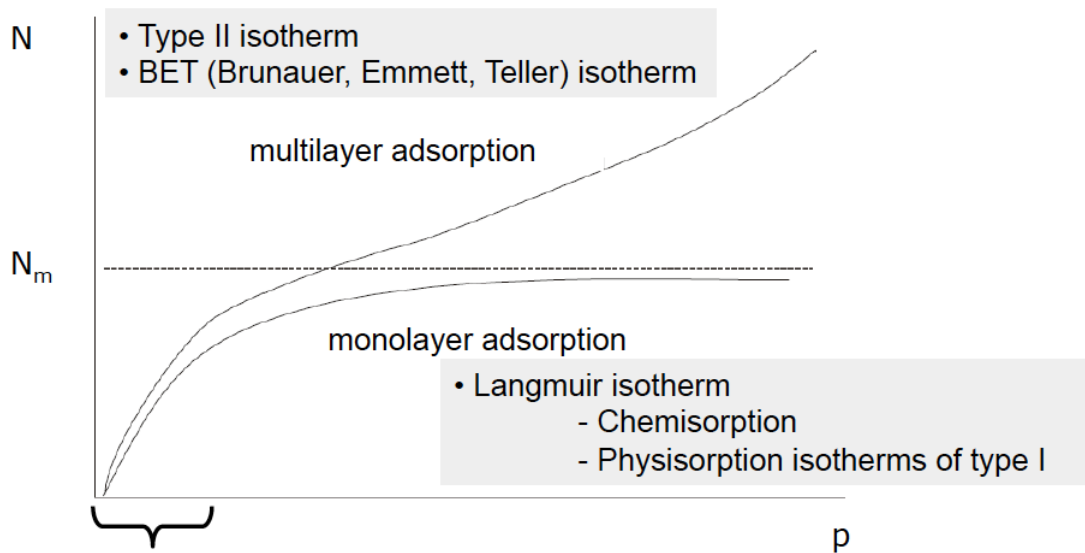


Figure 2-3. Theories to describe adsorption behavior: BET and Langmuir models

2.2.3 Additional Characterization Techniques: Specifications

High-resolution transmission electron microscopy (HRTEM) was done in a JEOL 2010F operated at 200 kV. The samples were suspended in ethanol, ground in an agate mortar and pestle, and then deposited on a holey carbon support film on Cu TEM grids. The images were recorded and analyzed using Digital Micrograph software.

Elemental composition was obtained using **energy dispersive X-ray spectroscopy (EDS)** using an Oxford X MaxN detector on a HITACHI S- 5200 scanning electron microscope (SEM). **Scanning Electron Microscopy** was carried out on the samples using the HITACHI S-5200 at voltages and currents of 10 – 20 kV and 10 – 20 mA as required.

A Kratos Ultra DLD spectrometer was used to carry out **X-ray photoelectron spectroscopy** to analyze the surface composition using a monochromatic AlK α source operating at a power of 200 mW and no charge neutralization. Charge neutralization was turned on for samples involving nafion and inks deposited on electrodes. High-resolution C 1s, O 1s and Mo 3d spectra were acquired at a pass energy of 20 eV. Three areas per sample were analyzed and CasaXPS was used to process spectra. Relative sensitivity factors provided by the manufacturer were used for quantification. Chemical composition was derived from Mo 3d component based on reference databases

Thermogravimetric Analysis was carried out in a TA Instruments SDT Q600 instrument. Experiments were carried out in inert atmosphere (nitrogen or argon), forming gas (~5.6% hydrogen in nitrogen) and air. Around 20 mg of sample and a gas flow of 20 – 50 ml/min were used.

Raman Spectroscopy was carried out in a 532 nm confocal Raman microscope Witec Alpha300R. Single spectra were obtained at different points of the samples at 20x magnification.

Fourier Transform Infrared Spectroscopy was carried out in Nicolet 6700 spectrometer.

Point of Zero Charge measurements were done in the Stabino Particle Charge analyzer by Particle Metrix using a background salt of 10^{-3} M KNO₃ and 0.025 M HNO₃ and KOH solutions for the titrator to adjust the pH.

2.2.4 Electrochemical Measurements

About 5-6 mg of molybdenum carbide sample was crushed and dissolved in 200 μl of ethanol and 50 μl of Nafion and sonicated for 30 minutes after each addition. Electrocatalyst slurry was deposited on a smooth glassy carbon electrode with an area of 0.1964 cm^2 . Enough ink was deposited to cover the entirety of the glassy carbon electrode.

All electrochemical measurements were carried out in PineWaveDriver equipped with a rotating disk electrode system. A three-electrode system was utilized to explore the activities of the molybdenum carbide composed of Ag/AgCl reference electrode and Pt mesh counter electrode. The experiments at ~ 0 pH were carried out in 0.5M sulfuric acid solution and the solution was degassed with a steady flow of argon into the cell. The measurements were performed with a sweep rate of 25 mV/sec and at 2000 RPM. The electrolyte was replaced for every measurement. All potentials are reported with respect to Standard Hydrogen Electrode (SHE).

REFERENCES:

1. http://web.mit.edu/2.813/www/readings/Ellingham_diagrams.pdf
2. Kishimoto et al. Journal of Mining and Metallurgy 44 B (2008) 39 – 48
3. Modern Methods in Heterogeneous Catalysis Research; 01 Nov 2013; Surface Area and Pore Size Determination; A. Trunschke

Chapter 3: Thermochemical Modeling

The molybdenum-carbon phase behavior is not well established and there are contradictory reports throughout literature. Hexagonal, cubic, and orthorhombic phases have all been reported but with different stoichiometries as was explained in Chapter 1. The phases of molybdenum carbide under study here are: metastable cubic MoC and thermodynamically stable hexagonal Mo₂C and shown in Figure 3-1.

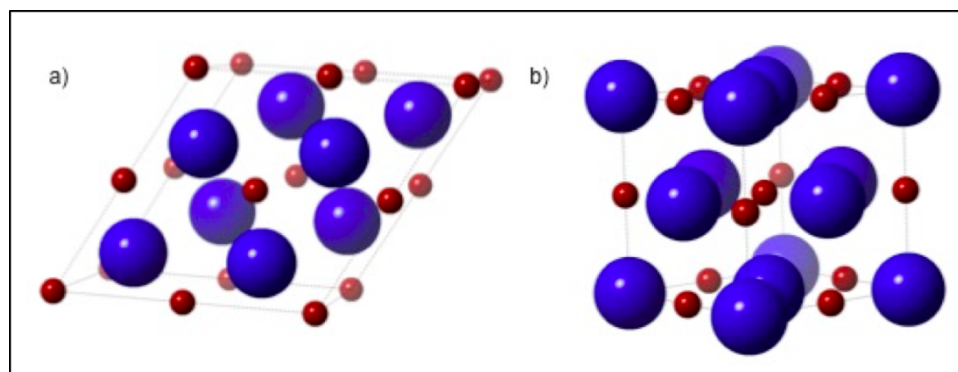


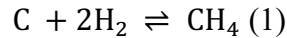
Figure 3-1. (a) Hexagonal Mo₂C and (b) cubic MoC molybdenum carbide structures.

Thermodynamic modeling is an essential part of understanding the structural formation of materials and helps refine the parameters for synthesizing the desired carbide and was carried out to better understand the Mo-C-H system using available thermodynamic data (1,2). These calculations were used to plot Ellingham and phase diagrams of Mo₂C in hexagonal phase and MoC in the cubic phase. Ellingham diagrams demonstrate the relative ease for certain reactions such as formation, oxidation, reduction, *etc.* to take place with respect to temperature and pressure. Here the formation of phases of molybdenum carbide with respect to temperature and partial pressures of hydrocarbon and hydrogen in the system was investigated. These also were utilized to theoretically explore all possible reactions in the system. Phase diagrams on the other hand display the relationships between the various phases of molybdenum-carbon when the system is

at equilibrium, which were instrumental in the refinement of the synthesis pathways discussed later in Chapter 4.

3.1 Ellingham Diagrams

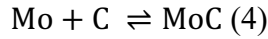
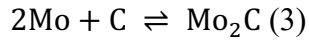
Ellingham diagrams were constructed to study the formation of cubic MoC and hexagonal Mo₂C with respect to various hydrocarbons such as methane, ethylene, and acetylene. Equation 1 shows hydrogen is being used to gasify carbon into methane. While it is important to dispose of the excess carbon, it is equally important to avoid the reduction of the MoC nanoparticles, which is a possibility when they are treated in H₂.



$$K = P_{\text{CH}_4}/P_{\text{H}_2}^2 \quad (2)$$

In order to find a balance between eliminating excess carbon and not reducing the carbide, a mixture of H₂ and CH₄ can be used to shift the equilibrium of the reaction. Equation 2 shows the thermodynamic equilibrium constant (K) being equal to a ratio of the partial pressures of the two gases. The standard enthalpy of reaction, $\Delta H^\circ_{298\text{K}}$ and the entropy, $\Delta S^\circ_{298\text{K}}$ were calculated to be -74800 J/mol and -80.6 J/K mol. Taking into account ΔC_p as a function of temperature, ΔG° values were calculated for a range of 25°C - 1000°C. Using thermodynamic equations mentioned in Chapter 2, ΔG of Reaction 1 can be related to the partial pressures of the gases in the system (K). The thermodynamic equations mentioned in Chapter 2 were utilized to calculate the thermodynamic parameters for the reaction 1 for temperatures ranging from 200-1000 °C for various values of K . This is illustrated in Ellingham diagrams in Figure 3-2 that plot ΔG as a function of temperature in which each colored line represents an equilibrium constant (CH₄/H₂ ratio). In order to study the thermodynamics of the formation of molybdenum carbide with respect to methane, it is essential to calculate $\Delta G^\circ(T)$ of the carbides. This was done for both phases of the

carbide, MoC and Mo₂C, using thermodynamic equations mentioned in Chapter 2 with respect to the following formation reactions:



These values are shown on the Ellingham diagrams as dotted lines. In order to ensure that the formation of carbide is more favorable than the formation of methane, an equilibrium constant that has a greater ΔG than the carbide formation must be chosen. This ensures there is enough carbon to form the carbide while simultaneously; there is not too much hydrogen to reduce the carbide to Mo metal and form the hydrocarbon. For example, from Figure 3b, at 800 °C the formation of Mo₂C is favorable if the value of the thermodynamic equilibrium constant, K , is equal to or greater than 10⁻⁴. This K value translates to a ratio of partial pressures of methane to hydrogen to be ≥ 0.01 in order to synthesize Mo₂C at 800 °C.

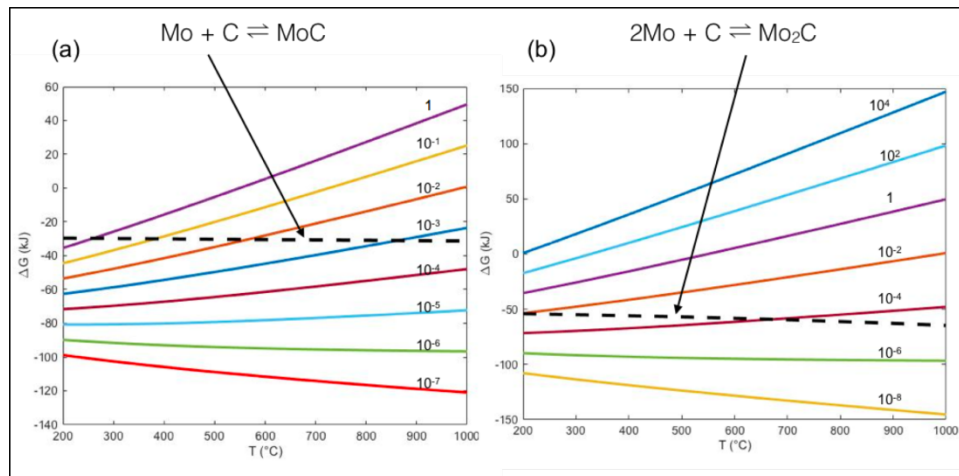


Figure 3-2. Ellingham diagram showing the formation of MoC (left, a) and Mo₂C (right, b) with respect to CH₄. The solid lines correspond to the free energy of formation of methane with respect to temperature. The numbers mentioned on the solid lines represent the equilibrium constant, K .

Similar calculations were conducted using ethylene and acetylene. Ellingham diagrams for the formation of Mo_2C with respect to ethylene and acetylene are shown in Figures 3-3 and 3-4 respectively.

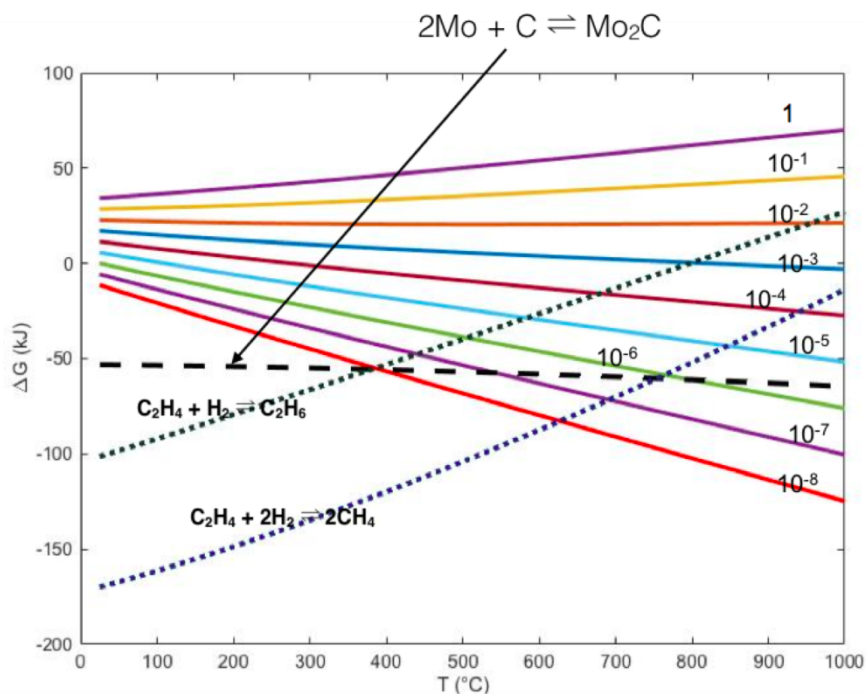


Figure 3-3. Ellingham diagram showing the formation of Mo_2C with respect to C_2H_4 . The solid lines correspond to free energy of formation of ethylene with respect to temperature. The numbers mentioned on the solid lines represent the equilibrium constant, K .

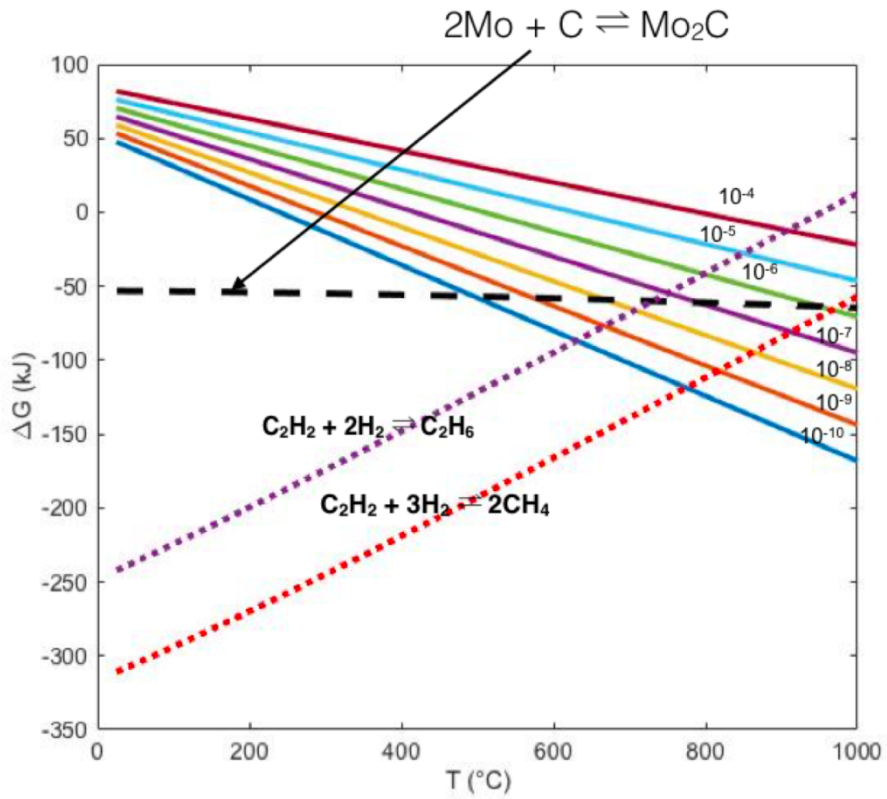


Figure 3-4. Ellingham diagram showing the formation of Mo_2C with respect to C_2H_2 . The solid lines correspond to free energy of formation of acetylene with respect to temperature. The numbers mentioned on the solid lines represent the equilibrium constant, K .

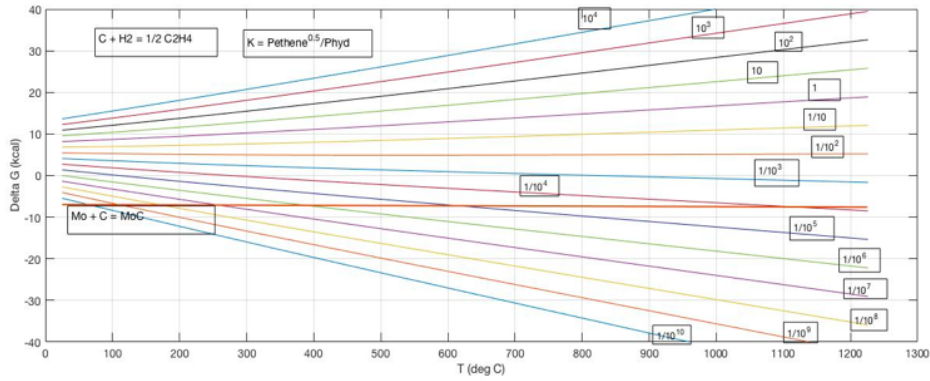


Figure 3-5. Ellingham diagram showing the formation of MoC with respect to C_2H_4 . The solid lines correspond to free energy of formation of ethylene with respect to temperature. The numbers mentioned on the solid lines represent the equilibrium constant, K .

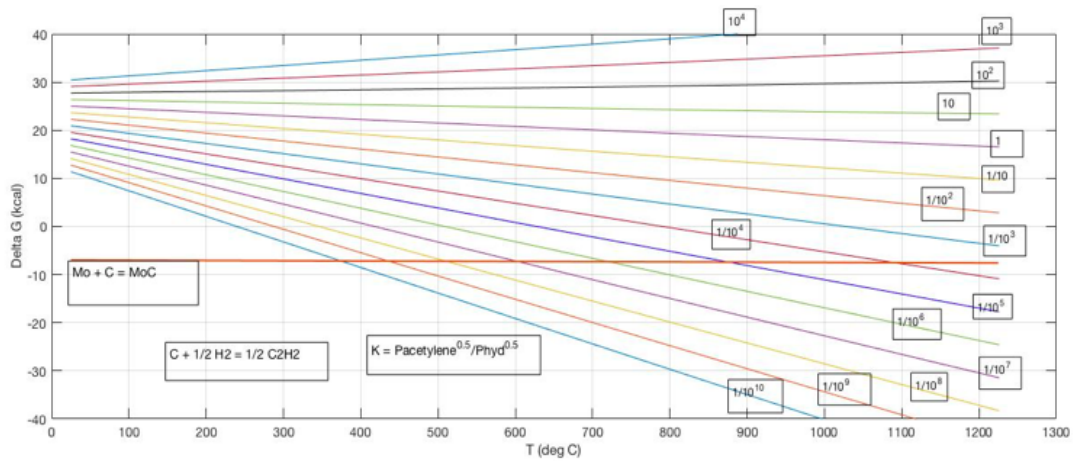


Figure 3-6. Ellingham diagram showing the formation of MoC with respect to C_2H_2 . The solid lines correspond to free energy of formation of acetylene with respect to temperature. The numbers mentioned on the solid lines represent the equilibrium constant, K .

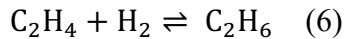
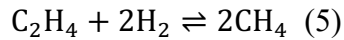
Similar observations in case of ethylene show that beyond $800\text{ }^\circ\text{C}$ (Figure 3-3), the ratio of ethylene to hydrogen should be at or above $1:10^5$ in order to form the carbide, Mo_2C . In the case of acetylene (Figure 3-4), within the range of around $800\text{ }^\circ\text{C} - 950\text{ }^\circ\text{C}$, the ratio of acetylene to hydrogen should be at or above $1:10^{12}$ in order to form the carbide. But beyond $950\text{ }^\circ\text{C}$, the formation of the

hydrocarbon becomes more favorable (at a ratio of 1:10¹²). In such a case, the hydrogen in the system would reduce the carbide to Mo metal and form acetylene. However, maintaining such ratios of gases in the system is not feasible in experimental setups.

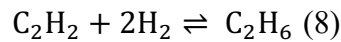
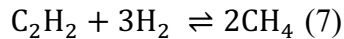
In the case of cubic MoC, at a temperature range of 600 °C – 1100 °C, the ratio of ethylene to hydrogen should be at or above 1:10⁴ to synthesize the carbide as seen in Figure 3-5. Beyond 1100 °C, at these partial pressures, the formation of hydrocarbon becomes more favorable.

The experimental unfeasibility of ratios of partial pressures of gases is not the only reason to avoid the use of hydrocarbons such as ethylene and acetylene. Figures 3-3 and 3-4 show the occurrence of undesirable side reactions, which are more favorable than the formation of the carbide.

These reactions in case of ethylene are as follows:



In case of acetylene, the following reactions can take place:



These side reactions are more thermodynamically favorable than the formation of carbide for much of the temperature range shown. For instance, in case of acetylene (Figure 3-4), the side reactions are more favorable than the formation of Mo₂C at temperatures from 25 °C - 900 °C for most ratios of partial pressures of acetylene to hydrogen.

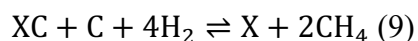
In order to avoid the occurrence of undesirable side reactions, methane was chosen as the hydrocarbon for the both further modeling as well as synthesis processing conditions (discussed in Chapter 4).

REACTION	$\Delta H_{298}^{\circ} (rxn)$ (J/mol)	$\Delta S_{298}^{\circ} (rxn)$ (J/deg mol)	$\Delta C_p^{\circ} (rxn) = A + BT + \frac{C}{T^2} + DT^2$ (J/deg mol)
$C + 2H_2 \rightleftharpoons CH_4$	-74800	-80.6	$-42.4 + 31.54 \times 10^{-3}T + 2.93 \times \frac{10^5}{T^2} - 0.61 \times 10^{-6}T^2$
$C + H_2 \rightleftharpoons \frac{1}{2}C_2H_4$	26250	-26.9	$-11.16 - 11.905 \times 10^{-3}T + 1.48 \times \frac{10^5}{T^2} + 17.38 \times 10^{-6}T^2$
$C + \frac{1}{2}H_2 \rightleftharpoons \frac{1}{2}C_2H_2$	113400	29.2	$8.02 - 24.33 \times 10^{-3}T + 5.235 \times \frac{10^5}{T^2} + 10.54 \times 10^{-6}T^2$
$C_2H_4 + H_2 \rightleftharpoons C_2H_6$	-137200	-120.3	$-31.85 + 60.47 \times 10^{-3}T - 9.12 \times \frac{10^5}{T^2} - 27.82 \times 10^{-6}T^2$
$C_2H_4 + 2H_2 \rightleftharpoons 2CH_4$	-202100	-107.8	$-62.48 + 27.06 \times 10^{-3}T + 2.9 \times \frac{10^5}{T^2} - 35.98 \times 10^{-6}T^2$
$C_2H_2 + 3H_2 \rightleftharpoons 2CH_4$	-376400	-220	$-100.84 + 111.74 \times 10^{-3}T + 10.41 \times \frac{10^5}{T^2} - 29.66 \times 10^{-6}T^2$
$C_2H_2 + 2H_2 \rightleftharpoons C_2H_6$	-311500	-232.5	$-70.18 + 84.32 \times 10^{-3}T - 1.61 \times \frac{10^5}{T^2} - 21.5 \times 10^{-6}T^2$
$Mo + \frac{1}{2}CH_4 \rightleftharpoons \frac{1}{2}Mo_2C + H_2$	11250	41.75	$24.76 - 18.795 \times 10^{-3}T - 1.855 \times \frac{10^5}{T^2} + 6.955 \times 10^{-6}T^2$
$\frac{1}{2}Mo_2C + \frac{1}{2}CH_4 \rightleftharpoons MoC + H_2$	35032.98	41.21	$21.45 - 35.015 \times 10^{-3}T - 0.725 \times \frac{10^5}{T^2} + 8.995 \times 10^{-6}T^2$

Table 3-1. Calculated enthalpy, entropy and heat capacity values of reactions used in Ellingham and gas phase equilibrium figures (in Section 3.2 of this chapter). Thermochemical data for each substance was obtained from (1,2).

3.2 Gas Phase Equilibrium Diagrams

Gas phase equilibrium figures were plotted to understand the relationships between Mo, Mo₂C and MoC phases with respect to partial pressures of methane and hydrogen at various chosen temperatures relevant to synthesis processes outlined in Chapter 4. With respect to these synthesis processes, these studies were also vital to deduce conditions to gasify excess carbon in the samples while keeping the metastable cubic phase (MoC) intact. The following equation shows that a metal carbide (XC) – carbon composite can be theoretically reduced with hydrogen to form the corresponding metal and methane:



While it is desirable to remove as much excess carbon as possible, it is essential to not get rid of the carbide in the process. The addition of methane to the hydrogen gas in the feed shifts the equilibrium of the reaction in a manner to prevent the reduction of MoC during the gasification of the residual carbon. The methane to hydrogen ratio used is extremely important; the excess carbon must be methanized while leaving the existing MoC nanoparticles intact. As mentioned in this chapter as well as Chapter 1, MoC is metastable and therefore, carbon can be easily removed from the carbide to form the more stable Mo₂C. As a result, gas phase equilibrium studies are essential they outline the regions of stability for MoC as well as possible products of a hydrogen methanization treatment such as Mo and Mo₂C.

Phase diagrams were calculated at temperatures of 700 °C, 800 °C, 900 °C, 1000 °C and 1100 °C. DFT assisted studies carried out in (3) helped provide thermodynamic data for MoC phase and are shown in Figure 3-7. This result also shows that under the standard conditions, the hexagonal MoC phase is the more stable phase of carbide at low temperatures, while at high temperatures (~1100 °C) the cubic phase of MoC is expected to be more stable. However, an estimated error of ~6

kJ/mol in the DFT calculated free energy of formation relates to ~300 °C error in the range of temperature stability and; therefore, it is reasonable to assume that the stability region of cubic MoC extends to temperatures as low as 900 °C under the standard conditions. This has been further observed in the thermochemical modeling detailed in this chapter and the synthesis and characterization studies in Chapter 4. Figure 3-7 also postulates the presence of hexagonal MoC however, the thermochemical modeling in this chapter deals with only two phases as mentioned above: cubic MoC and hexagonal Mo₂C. The reason for this is that these are the phases observed in the synthesis processes developed and detailed in Chapter 4.

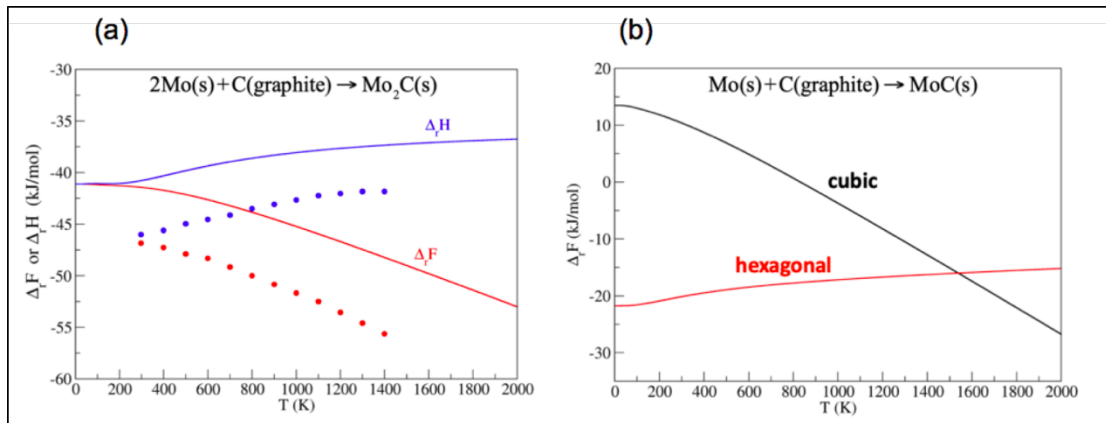
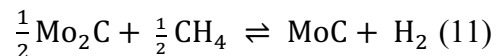
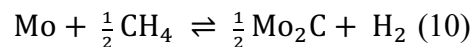


Figure 3-7. DFT calculated phase diagrams of a) hexagonal Mo₂C and b) MoC in the cubic (black) and hexagonal phase (red). Dotted data on the left figure correspond to the experimental data for the Mo₂C heat and free energy of formation taken from (4). Figure taken from (3).

With the help of thermodynamic equations at equilibrium, the formation of the carbides, Mo₂C and MoC, are related to the partial pressures of methane and hydrogen in the system. The reactions with respect to which these equations were designed are as follows:



With the Ellingham diagrams solely the formations of Mo₂C and MoC from Mo metal were studied. Here in the phase diagrams, reactions specific to synthesis processes outlined in Chapter 4 were investigated (Mo to Mo₂C and Mo₂C to MoC; as seen from the reactions 10 and 11). At the chosen temperatures, the thermodynamics of the reactions 10 and 11 were calculated using equations in Chapter 2 as shown in Table 3-1. At equilibrium, $\Delta G=0$, which leads to $\Delta G^\circ = -RT \ln(K)$. By substituting for K with respect to both reactions, the following relationship is obtained:

$$P_{\text{H}_2} = \exp(-\Delta G^\circ/RT) \cdot P_{\text{CH}_4}^{1/2} \quad (12)$$

The phase diagrams obtained as a result of these calculations are shown in Figure 3-8. As expected, according to the diagrams (Figure 3-8), Mo is stable at high partial pressures of hydrogen and MoC is stable at high partial pressures of methane. Mo₂C being the thermodynamically stable phase occupies a majority of the area in the phase diagram. At 800 °C for instance, there are a series of ratios of partial pressures of methane to hydrogen such as 1:1, 2:1 and 5:2 (to name a few) for which MoC would be stable as shown in Figure 3-9.

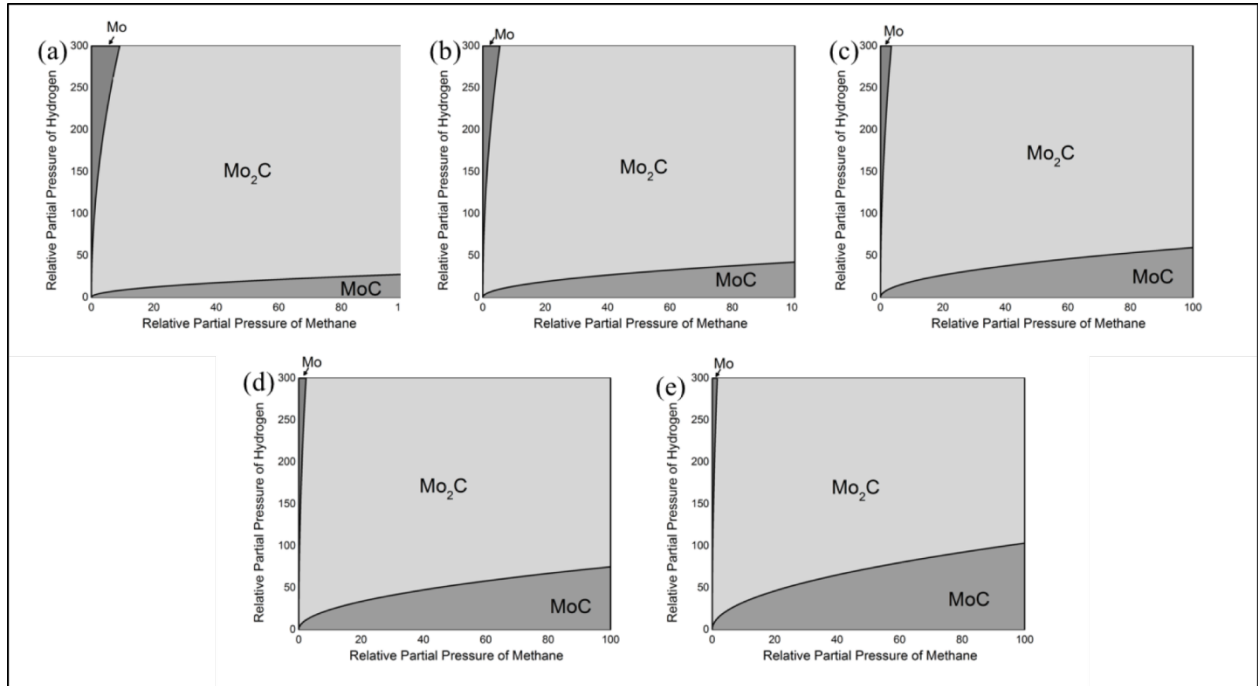


Figure 3-8. Gas phase equilibrium studies for the Mo-Mo₂C-MoC system with respect to hydrogen and methane relative partial pressures pertaining to temperatures of 700 °C (a), 800 °C (b), 900 °C (c), 1000 °C (d) and 1100 °C (e).

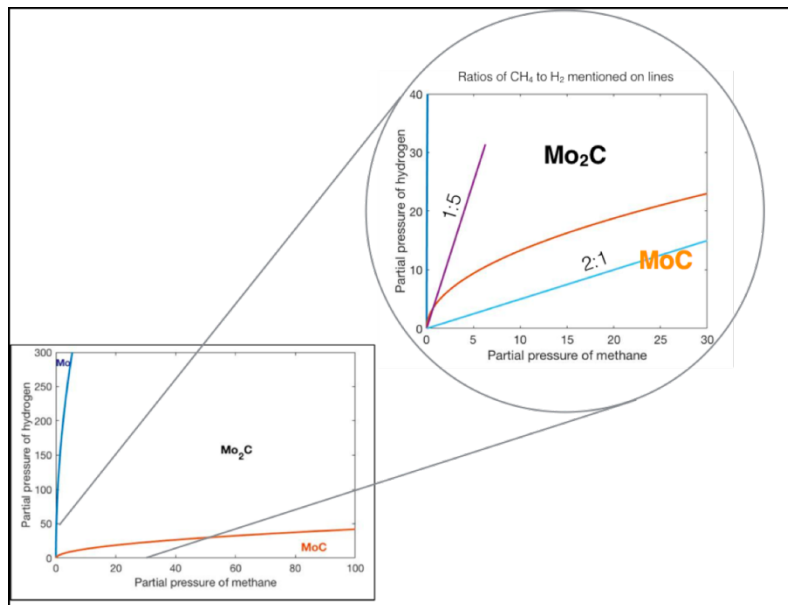


Figure 3-9. Appropriate methane to hydrogen ratios in order for the hydrogen methanization treatment at 800 °C.

Given the high uncertainties of the free energy data of MoC phase, the ratios of methane to hydrogen calculated are rather approximate. The estimated error in Gibbs free energies of reactions 10 and 11 at 298 K are ± 1080 J/mol and ± 1540 J/mol respectively. The ratios mentioned in Figure 3-9 ($\text{CH}_4:\text{H}_2 = 2:1$ and $1:5$) have been experimentally used and discussed in Chapter 4. These ratios were chosen as they are in different regions of stability as shown in Figure 3-9: MoC region (ratio of 2:1) and Mo_2C region (ratio of 1:5). The discussion in Chapter 4 also demonstrates a proof of concept for the theoretical thermochemical modeling. It is also important to note that there is error associated with using thermodynamic information relating to bulk phase to tune the synthesis of nanoparticles. There are many phenomena that take place at the nanoscale which bulk thermodynamics does not account for – such as Ostwald Ripening and particle migration and coalescence. The thermodynamic equations do not take surface enthalpy and entropy into account. The expectation is that if the nanoscale processes were accounted for the topology of the Ellingham and gas phase equilibrium diagrams would remain unchanged and the key take away points regarding the stability of the phases of molybdenum carbide would still be valid.

3.3 Summary

This chapter deals with the thermochemical analysis of the molybdenum carbon hydrogen system. The results of the analysis, which are Ellingham diagrams, revealed that methane is the suitable hydrocarbon for the synthesis of the molybdenum carbides. Use of hydrocarbons such as ethylene and acetylene lead to the undesirable side reactions such as formation of ethane and methane. This is useful information for researchers in search of appropriate carburizing agents as a carbon source for synthesis of molybdenum carbide. Phase diagrams have also been computed here to find optimal reaction conditions to synthesize single carbide phase cubic MoC nanoparticles by hydrogen methanization treatment. The gas phase equilibrium diagrams were computed for

reactions of Mo to Mo₂C and Mo₂C to MoC at temperatures between 700 – 1100 °C. The regions of stability for Mo, Mo₂C and MoC therefore obtained show that MoC is stable at high partial pressures of methane and Mo is stable at high partial pressures of hydrogen. Mo₂C being the thermodynamically stable phase occupies a major area of the phase diagrams. These figures also yielded ratios of partial pressures of methane to hydrogen where MoC would be stable and would not be reduced to form Mo₂C.

The results in this chapter were published in:

Nayak, Benavidez, Matanovic, Garzon. Thermochemical Analysis of Mo-C-H system for synthesis of molybdenum carbides. *Thermochimica Acta* 676 (2019) 27–32

REFERENCES:

1. Kouvetdkis J, Brewer L. Temperature stability range of the binary MoC phase. *J Phase Equilibria*. 1992;13(6):601–4.
2. Kubaschewski O, Alcock CB, Spencer PJ. *Materials Thermochemistry*. 1993.
3. Nayak SK, Benavidez AD, Matanovic I, Garzon FH, Thermochemical Analysis of Mo-C-H System for Synthesis of Molybdenum Carbides, *Thermochimica Acta* (2019).
4. Pankratz LB, King EG, Weller WW, States. U. Thermodynamic data for molybdenum carbide and tantalum carbide [Internet]. [Washington, D.C.]: U.S. Dept. of the Interior, Bureau of Mines; 1966. p. 10 p. (Report of investigations / United States Department of the Interior, Bureau of Mines ;6861). Available from: <file://catalog.hathitrust.org/Record/005951821>

Chapter 4

4.1 Ion Exchange synthesis

A fast, facile method was developed to synthesize the metastable cubic phase of MoC. It involves a combination of ion exchange synthesis followed by carburization and then methanization. This method has proved to yield 2 nm MoC nanoparticles with a surface area of about 350m²/g. The schematic of the entire process is shown on Figure 4-1.

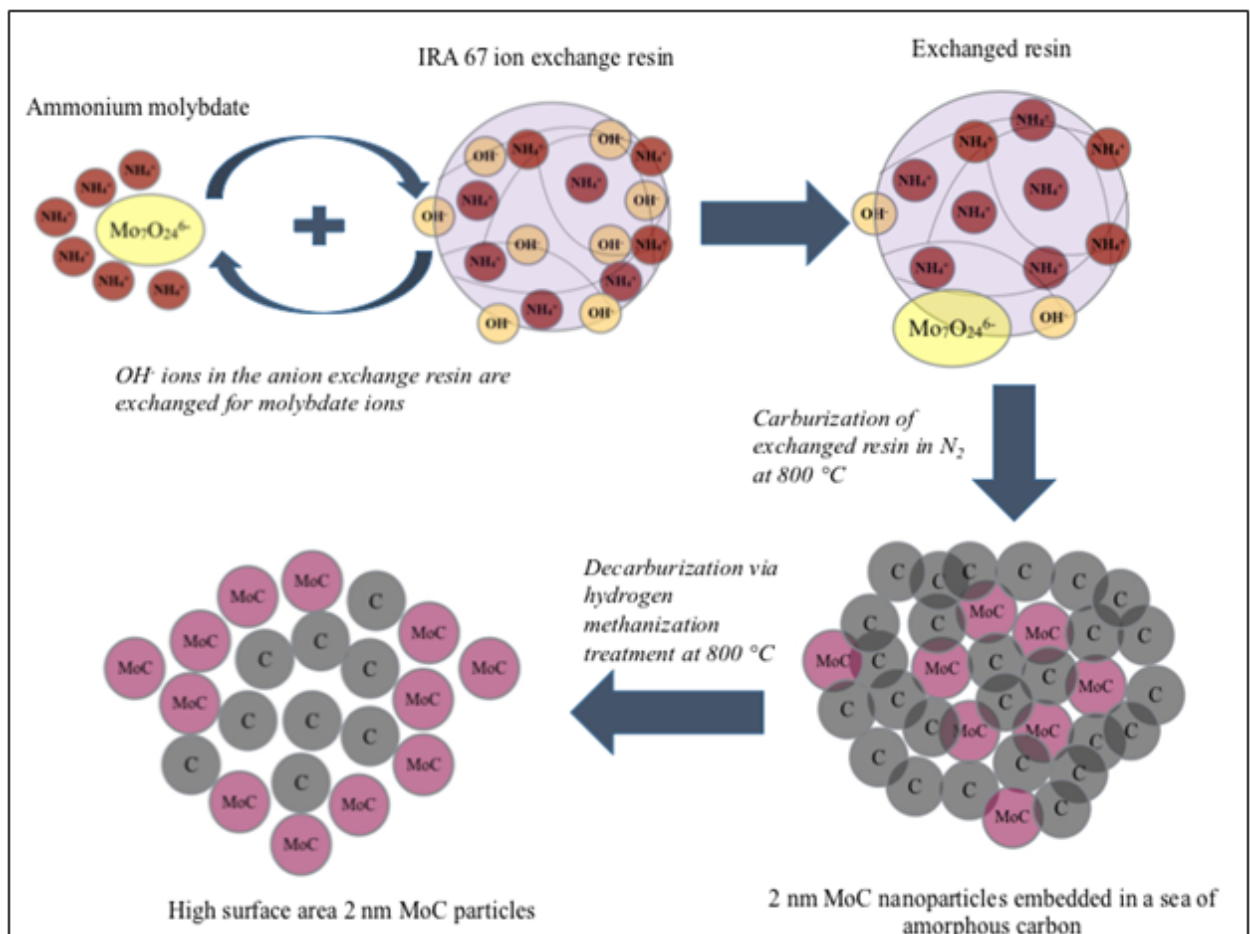


Figure 4-1: Synthesis of molybdenum carbide via ion exchange followed by pyrolysis and decarburization via hydrogen methanization.

Molybdenum carbide nanoparticles were synthesized using an ion exchange method (1). A quarternary ammonium divinylbenzene acrylic anion exchange resin (Amberlite IRA 67, Rohm

and Hass) was pretreated using 1 M sodium hydroxide and 1 M sodium hypochlorite solutions. The IRA 67 resin has a shipping weight of 700g/l and a theoretical total exchange capacity of 1.6 eq/l. Ammonium molybdate tetrahydrate was used as the molybdenum precursor. 1 mmol of ammonium molybdate was used for every 10 g of pre-treated resin in 100 ml of DI water. The solution was left for stirring overnight. After filtration, the exchanged resin was washed with DI water until the pH was 7 and then dried overnight at 80°C. A series of pyrolysis protocols were carried out as follows:

1. Pyrolysis of exchanged resin at 800 °C for 1 hour in nitrogen.
2. Pyrolysis of exchanged resin at 800 °C for 1 hour in argon.
3. Pyrolysis of exchanged resin at 800 °C for 6 hours in nitrogen.
4. Pyrolysis of exchanged resin at 1000°C for 1 hour in nitrogen.

Samples were analyzed at different points of the synthesis using a variety of techniques: Thermogravimetric Analysis, X-Ray Diffraction, Scanning Electron Microscopy – Energy Dispersive Spectroscopy, Transmission Electron Microscopy, X-Ray photoelectron spectroscopy, Gas Adsorption experiments, Raman Spectroscopy and FTIR. Thermogravimetric analyses were done on the IRA 67 resin (carbon precursor) as well as the ion-exchanged resin. The former shows that the resin is stable up until ~360 °C in an inert atmosphere as shown in Figure 4-2. The latter in Figure 4-3 shows a difference in mass between being run in air and argon. This is most likely because of the formation of an oxide when the sample is treated in air. The SEM images before and after pyrolysis are shown in Figure 4-4. The spherical shape is retained after pyrolysis. However, there is a shrinkage observed owing to the extra materials of the resin being burnt off. Figure 4-5 shows that after pyrolysis, the sample consists of spheres of 200 µm in diameter.

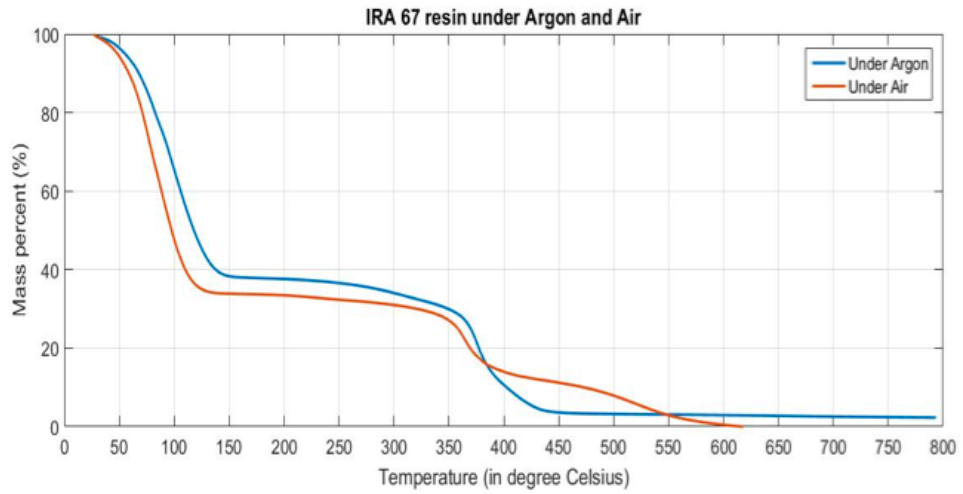


Figure 4-2. Thermogravimetric Analysis of Amberlite IRA 67 Resin.

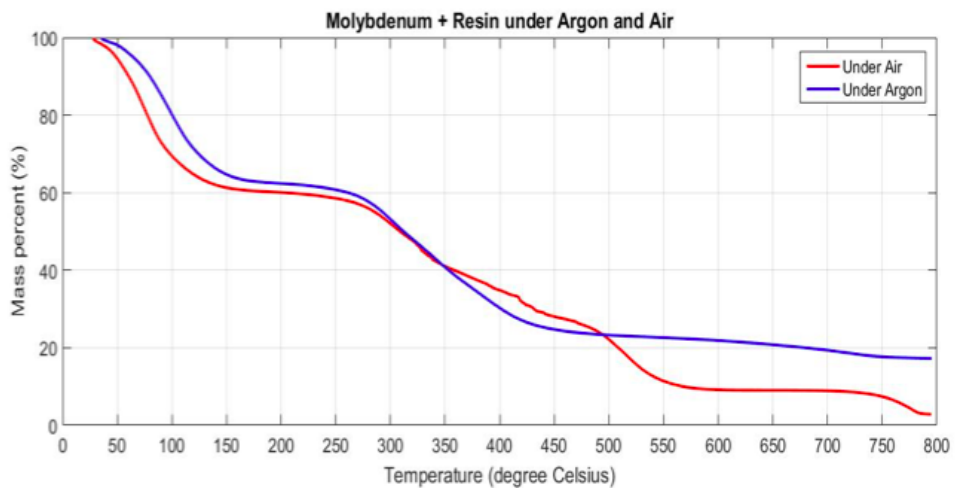


Figure 4-3. Thermogravimetric Analysis of ion-exchanged resin.

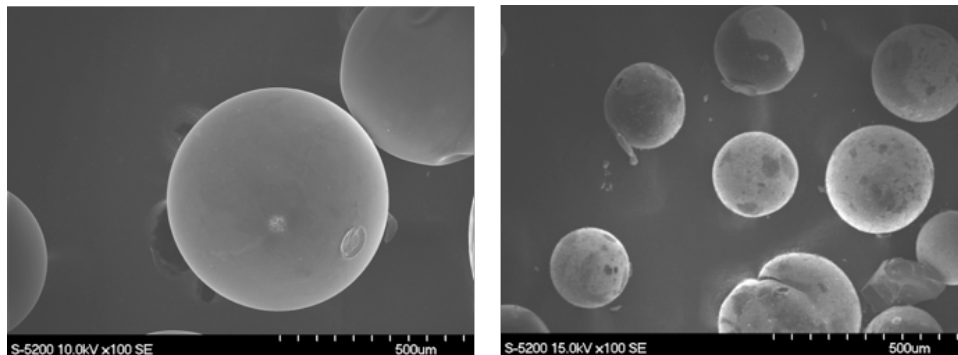


Figure 4-4. Scanning Electron Microscopy images of samples before (a) and after (b) pyrolysis (800°C, 1 hour in nitrogen).

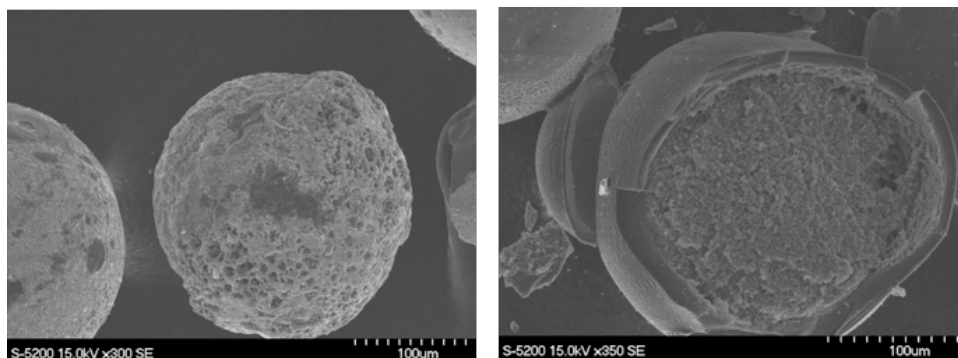


Figure 4-5. Scanning Electron Microscopy images of samples after pyrolysis at 800°C for 1 hour in nitrogen.

The X-Ray diffraction patterns of various pyrolysis conditions are shown in Figure 4-6, which display the changing phase relationships as a function of time and temperature. 800°C pyrolysis in argon or nitrogen yields cubic MoC, and amorphous carbon, while 1000°C pyrolysis shows mixed Mo₂C and MoC phases along with amorphous carbon. Similarly, increasing the hold time to 6 hours produces Mo₂C alongside cubic MoC. The Whole Profile Fitting for this protocol indicates around 36% Mo₂C. Pyrolysis conditions of 800 °C and 1 hour in an inert atmosphere (Ar or N₂) produces single carbide phase molybdenum carbide as shown in Figure 4-7. A broad peak at low angles (~23°) indicates amorphous carbon. The Whole Profile Fitting revealed a crystallite size of ~2 nm and no incoherent strain broadening of the cubic phase was observed in the

diffraction patterns which shows that there were no atoms bonded in a state of stress. Given the size of the nanocrystals ($\sim 2\text{nm}$), the theoretical surface area should be high ($\sim 330\text{ m}^2/\text{g}$); however, the surface area was only $5.6\text{ m}^2/\text{g}$ as is calculated from Figure 4-9. HRTEM images of the pyrolyzed materials in Figure 4-8 show the molybdenum carbide nanoparticles are surrounded by amorphous carbon. These images also indicate graphitic stacking around the molybdenum carbide nanoparticles but there is a high degree of disorder in the carbon. This explains the low surface area of pyrolyzed materials. It is evident from the micrographs that the amorphous carbon is impeding gas access to the high surface area MoC crystallites.

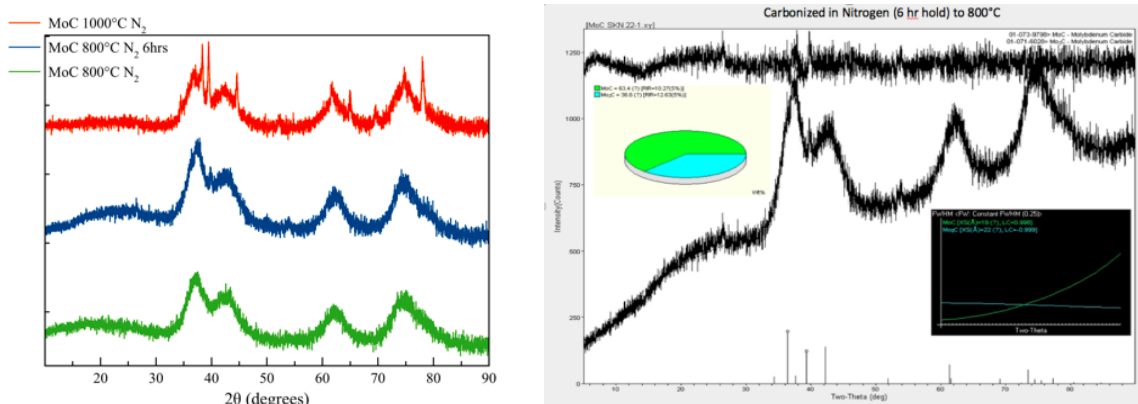


Figure 4-6. X-Ray Diffraction of samples under different pyrolysis condition. (left)

Whole profile fit of sample after being pyrolyzed in nitrogen for 6 hours (right). The fit shows 35% Mo₂C and 65% MoC.

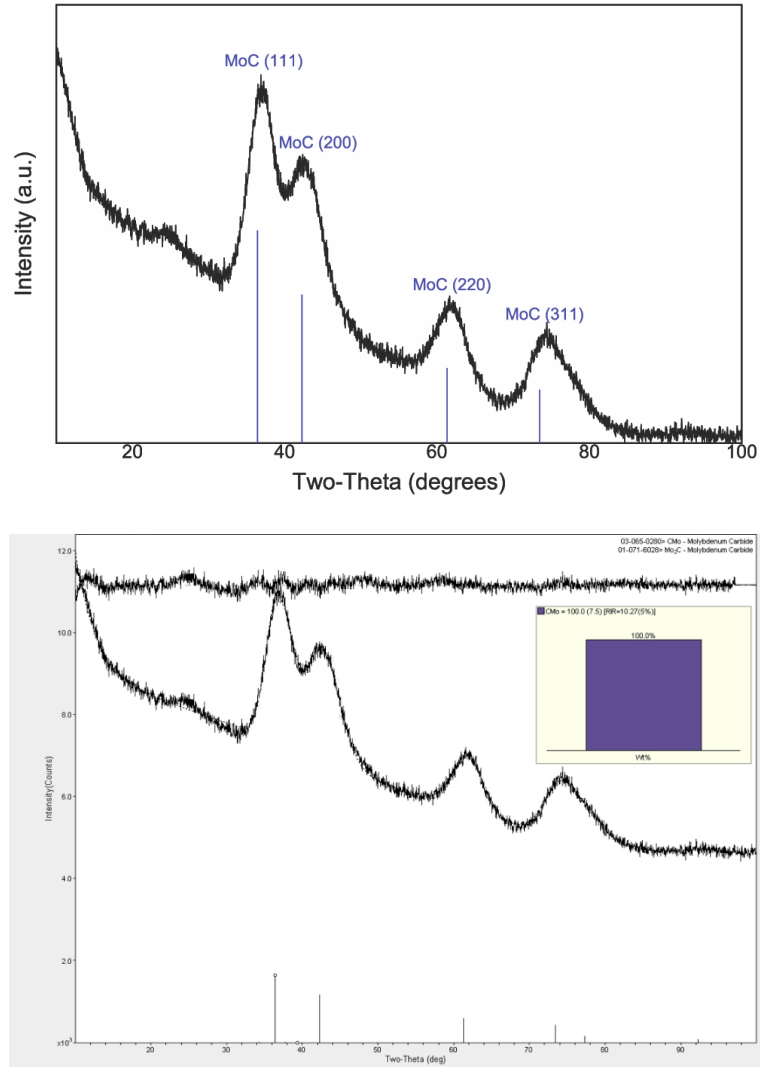


Figure 4-7 X-Ray diffraction pattern of molybdenum carbide (pyrolyzed at 800 °C for 1 hour in nitrogen) (top) and whole profile fitting refinement fit ($R = 1.61\%$), (bottom).

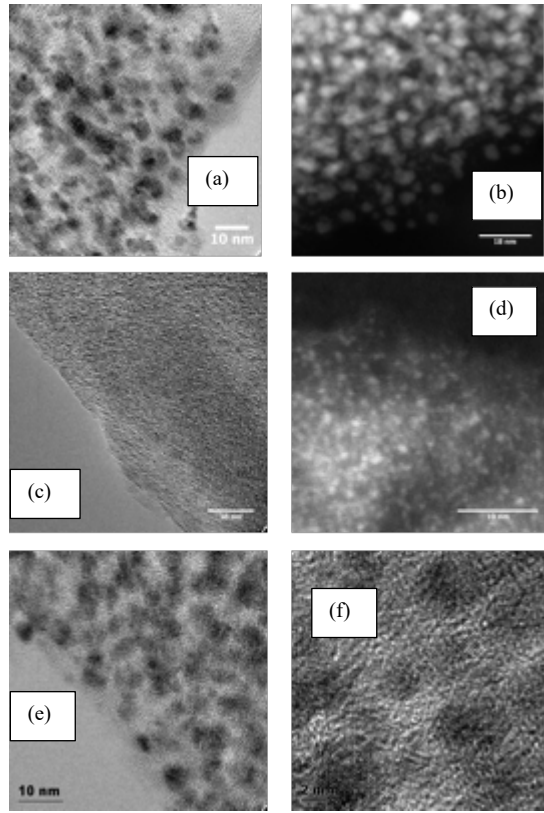


Figure 4-8. TEM images of molybdenum carbide: a) and b) molybdenum carbide prepared at 800°C in nitrogen; c) and d) molybdenum carbide prepared at 800 °C in argon; e) and f) molybdenum carbide prepared at 800 °C in nitrogen with 6 hour hold.

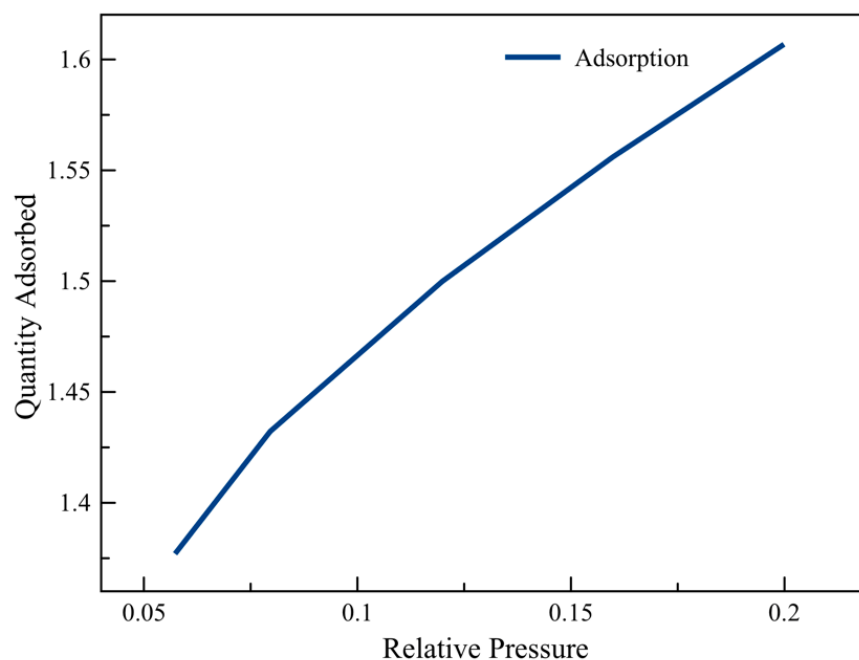


Figure 4-9. Adsorption isotherm of molybdenum carbide after pyrolysis at 800 °C in nitrogen. Efforts were carried out to reduce the carbon content of the prepared molybdenum carbide samples. Thermogravimetric analysis was done on samples in forming gas to observe the effect of hydrogen on the carbon surrounding the molybdenum carbide nanoparticles (Figure 4-10). X-Ray diffraction and Scanning Electron Microscopy was done on the samples to assess the phase composition and ratios of Mo to C in the sample. The EDS results shown on Figure 4-12 indicate that C:Mo ratios have decreased as a result of the forming gas treatment, however the XRD analyses in Figure 4-

11 indicate that the MoC is reduced to form Mo₂C.

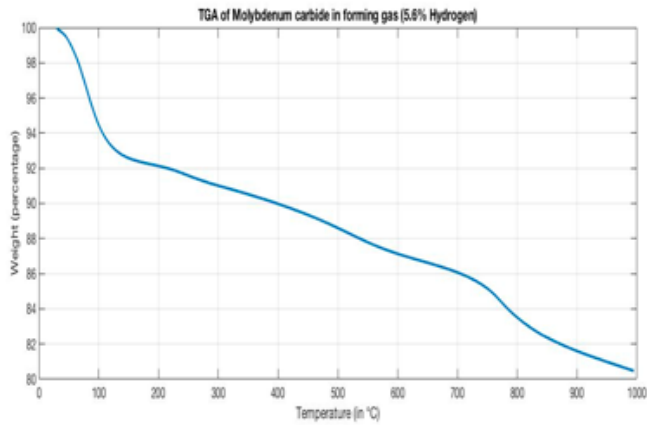


Figure 4-10. Thermogravimetric analysis of molybdenum carbide in forming gas.

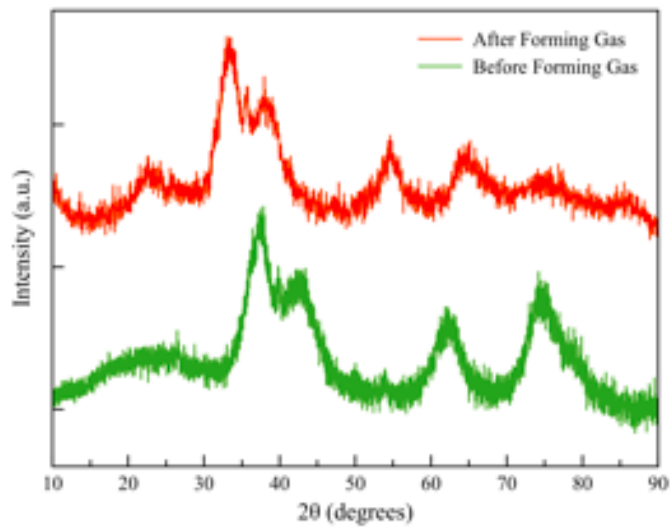


Figure 4-11. X-ray diffraction of post-TGA sample after forming gas treatment

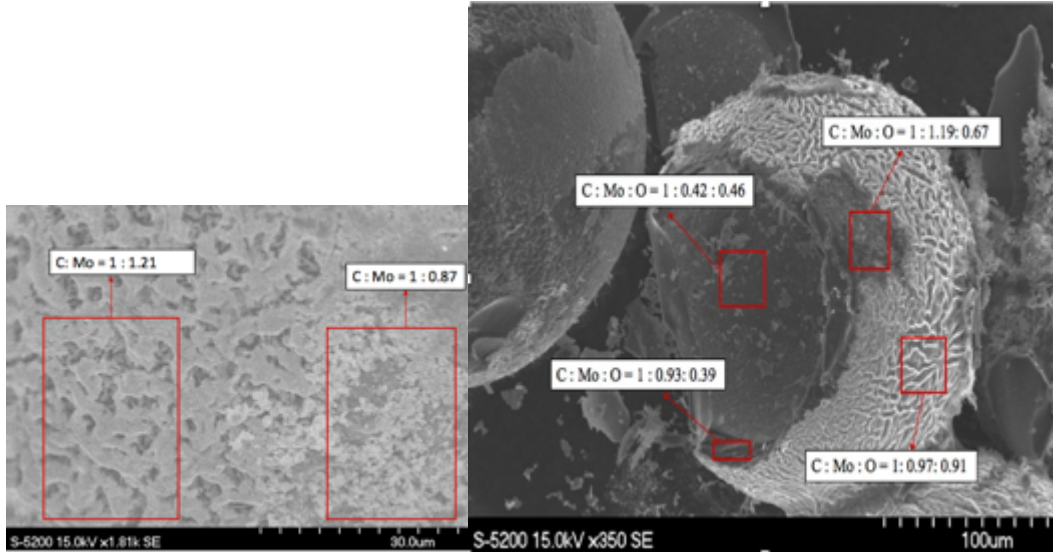


Figure 4-12. Scanning electron microscopy of molybdenum carbide after forming gas treatment. Based on the thermodynamic calculations (from Chapter 3), the methanization treatment was designed to treat the carbide nanoparticles in a mix of methane and hydrogen (ratio of relative partial pressures being 2:1). Hence, by using this gas mixture, the reduction of the MoC – C composite can be controlled and thus, circumvent the loss of MoC. The pyrolyzed materials were crushed and sieved. They were then treated in a mixture of methane and hydrogen (molar ratio of 2:1 and a total flow rate of 180 ccm; 1.6% CH₄ and 0.8% H₂ in nitrogen). This methanization treatment was carried out at 800 °C for 1 hour with a ramp rate of 10 °C/min.

Nitrogen gas adsorption experiments on molybdenum carbide exhibit strong chemisorption of nitrogen and neither BET nor Langmuir models fit the observed adsorption behavior. Mass spectroscopy on the molybdenum carbide further iterates this statement as shown in Figure 4-13, which shows strong adsorption of nitrogen that is desorbed only at high temperatures (> 600 °C). Table 4-1 shows the varying surface areas obtained as a result of the different adsorbates and models.

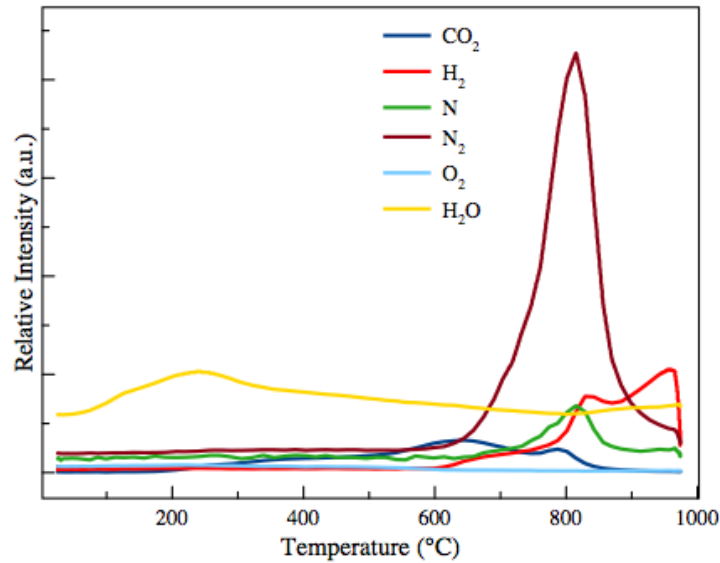


Figure 4-13. Mass spectroscopy on methanized molybdenum carbide sample.

Surface Area Model	BET	Langmuir
N ₂ as Adsorbate	310 m ² /g	413 m ² /g
Ar as Adsorbate	272 m ² /g	362 m ² /g

Table 4-1. Surface area of MoC post-methanization (CH₄:H₂=2:1 at 800 °C) using different adsorbates and surface area models.

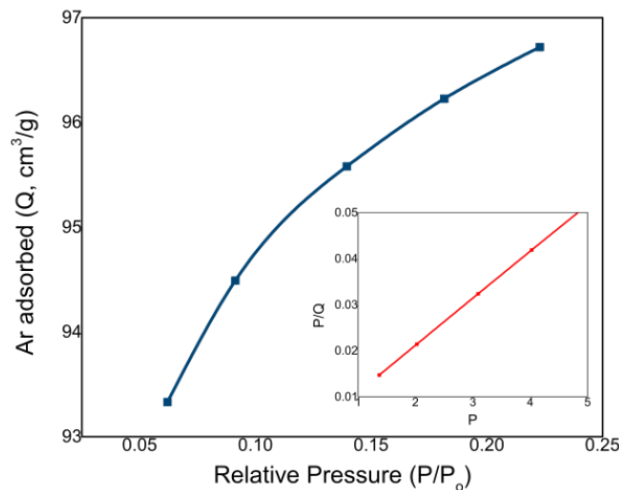


Figure 4-14. Surface area analysis of molybdenum carbide using argon as an adsorbate. (Inset:

Langmuir adsorption isotherm, $P/Q = P/Q_m + 1/KQ_m$, ($R^2 = 0.999$)

The adsorption-desorption isotherm using argon as adsorbate is shown in Figure 4-14 from which the Langmuir surface area was calculated to be 360 m²/g. This is a vast increase from 5.6 m²/g, which was the surface area before the decarburization via hydrogen methanization treatment.

The X-ray diffraction pattern alongside the WPF refinement of the MoC post-methanization is shown in Figure 4-15. No change in MoC peak widths is observed indicating that the crystallite size remained the same. WPF refinement identified only the presence of 2 nm cubic MoC; the introduction of Mo_xC hexagonal phases into the pattern fitting did not improve the goodness of fit pointing towards the unlikelihood of its presence.

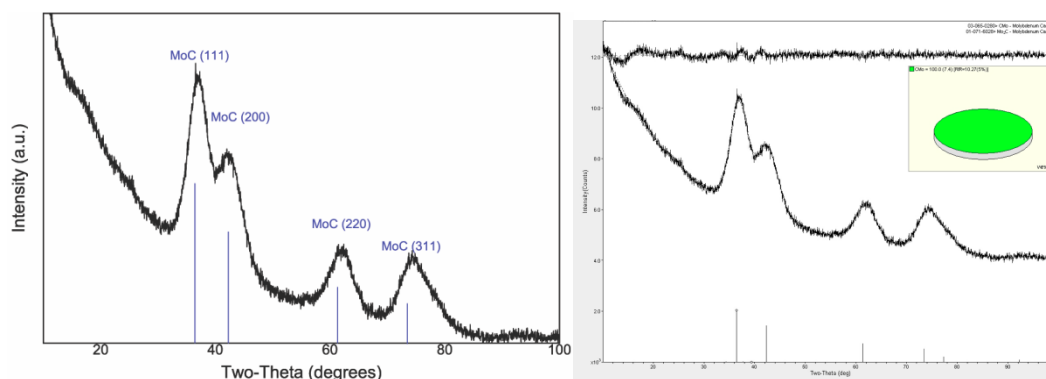


Figure 4-15. X-Ray diffraction pattern and whole profile fitting refinement of molybdenum carbide after methanization treatment.

This is further corroborated by the HRTEM images in Figure 4-16 that show 2-3 nm particles. This supports the observation that the MoC nanoparticles have not agglomerated as a result of the methanization treatment. A Fourier transform of the boxed region was used to index the prominent fringes as the (111) of cubic MoC.

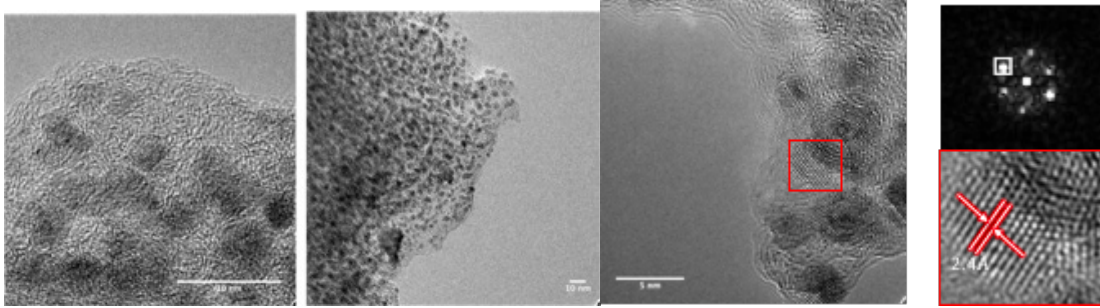


Figure 4-16. HRTEM images of molybdenum carbide post methanization treatment and Fourier transform of indicated region.

The atomic percentages of Mo, C and O pre- and post-methanization obtained through Energy Dispersive X-ray Spectroscopy (EDS) are shown in Table 4-2. There is a substantial increase in the Mo atomic percent post-methanization, which indicates that more of the carbon in the methanized sample exists as carbide. There is also a decrease in the O atomic percent due to methanization.

Atomic %	C	Mo	O	N
Pyrolyzed materials	81.75	0.91	17.34	0
Methanized materials	76.17	15.62	7.07	1.14

Table 4-2. EDS analyses of molybdenum carbide materials before and after the decarburization via hydrogen methanization treatments.

Valence state information and elemental composition pre- and post- methanization treatment is obtained through X-ray photoelectron spectroscopy as shown in Table 4-3, Table 4-4 and Figure 4-17. It is important to note that these samples were exposed to air before on transfer to XPS, thus affecting the reliability of the measurements. High resolution Mo 3d spectrum was fit using multiple symmetrical peaks due to following valence states: two peaks due to Mo coordinated to

C (peaks at 228.2 and 228.6 eV), Mo(IV) at 229.7 eV, Mo(V) at 230.6 eV and Mo(VI) at 232.2 eV according to the reference data base (2) and reports in literature (3-5). A substantial increase in Mo-C bonding is observed post-methanization implying more of the carbon exists as the carbide, which agrees with our results from EDS.

Sample	Mo ⁰ %	Mo ³⁺ %	Mo ⁴⁺ %	Mo ⁶⁺ %
Pre-methanized	24.3	21.5	11.1	43.1
Post-methanized	60.0	14.8	11.3	13.9

Table 4-3. Relative molybdenum compositions from XPS analysis of synthesized MoC powders before and after the methanization treatment.

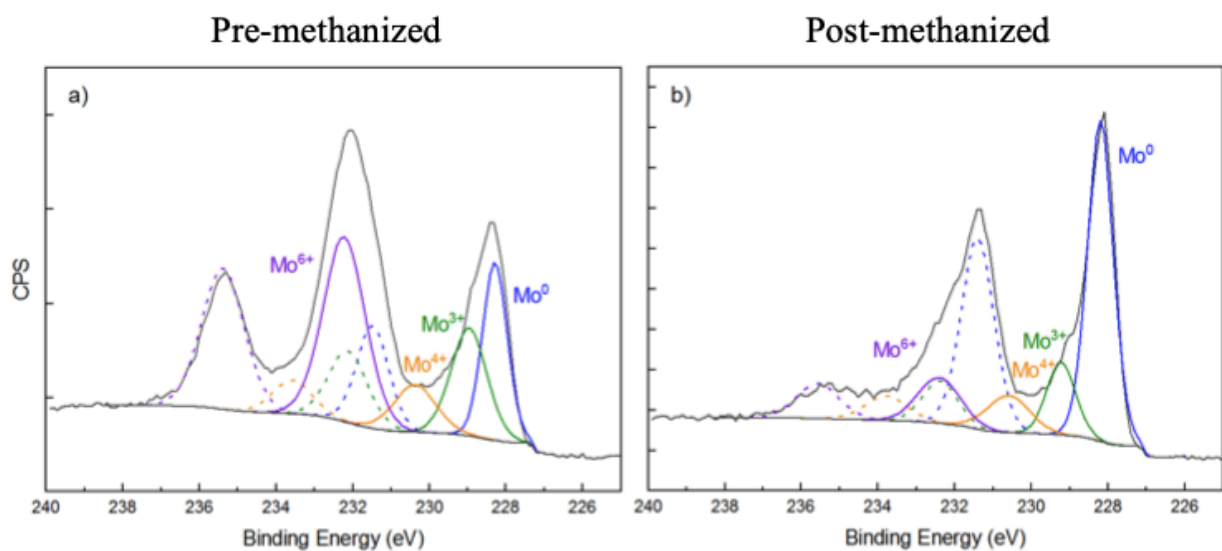


Figure 4-17. XPS analyses of molybdenum carbide samples before (a) and after (b) methanization.

Sample	C 1s %	O 1s %	Mo 3d %	N 1s %
Pyrolyzed materials	77.7	17.3	4.0	0.92

Other methanization ratios were attempted as well such as $\text{CH}_4 : \text{H}_2 = 1:1$, $1:5$ and $5:2$. The ratio of methane to hydrogen of $1:5$ is in the Mo_2C stability region as demonstrated in Chapter 3. The X-ray diffraction of the carbide materials obtained via decarburization via hydrogen methanization ($1:5$) is shown in Figure 4-19. Whole Profile Fitting technique indicates around 40 percent hexagonal Mo_2C alongside cubic MoC .

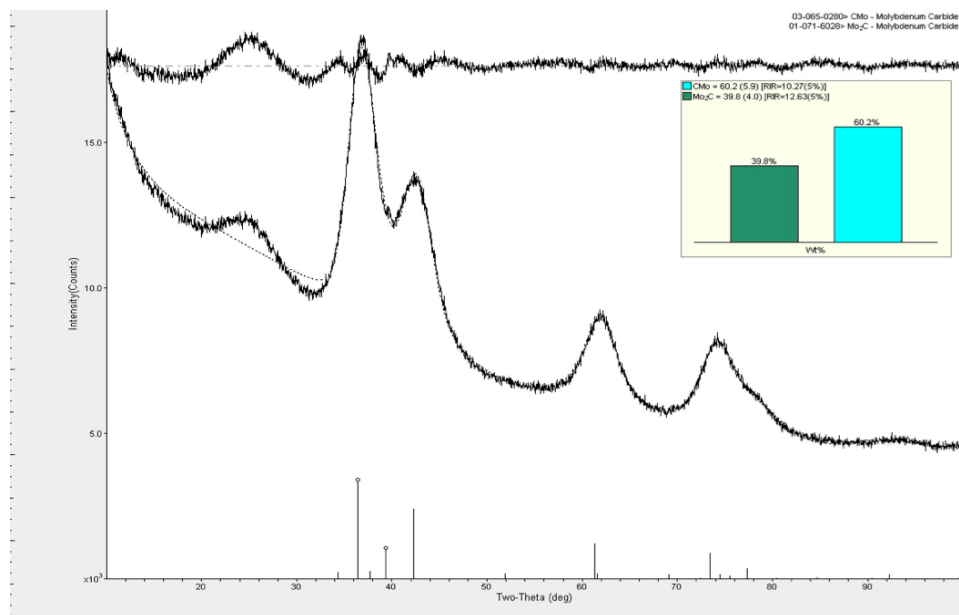


Figure 4-19. X-ray diffraction of molybdenum carbide materials after methanization at $\text{CH}_4 : \text{H}_2 = 1:5$.

The X-ray diffraction patterns of other ratios indicate crystallite sizes of around 2-3 nm. The surface areas of carbide materials using different decarburization via hydrogen methanization protocols are shown in Figure 4-20. Surface areas of these carbides range from 200 – 360 m^2/g and it has been observed that molybdenum carbide is obtained at $\text{CH}_4 : \text{H}_2 = 2:1$.

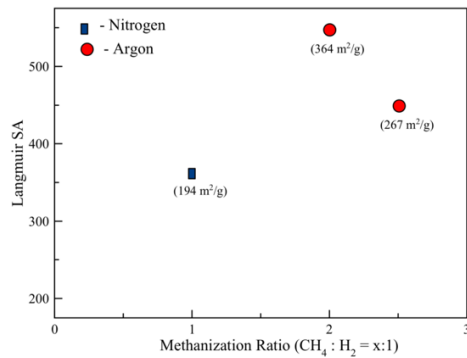


Figure 4-20. Surface areas of carbide materials obtained via different decarburization protocols.

4.2 Ammonolysis and methane treatment of molybdenum oxide

Lee et al.'s (6) method was used to synthesize a different batch of molybdenum carbide. This method is different from the ion exchange synthesis as it involves an oxide precursor and carburizing gas (methane) as carbon source. As stated in Chapter 3 the type of synthesis route affects the phase and composition of carbide produced. Both synthesis processes yield cubic MoC (under certain circumstances), however the parameters such as particle size, surface area and contaminants are different. The schematic for the process is shown in Figure 4-21.

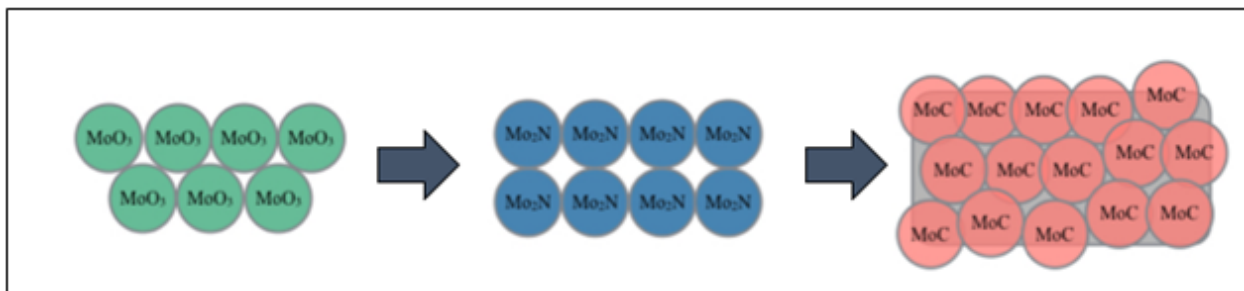


Figure 4-21. Schematic for synthesis process using molybdenum oxide as a precursor.

The synthesis process has two distinct steps:

1. Ammonolysis of molybdenum precursor, MoO₃: The oxide, MoO₃, is treated in 60 scfm of ammonia and different protocols were used:
 - a. 350°C – 450°C @ 1.5°C/min and 450°C – 700°C @ 5°C/min. The space velocity is

137.4 hr⁻¹ (mol of NH₃/mol of MoO₃).

b. 350°C – 450°C @ 0.6°C/min and 450°C – 700°C @ 3°C/min. The space velocity is

181.425 hr⁻¹ (mol of NH₃/mol of MoO₃)

2. Methane treatment: The nitride materials formed in the previous step are subjected to a methane treatment, the protocols being:

a. RT - 670°C at 0.5°C/min in 0.3% CH₄, 1.2%H₂ in N₂

b. RT - 670°C at 0.5°C/min in 3% CH₄ in N₂ (155 sccm).

A series of characterization tests have been done to understand the properties of the molybdenum precursor, MoO₃. The X-Ray diffraction pattern of the oxide is shown in Figure 4-22.

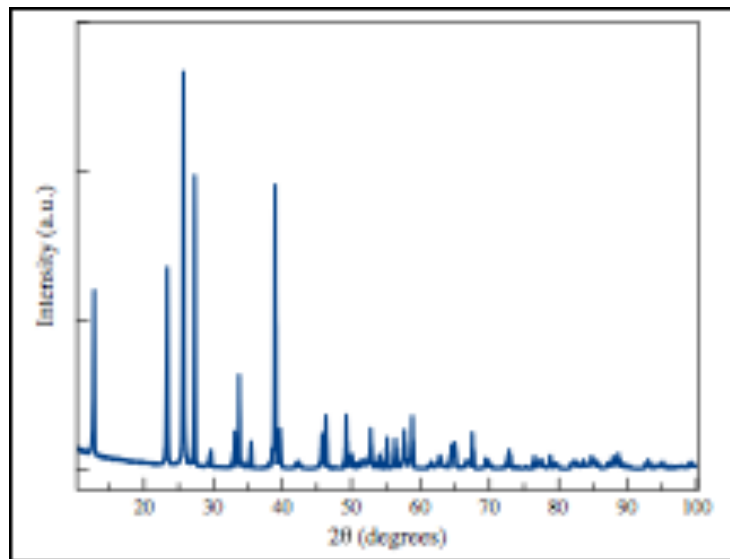


Figure 4-22. The X-ray diffraction pattern of molybdenum oxide.

Point of zero charge measurements were done to understand the surface charge of the molybdenum oxide particles which is important to understand solution dispersal behavior. The experiments were carried out in a Stabino Particle Charge analyzer. The background salt used was 10⁻³ M KNO₃ and 0.025 M HNO₃ and KOH solutions were used as the titrators to adjust the pH. The initial pH of the MoO₃ sample was observed to be around 3.5 and over the course of the experiment, the pH

was slowly raised to 10 and then titrated back to around 4. Figure 4-23 shows three rising pH curves and two falling pH curves. The rising pH curves are all strongly negative in zeta potential over the entire pH range. In the falling curves, there is a drop in the strength of the zeta potential, but at acidic conditions, the zeta potential value increases again (becomes more negative). These observations indicate that surface structure of the oxide changes when the pH is adjusted to basic conditions.

The surface area of molybdenum oxide was measured to be $0.8 \text{ m}^2/\text{g}$ as shown in Figure 4-24.

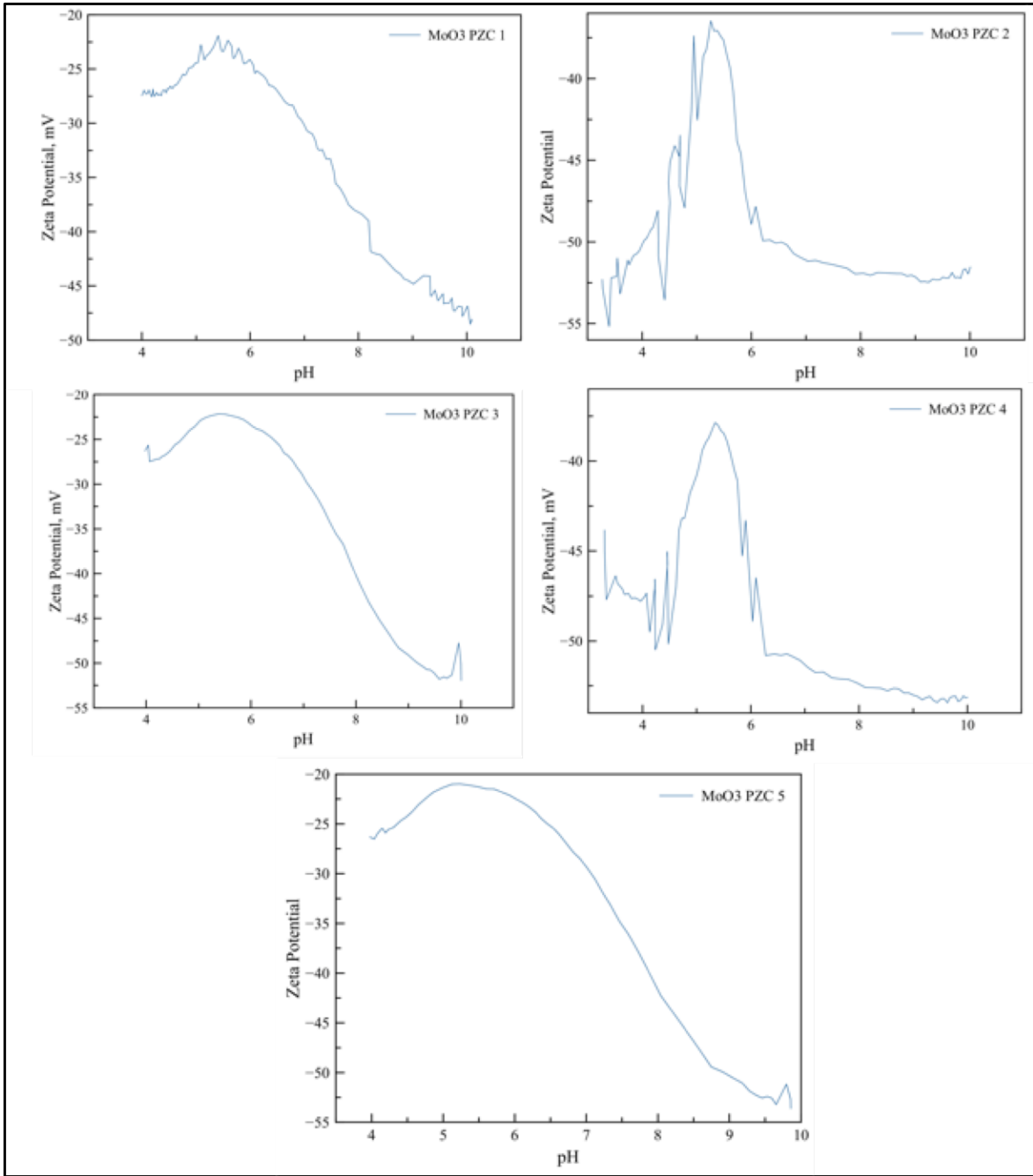


Figure 4-23. Point of zero charge measurements done on molybdenum oxide.

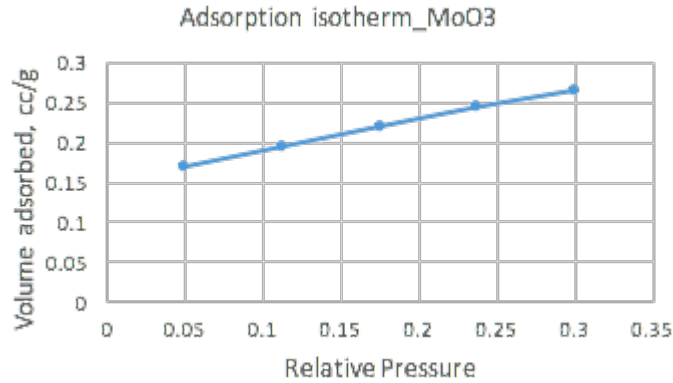


Figure 4-24. Adsorption isotherm for molybdenum oxide.

The particle size of the oxide was reduced by milling prior to the ammonolysis treatment in ethanol and 0.5 mm YSZ beads.

The product of the ammonolysis treatment (a) is a nitride that is air-sensitive hence, is difficult to characterize. Care is taken to ensure the intermediate product is not exposed to air when transitioning from step 1 to 2 in the process. However, in order to run XRD on the intermediate product, kapton tape was used to ensure the sample is not exposed to air while testing. The pattern is shown in Figure 4-25. The WPF refinement indicates 6 nm crystallites of $\text{Mo}_2\text{N}_{0.92}$ (PDF #01-076-6129).

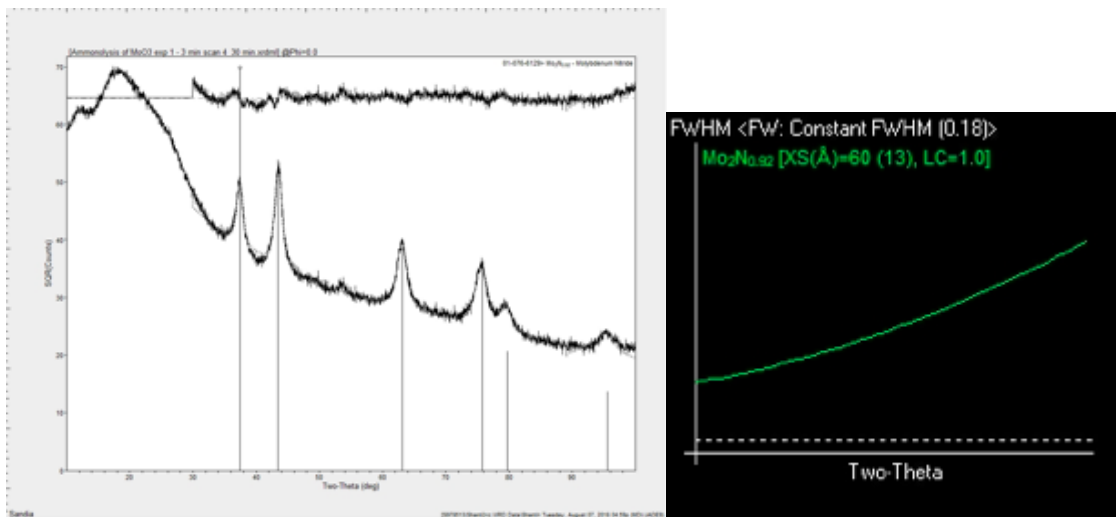


Figure 4-25. X-ray diffraction pattern of samples post-ammonolysis (a) treatment.

A combination of ammonolysis protocol (a) and methane treatment (a) yielded nanomaterials that had not been entirely carburized. This is shown by the X-ray diffraction pattern in Figure 4-26. The WPF refinement shows the sample is composed of oxides, Mo_4O_{11} and MoO_2 and nitride, Mo_3N_2 . These oxides are most likely the intermediates of the ammonolysis and methane treatments.

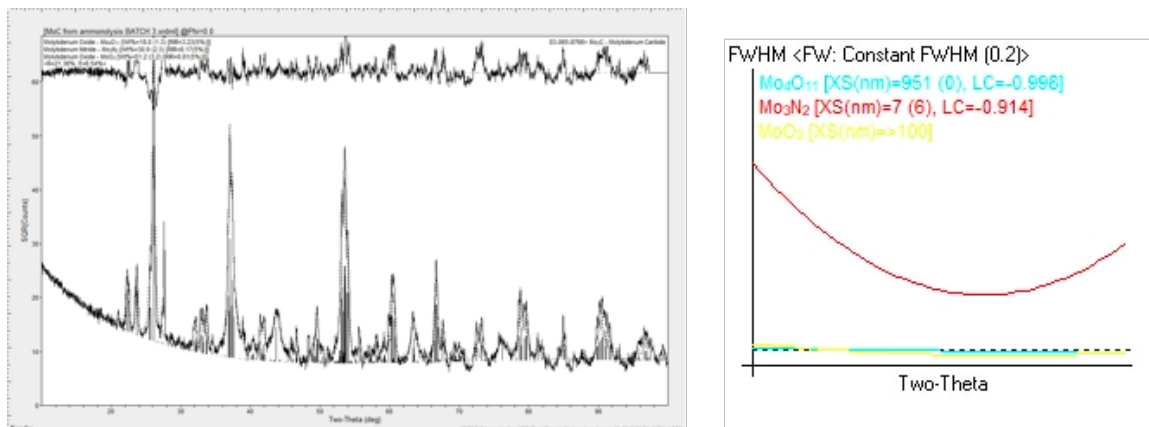


Figure 4-26. (Left) X-ray diffraction pattern of samples after ammonolysis protocol (a) and methane treatment (a). (Right) The WPF fit showing crystallite sizes of Mo_4O_{11} , Mo_3N_2 and MoO_2 .

A combination of ammonolysis treatment (b) and methane treatment (b) yielded molybdenum carbide nanoparticles as seen via X-ray diffraction pattern in Figure 4-27. These routes produce 7.3 nm crystallites of cubic MoC (~97%) and 17 nm crystallites of hexagonal MoC (~3%).

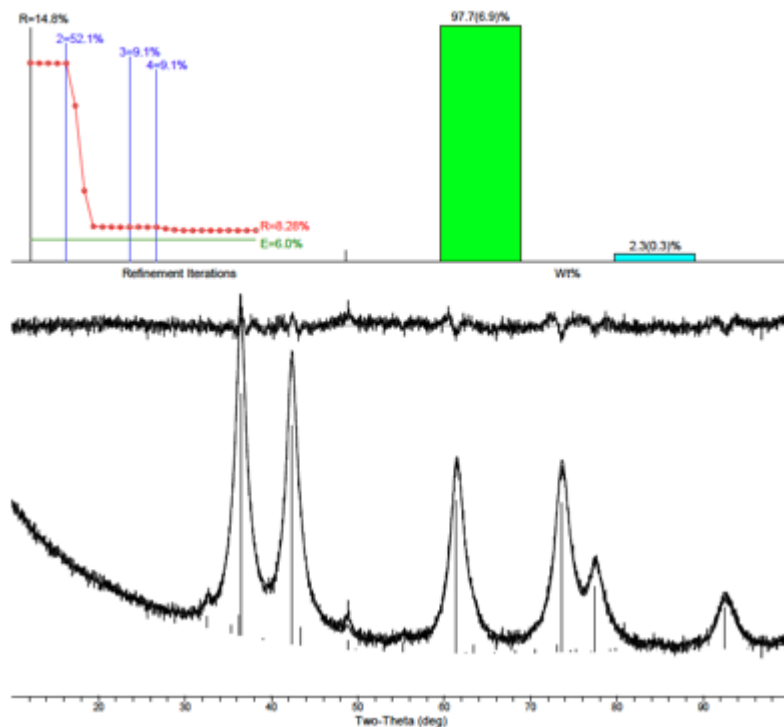


Figure 4-27. X-ray diffraction pattern of samples after ammonolysis protocol (b) and methane treatment (b).

Scanning electron microscopy was done on the samples and is shown in Figure 4-28. The atomic percentages from EDS analysis are also shown alongside in Table 4-5. These analyses show around 30 atomic % of Mo which is almost twice as that of high surface area MoC prepared via Ion Exchange Synthesis protocol discussed in Section I of this chapter. The oxygen atomic percent is low as well indicating there is little possibility of an oxycarbide or oxynitride formed. Moreover, the absence of a broad peak in the low angles ($\sim 23^\circ$) in the diffraction pattern (Figure 4-28) indicates the absence of excess amorphous carbon. This in combination with EDS analyses show there is much less excess carbon in this carbide sample as compared to that formed via Ion Exchange Synthesis protocol.

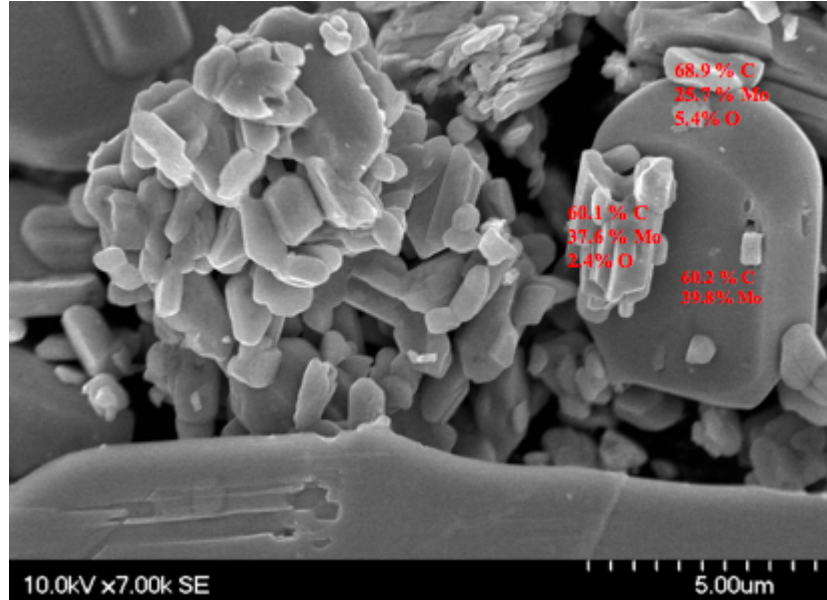


Figure 4-28. SEM image of sample after ammonolysis protocol (b) and methane treatment (b).

Element	C	O	Mo
Atomic %	68.62	0.86	30.52

Table 4-5. EDS analysis of sample after ammonolysis protocol (b) and methane treatment (b).

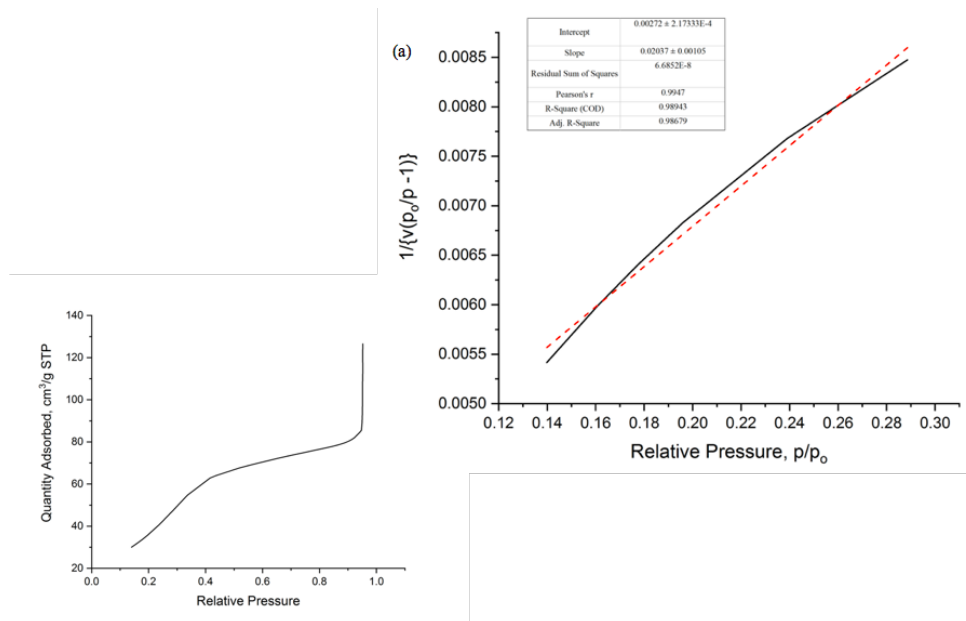


Figure 4-29. Adsorption studies of sample after ammonolysis protocol (b) and methane treatment

(b).

Surface area measurements were done on the sample via argon adsorption as shown in Figure 4-29. The surface area is around 180 m²/g, which matches reports in literature.

XPS analyses done on the sample and compared with molybdenum carbides obtained from the Ion Exchange Synthesis Protocol are shown in Figure 4-30.

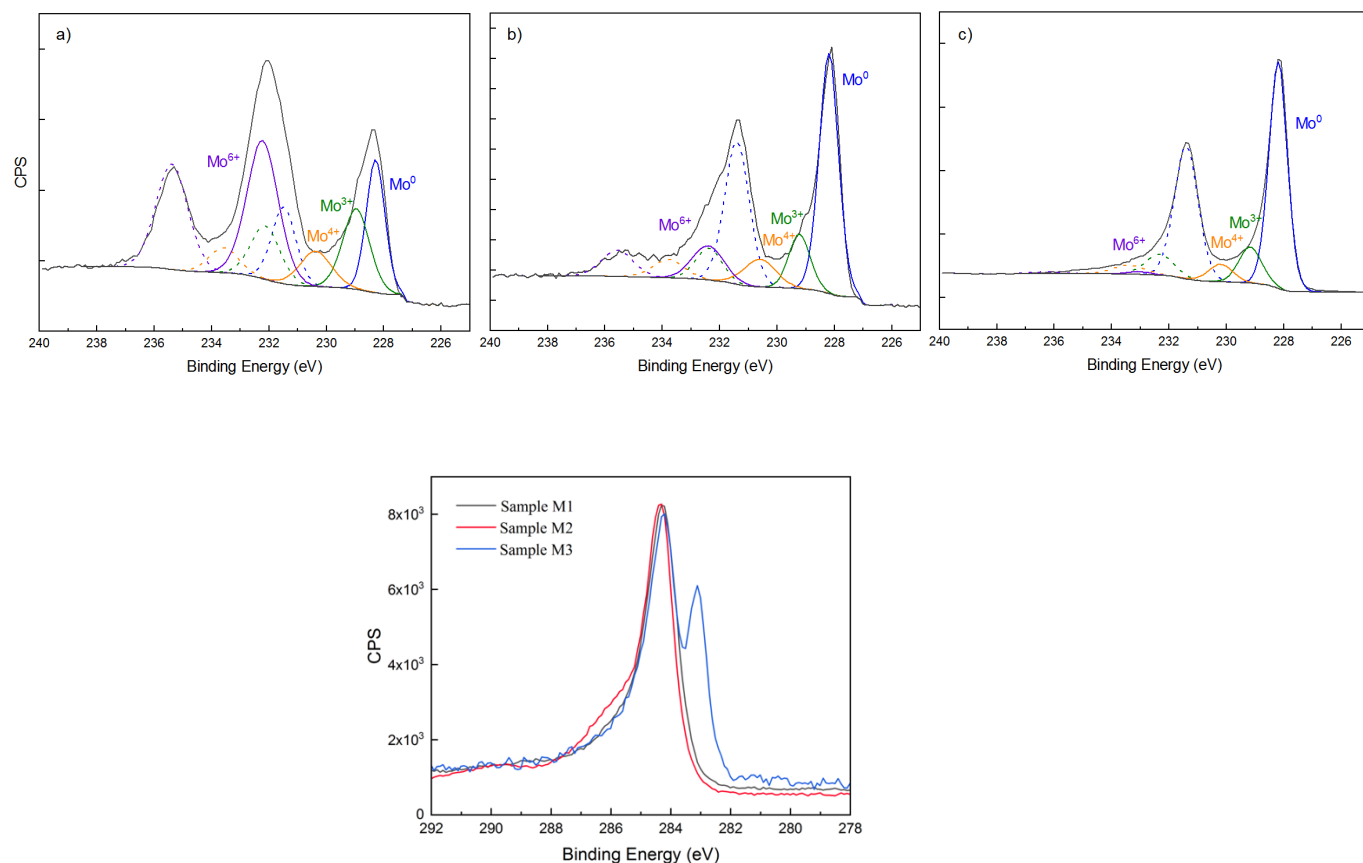


Figure 4-30. (Top) XPS analysis (Mo spectra) of molybdenum carbide samples (a) pyrolysis of exchanged resin (b) decarburized sample post-pyrolysis of exchanged resin and (c) molybdenum carbide from oxide precursor.

(Bottom) Comparison of C 1s spectra for three carbide samples prepared: Sample M1: pyrolysis of exchanged resin. Sample M2: decarburized sample post-pyrolysis of exchanged resin. Sample M3: molybdenum carbide from oxide precursor

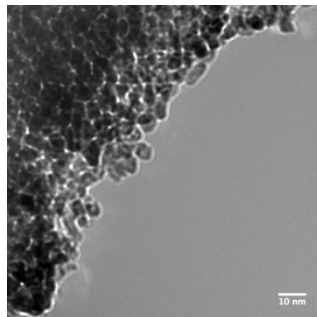


Figure 4-31. TEM micrograph of sample after ammonolysis protocol (b) and methane treatment (b).

It is known from XRD that there is no metallic molybdenum in the sample. As a result, the Mo^0 peak is used to characterize the Mo-C bond. The HRTEM micrograph in Figure 4-31 also further confirms that the particle size is around 8 nm.

4.3 Other characterization studies

Other characterization tests were carried out via Raman spectroscopy, FTIR, and conductivity measurements to understand the properties of the carbide nanomaterials synthesized using protocols I and II discussed in this chapter.

Raman spectroscopy and FTIR analyses were utilized to differentiate between the molybdenum carbide samples prepared via different methods in Ion Exchange Synthesis Protocol I and Protocol II.

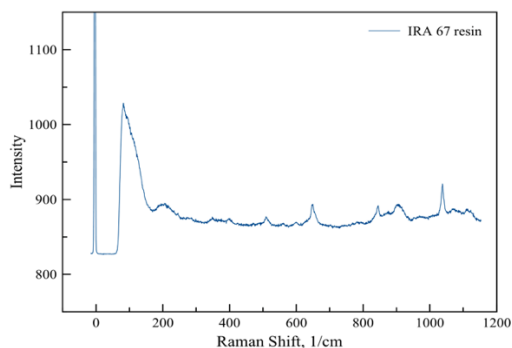


Figure 4-32. Raman spectrum of IRA 67 resin.

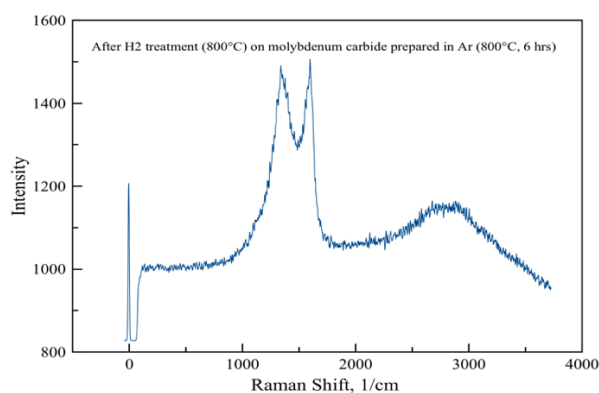
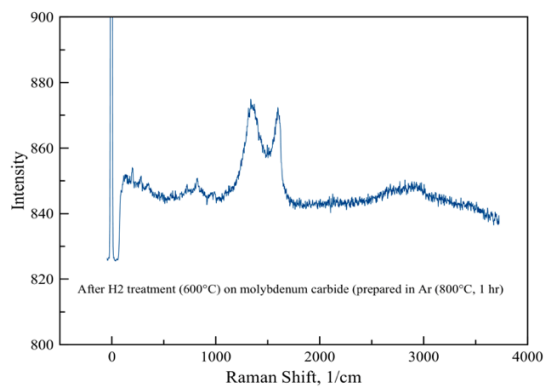


Figure 4-33. Raman spectrum of the sample after hydrogen treatment at 600 °C done on molybdenum carbide prepared in (top) Ar (800 °C, 1 hr) (bottom) Ar (800 °C, 6 hrs).

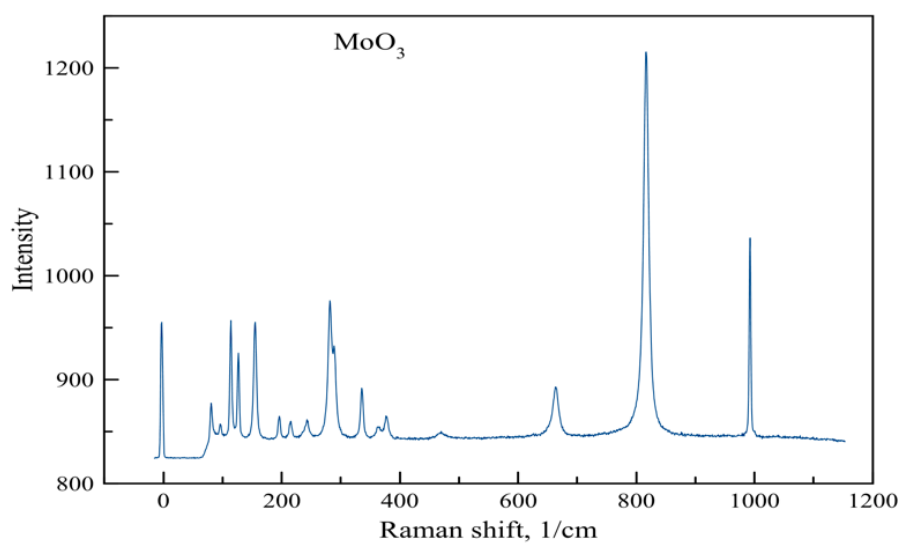


Figure 4-34. Raman spectrum of molybdenum oxide (precursor for Synthesis Protocol II).

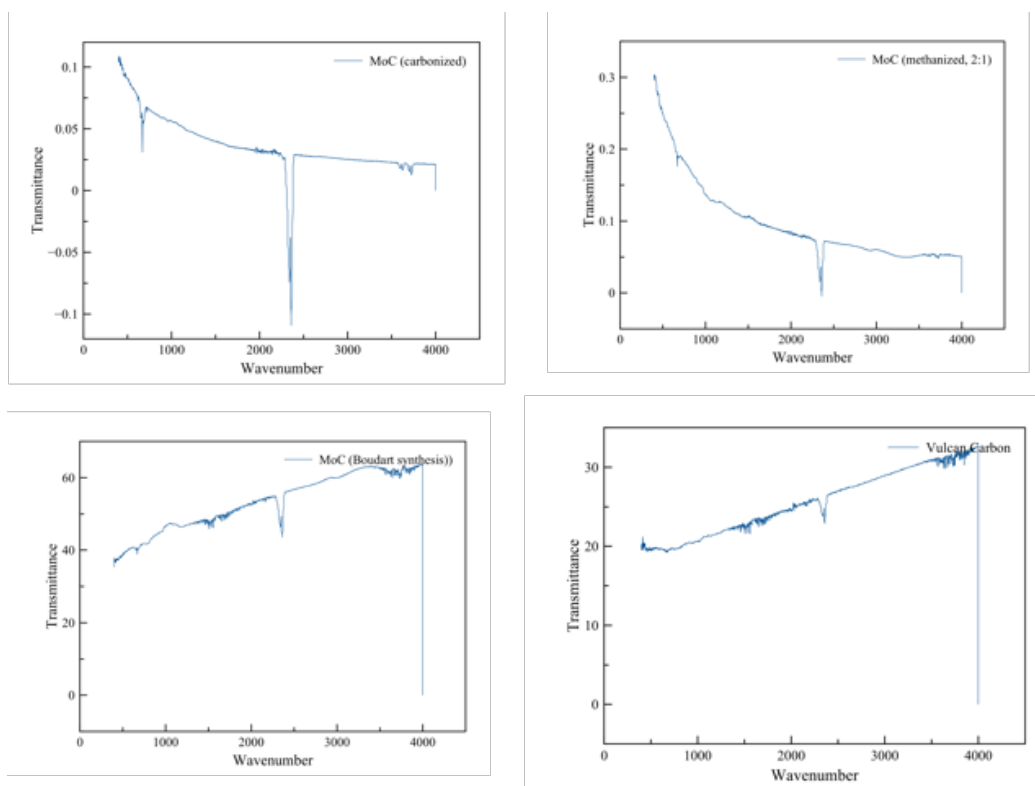


Figure 4-35. FTIR analyses done on molybdenum carbide samples prepared via various synthesis routes as well as Vulcan carbon.

These analyses look similar possibly due to the carbon in the samples and were therefore unsuccessful in differentiating between the properties of the carbide samples synthesized via different protocols.

Conductivity measurements were also done on the molybdenum carbide samples to ensure the synthesized nanomaterials are electrically conductive. In order to be effective catalysts for electrochemical reactions, the materials need to be electrically conductive. These measurements were done using 4 probe setup consisting of a copper foil and nickel rod. A constant current of 1 μA was applied and the voltage was measured.

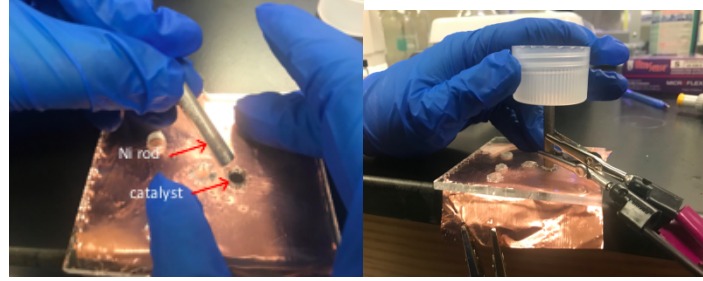


Figure 4-36. 4-probe conductivity measurement setup consisting of a copper foil and nickel rod. The results as shown in Table 4-6 and indicate that all molybdenum carbide samples synthesized have high electrical conductivity.

Sample Details	Conductivity
2 nm particles of cubic MoC in amorphous carbon (ion exchange synthesis)	28.71 S/m
MoC (2 nm; 360m ² /g; methanized CH ₄ :H ₂ = 2:1)	126.302 S/m
MoC (methanized CH ₄ :H ₂ = 1:5; sample consists of MoC, Mo ₂ C & amorphous and graphitic carbon)	24.28 S/m
MoC (synthesized by Synthesis Protocol II)	631.51 S/m
Sample with 46% Mo ₂ C + 40% graphitic carbon + 14% MoC	98.67 S/m

Table 4-6. Conductivity measurements of all molybdenum carbide samples.

4.4 Attempts to use molybdenum carbide as support for precious metals

In order to improve the catalytic properties of molybdenum carbide, attempts have been made to use it as a support for precious metals such as ruthenium and platinum.

a. Ru/carbon

Ruthenium deposited on Vulcan XC-72 carbon was prepared in order to help refine the synthesis parameters to deposit Ru on molybdenum carbide. The following methods were used:

* Incipient Wetness Method: 20 weight percent Ru/Vulcan XC-72 Carbon (~200 mg) was prepared using incipient wetness method. The RuCl_3 required to achieve 20 weight% metal loading was dissolved in sufficient ethanol to reach the saturation point of the support. This solution was then gradually added to the carbon support and dried at 100°C in between depositions. Around thirty such depositions were carried out in order to maximize the effect of the capillary action that draws the Ru solution into the pores of the carbon support. The catalyst was then reduced at 400°C in 2% H_2/N_2 for 2 hours at $1^\circ\text{C}/\text{min}$. Samples were also synthesized using lower number of depositions (~10) while retaining the amount of ruthenium precursor, which have either yielded bigger nanoparticles of Ru and/or lower weight loadings of Ru as shown in the characterization studies below.

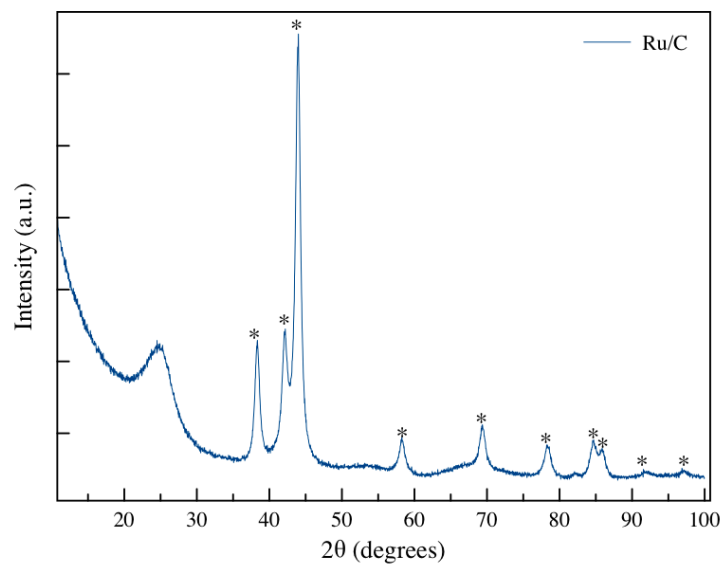


Figure 4-37. XRD pattern of Ru/C prepared via incipient wetness (10 depositions), ‘*’ represents hexagonal Ru.

Element	C	O	S	Cl	Ru
Weight %	81.78	6.64	0.36	0.49	10.73

Table 4-7. EDS analysis of Ru/C prepared via incipient wetness (10 depositions).

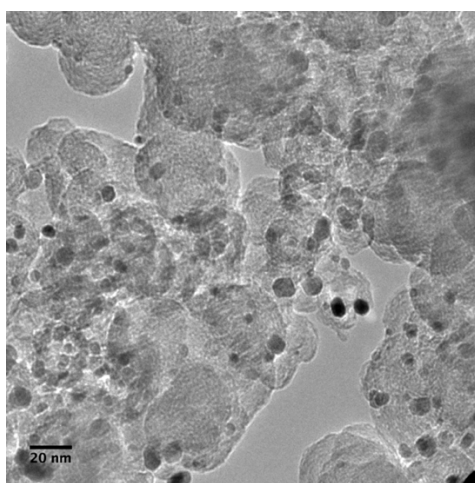


Figure 4-38. HRTEM micrograph of Ru/C prepared via incipient wetness (10 depositions).

Figure 4-37 (XRD analysis) shows 10 nm crystallites of Ru that is further iterated by HRTEM micrograph (Figure 4-38). Table 4-7 shows EDS analysis which indicates around 11 weight% of Ru in the sample.

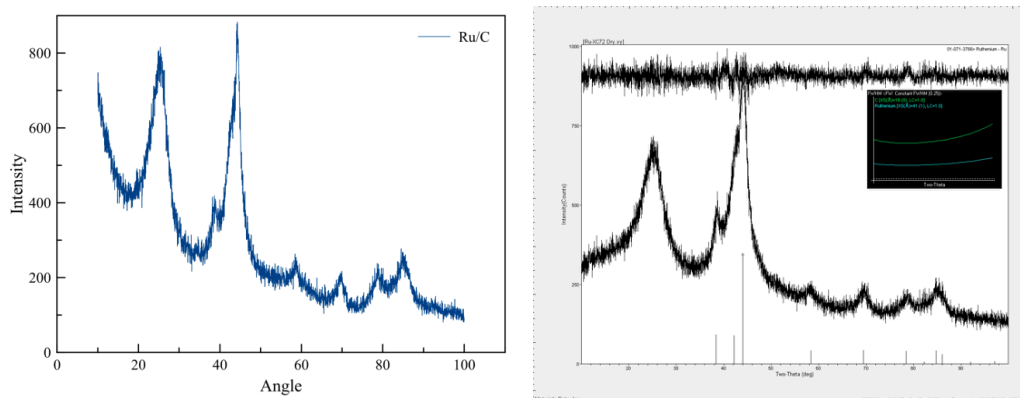


Figure 4-39. XRD pattern of Ru/C prepared via incipient wetness (30 depositions) (left). WPF fit showing 10 nm crystallites of Ru. (Right).

X-Ray diffraction analysis of Ru/C prepared via incipient wetness (30 depositions) is shown in Figure 4-39. The WPF refinement indicates ~ 4 nm crystallites of Ru. Scanning electron microscopy images of the same are shown in Figure 4-40 which indicate a similar particle size. EDS analyses shown in Table 4-7 indicate 19.5 wt% Ru which was the aim of the synthesis process.

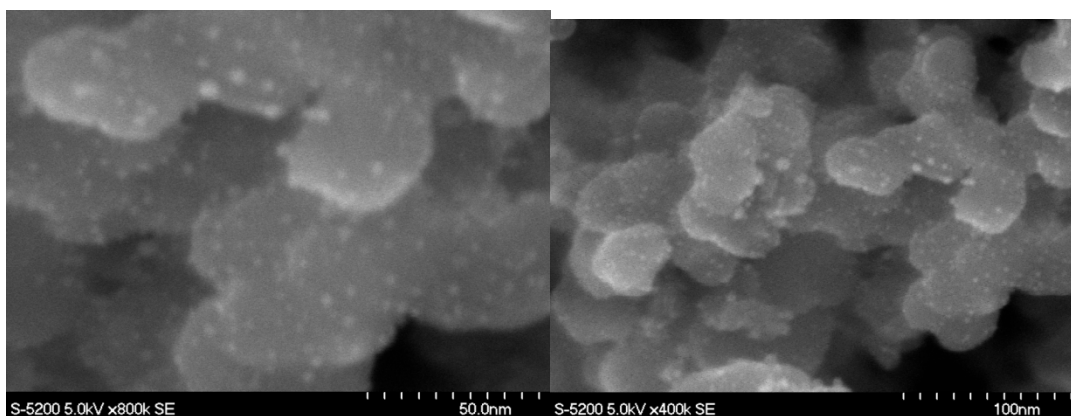


Figure 4-40. SEM images of Ru/C prepared via incipient wetness (30 depositions).

Element	C	Ru	O	S	Cl
Wt %	76.8	19.5	2.76	0.85	0.25

Table 4-8. EDS analysis of Ru/C prepared via incipient wetness (30 depositions).

*Wet Impregnation Method: Ruthenium chloride was added to a solution of DI water and ethanol (1:1, v/v), added to the carbon support and dried at 100 °C for 4 hours. It was then reduced in 2% hydrogen for 2 hours at 400 °C at 1°C/min. The XRD pattern shown in Figure 4-41 shows prominent peaks of carbon.

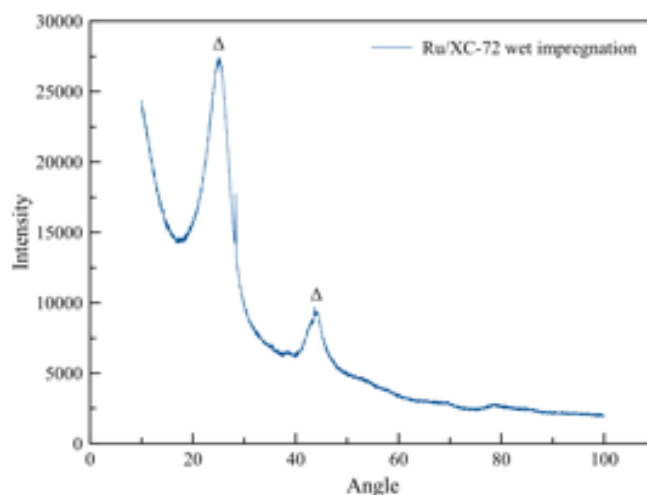


Figure 4-41. XRD pattern of Ru/C synthesized via wet impregnation method (Δ indicates carbon peaks)

*Polyol Synthesis: A polyol-glycol reduction method was attempted to synthesize Ru/C. The X-ray diffraction pattern of the same is shown in Figure 4-42. The method yielded 2 nm crystallites of Ru, however, the weight percent of Ru was 12%, which is considerably lower than the required weight loading.

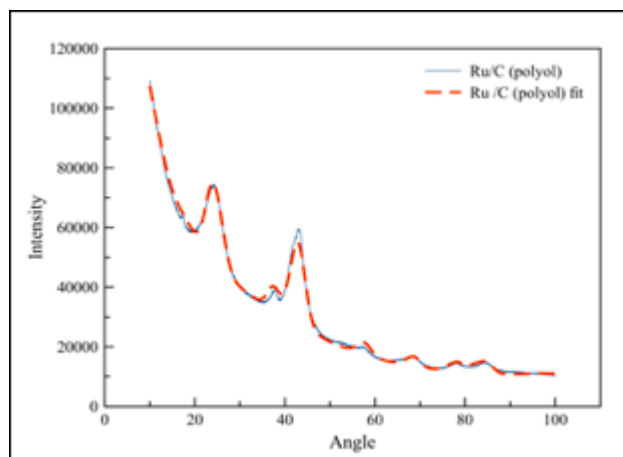


Figure 4-42. XRD pattern of Ru/C prepared via polyol method.

b. Ru/MoC synthesis

Methods of incipient wetness and wet impregnation were used to synthesize Ru/MoC. High surface area molybdenum carbide prepared via Ion Exchange Synthesis Protocol I was used for the deposition technique.

*Incipient Wetness: Using this process, RuCl_3 required to achieve 10 weight% metal loading was dissolved in sufficient DI water to reach the saturation point of the support which was found to be $0.7 \mu\text{L}/\text{mg}$ of MoC. This solution was then gradually added to $\sim 90 \text{ mg}$ MoC support in $10\text{-}20 \mu\text{L}$ aliquots and dried at 100°C in between depositions. The catalyst was then reduced at 400°C in $2\%\text{H}_2/\text{N}_2$ for 2 hours at $1^\circ\text{C}/\text{min}$. Figure 4-43 shows the XRD diffraction pattern and WPF refinement fit details. The WPF refinement indicates around 16 nm crystallites of Ru whereas the crystallite size of MoC nanoparticles is retained (2-3 nm).

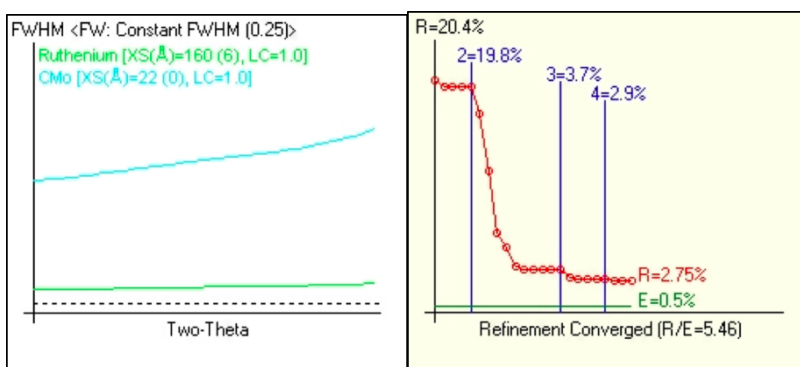
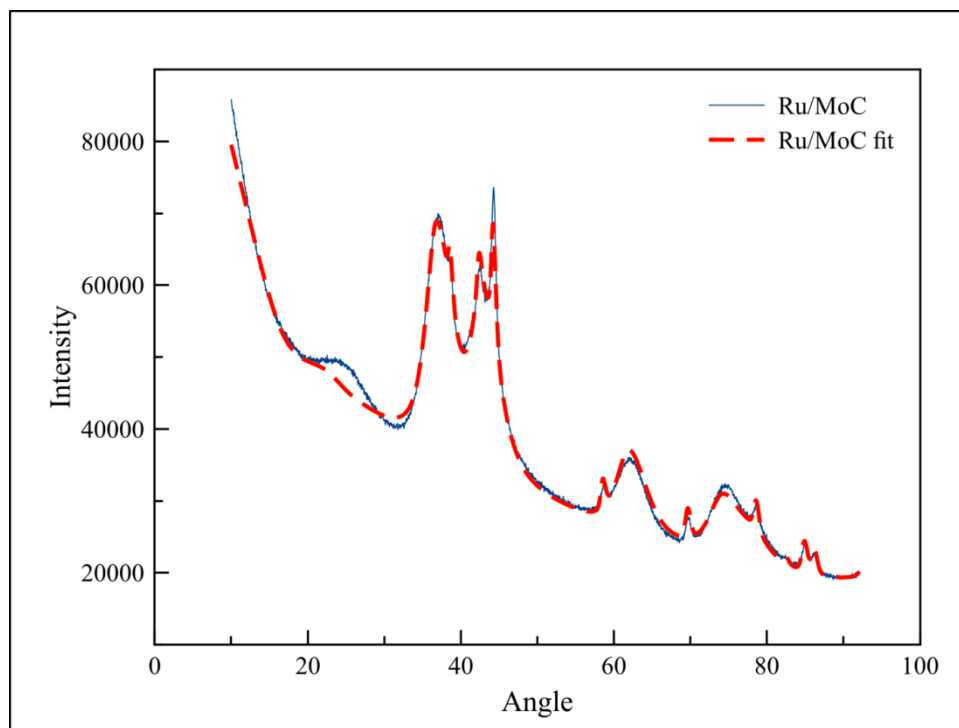


Figure 4-43. XRD pattern of Ru/MoC prepared via incipient wetness method.

Elements	C	O	Mo	Ru
Wt%	70.17	8.81	13.96	7.07

Table 4-9. EDS analysis of Ru/MoC prepared via incipient wetness method.

EDS analysis of sample shown in Table 4-9 indicates around 7 weight percent of Ru. While the metal loading was close to the desired quantity, the Ru crystallite size is bigger than that in Ru/C samples prepared via the same method.

*Wet impregnation method: The wet impregnation method involved dissolving the RuCl₃ required for the same metal loading (10 weight percent) in water: ethanol (1:1, v/v) and adding it to the MoC support. The catalyst was dried at 100°C for four hours. It was then reduced at 400°C in forming gas for 2 hours at 1°C/min. The XRD analysis shown in Figure 4-44 indicates crystallite sizes of 40 nm (Ru) and 2.6 nm (MoC).

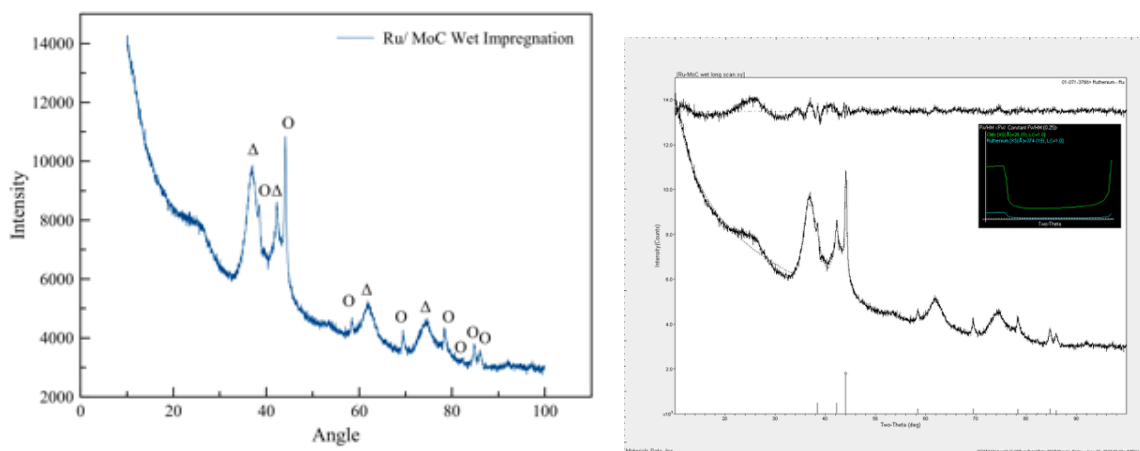


Figure 4-44. (Left) XRD pattern of Ru/MoC prepared via wet impregnation ('Δ' indicates MoC and 'O' indicates Ru). (Right) WPF of diffraction pattern showing 2.6 nm of MoC and 40 nm Ru.

c. Pt/MoC synthesis

The Pt based catalysts were prepared via wet impregnation synthesis. The metal precursor, chloroplatinic acid (H₂PtCl₆) for 20 wt%, was dissolved in DI water and formic acid. The MoC was added to the solution and sonicated for 15 minutes. The solution was left stirring overnight at 50°C before being washed with DI water and isopropanol. The XRD analysis and WPF refinement shown in Figure 4-45 and they indicate about 25 nm crystallites of Pt and 3 nm crystallites of MoC. The SEM micrograph as shown in Figure 4-46 indicates a uniform distribution of Pt nanoparticles.

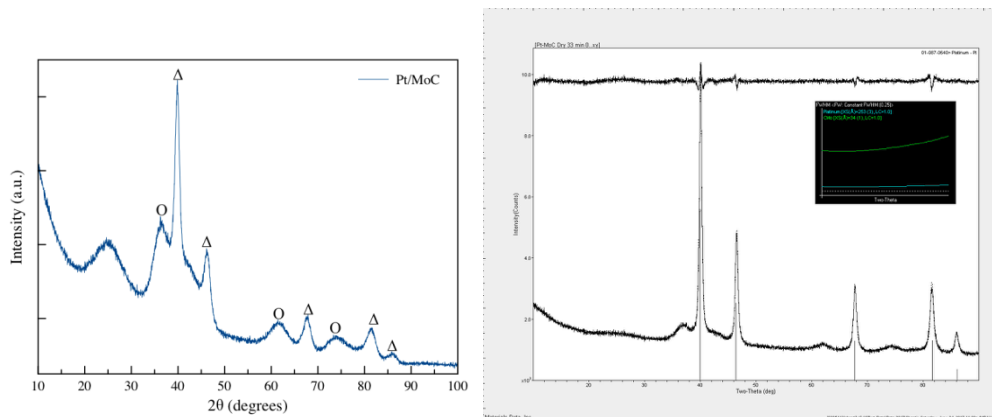


Figure 4-45. XRD pattern of Pt/MoC.

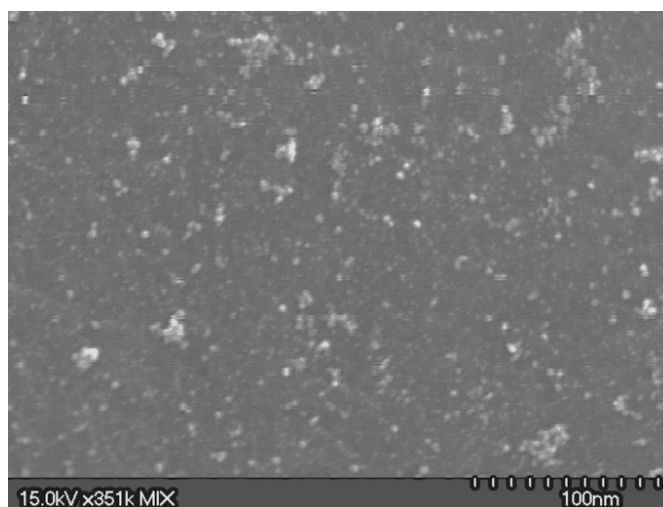


Figure 4-46. SEM micrograph of Pt/MoC.

4.5 Summary

This chapter shows the significance of the thermochemical analyses when developing synthesis methods to produce single carbide phase cubic MoC. The molybdate is ion exchanged for hydroxide ions within a quaternary ammonium divinylbenzene polystyrene anion exchange resin. The ion exchange resin acts as carbon source and importantly it provides a uniform dispersion of the molybdenum decreasing particle size growth. The pyrolysis of the ion exchanged resin leads to the formation of 2-3 nm particles of cubic MoC surrounded by excess carbon. Different pyrolysis conditions lead to the formation of different phases of the carbide reiterating the fact that

the cubic MoC is the metastable phase at temperatures below ~ 1200 °C while the hexagonal Mo₂C is the thermodynamically stable phase. The thermodynamically calculated ratios of partial pressures in Chapter 3 were used to reduce the content of excess carbon and improve access to the active phase of the sample, which is 2 nm particles of cubic MoC. The result is a vast increase in surface area from 5.6 m²/g to 360 m²/g, which is the highest surface area reported in literature so far. However, it is unknown what fraction of the high surface area is because of the carbon. Another synthesis process reported in Chapter 4 is that of Lee et al. The synthesis conditions yielded MoC nanoparticles with a surface area of around 180 m²/g. A comparison of molybdenum carbides synthesized by both processes leads to the following conclusions:

- Sample from the ion-exchange process has single-carbide phase MoC (2 nm particles) with a considerable amount of excess carbon (even after the decarburization treatment) and a high surface area of 360 m²/g.
- Sample from the second method has a mix of cubic and hexagonal phases of MoC (7 nm particles) with much less excess carbon but with about half the surface area as former ~ 180 m²/g.

This chapter also shows the attempts to utilize MoC as a support. While the experiments to synthesize Ru/C were successful, similar protocols with MoC did not yield similar results. However, the Pt has been successfully deposited on MoC as observed in the chapter.

The results of this study have been published in:

Nayak, Benavidez, Garzon. Facile Synthesis of High Surface Area Molybdenum Carbide Nanoparticles. J Am Ceram Soc. 2019; 102. 3738–3744.

REFERENCES

1. He G, Yan Z, Ma X, Meng H, Shen PK, Wang C. A universal method to synthesize nanoscale carbides as electrocatalyst supports towards oxygen reduction reaction. 2011;3(9):3578.
2. NIST X-ray Photoelectron Spectroscopy Database. National Institute of Standards and Technology.
3. Baltrusaitis J, Mendoza-Sanchez B, Fernandez V, Veenstra R, Dukstiene N, Roberts A, et al. Generalized molybdenum oxide surface chemical state XPS determination via informed amorphous sample model. 2015;326:151–61.
4. Kabir S, Lemire K, Artyushkova K, Roy A, Odgaard M, Schlueter D, et al. Platinum group metal-free NiMo hydrogen oxidation catalysts: high performance and durability in alkaline exchange membrane fuel cells. 2017;5(46):24433–43.
5. Scanlon DO, Watson GW, Payne DJ, Atkinson GR, Egdell RG, Law DSL. Theoretical and Experimental Study of the Electronic Structures of MoO₃ and MoO₂. 2010;114(10):4636–45.
6. Lee JS, Oyama ST, Boudart M. Molybdenum Carbide Catalysts. 1987;106:125–33.

Chapter 5: Investigation of Electrochemical Properties

As seen in Chapter 1, past studies relating to development of molybdenum carbide are often rampant with synthesis procedures yielding materials with contaminants and incomplete characterization studies leading to incorrect phase analysis of the carbide. As a result, there is very little or no information regarding the stabilities of different phases of the carbide under varying conditions of pH, cell potential, and temperature. Such studies dealing with the stabilities of the carbide are absolutely required in order to develop molybdenum carbide as an electrocatalyst or support in the commercial setting. In this chapter, the electrochemical characteristics of different samples of molybdenum carbide (synthesized in Chapter 4 and reported in (1)) are analyzed.

Cyclic voltammetry experiments were carried out using the parameters explained in Chapter 2. These experiments were carried out in 0.5M sulfuric acid solution, and the electrolyte solution was degassed with a steady flow of argon into the cell. Argon was chosen because molybdenum carbides chemisorb nitrogen as observed in Chapter 4. The materials tested are indicated by sample codes shown in Table 5-1.

Studies done here the stability of molybdenum carbide samples under varying conditions of pH, temperature, and cell potential. These studies provided a theoretical basis for the measurements. These studies were vital in performing cyclic voltammetry on the different carbide samples synthesized, which then showed how electrochemical characteristics vary with respect to properties such as particle size, surface area and excess carbon content.

Sample Code	Synthesis Route	Properties
M1	MoC prepared via pyrolysis of ion exchanged resin (ammonium molybdate and IRA 67) in an inert atmosphere at 800°C.	Single carbide phase cubic MoC, low surface area (~10 m ² /g), high carbon
M2	Decarburization via methanization of Sample M1 in a mix of hydrogen and methane at 800°C	Single carbide phase cubic MoC, high surface area (~330 m ² /g), less carbon than M1
M3	Ammonia treatment of MoO ₃ followed by methane treatment of the nitride formed in the first step.	Much less carbon than both M1 and M2. Surface area ~180 m ² /g
Ru/C	Incipient wetness deposition method	20 weight% Ruthenium on Vulcan XC-72 carbon. 4 nm crystallites of Ru.
Carburized Resin	Amberlite IRA 67 resin was heated in nitrogen to 800°C at 10°C/min for 1 hour.	Carbon

Table 5-1. Samples and their corresponding synthesis routes and properties for cyclic voltammetry measurements.

It has been established in (2) that oxidation and subsequent dissolution of the oxides is known to limit the performance of Mo_2C by decreasing its stability. Using HSC Chemistry (3) and quantum chemistry code VASP (4-8), the stabilities of cubic and hexagonal MoC phases were predicted here. It was observed in this study that a change in composition from Mo_2C to MoC in the hexagonal phases does not affect the stability. The oxidation of both carbides, Mo_2C and MoC to MoO_2 occurs at ~ -0.08 V vs SHE at ~ 0 pH. However, the cubic MoC was predicted to be less stable compared to its hexagonal counterparts. Based on consideration of thermodynamics it is concluded that at pH=0 the oxidation of cubic MoC to MoO_2 and graphite becomes thermodynamically favorable at -0.16 V vs SHE. The stability regions are also dependent largely on pH changes and not temperatures (in the range of 25 °C - 80 °C). Additionally, increase in pH decreases the stability regions by decreasing the oxidation potentials for -0.059 V per pH unit. This has been demonstrated in Figure 5-1 and Table 5-2.

Figure 5-1 provided regions of stability and instability for the cyclic voltammetry experiments carried out in the later section in this chapter. The investigation into the electrochemical stability of molybdenum carbide provides a roadmap for developing stable molybdenum carbide catalysts and supports for electrochemical reactions.

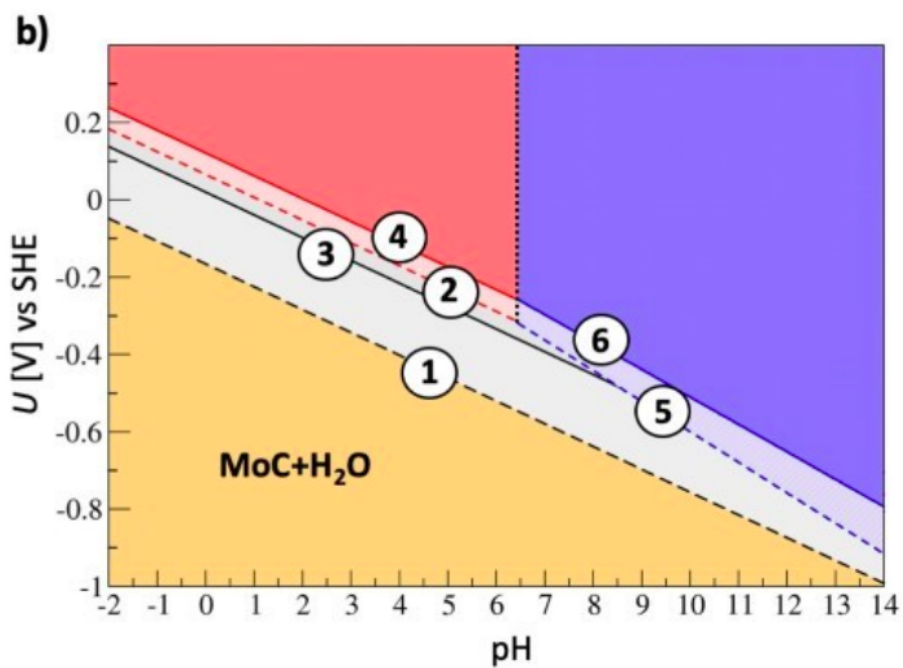


Figure 5-1. Stability regions of cubic MoC in water as a function of applied potential and pH at 25 °C. The lines correspond to the dependence of formation potential (vs SHE) on pH as listed in the Table 6-2. (1)

No	Process	Dependence of formation potential in V (vs SHE) on pH	
		hexagonal MoC	cubic MoC
1	$\text{MoC} + 2\text{H}_2\text{O} \rightarrow \text{MoO}_2 + \text{C} + 2\text{H}_2$	$U = -0.08 - 0.059\text{pH}$	$U = -0.16 - 0.059\text{pH}$
2	$\text{MoC} + 4\text{H}_2\text{O} \rightarrow \text{MoO}_2 + \text{CO}_2 + 4\text{H}_2$	$U = +0.07 - 0.059\text{pH}$	$U = +0.03 - 0.059\text{pH}$
3	$\text{MoC} + 3\text{H}_2\text{O} \rightarrow \text{MoO}_3 + \text{C} + 3\text{H}_2$	$U = +0.13 - 0.059\text{pH}$	$U = +0.07 - 0.059\text{pH}$
4	$\text{MoC} + 5\text{H}_2\text{O} \rightarrow \text{MoO}_3 + \text{CO}_2 + 5\text{H}_2$	$U = +0.17 - 0.059\text{pH}$	$U = +0.13 - 0.059\text{pH}$
5	$\text{MoC} + 4\text{H}_2\text{O} \rightarrow \text{MoO}_4^{2-} + \text{C} + 8\text{H}^+ + 6\text{e}^-$	$U = +0.24 - 0.079\text{pH}$	$U = +0.19 - 0.079\text{pH}$
6	$\text{MoC} + 6\text{H}_2\text{O} \rightarrow \text{MoO}_4^{2-} + \text{CO}_2 + 12\text{H}^+ + 10\text{e}^-$	$U = +0.23 - 0.071\text{pH}$	$U = +0.20 - 0.071\text{pH}$

Table 5-2. Stability regions of hexagonal and cubic MoC in water at 25 °C. (1)

Cyclic voltammetry experiments were carried out on three molybdenum carbide samples – the carbonized (low surface area) molybdenum carbide, the methanized (high surface area) molybdenum carbide and the molybdenum carbide from the oxide precursor.

5.1 Cyclic Voltammetry Experiments (Molybdenum Carbide from oxide precursor)

The electrochemical behavior of molybdenum carbide (from oxide precursor) with a loading of 1.12 mg/cm^2 was observed between the potentials of -0.1 V and -0.6 V vs SHE. The carbide shows an overpotential of -0.29 V vs SHE at a current density of -0.01 A/cm^2 . The cyclic voltammetry scans as well as the magnified sweeps in the negative direction are shown in Figure 5-2.

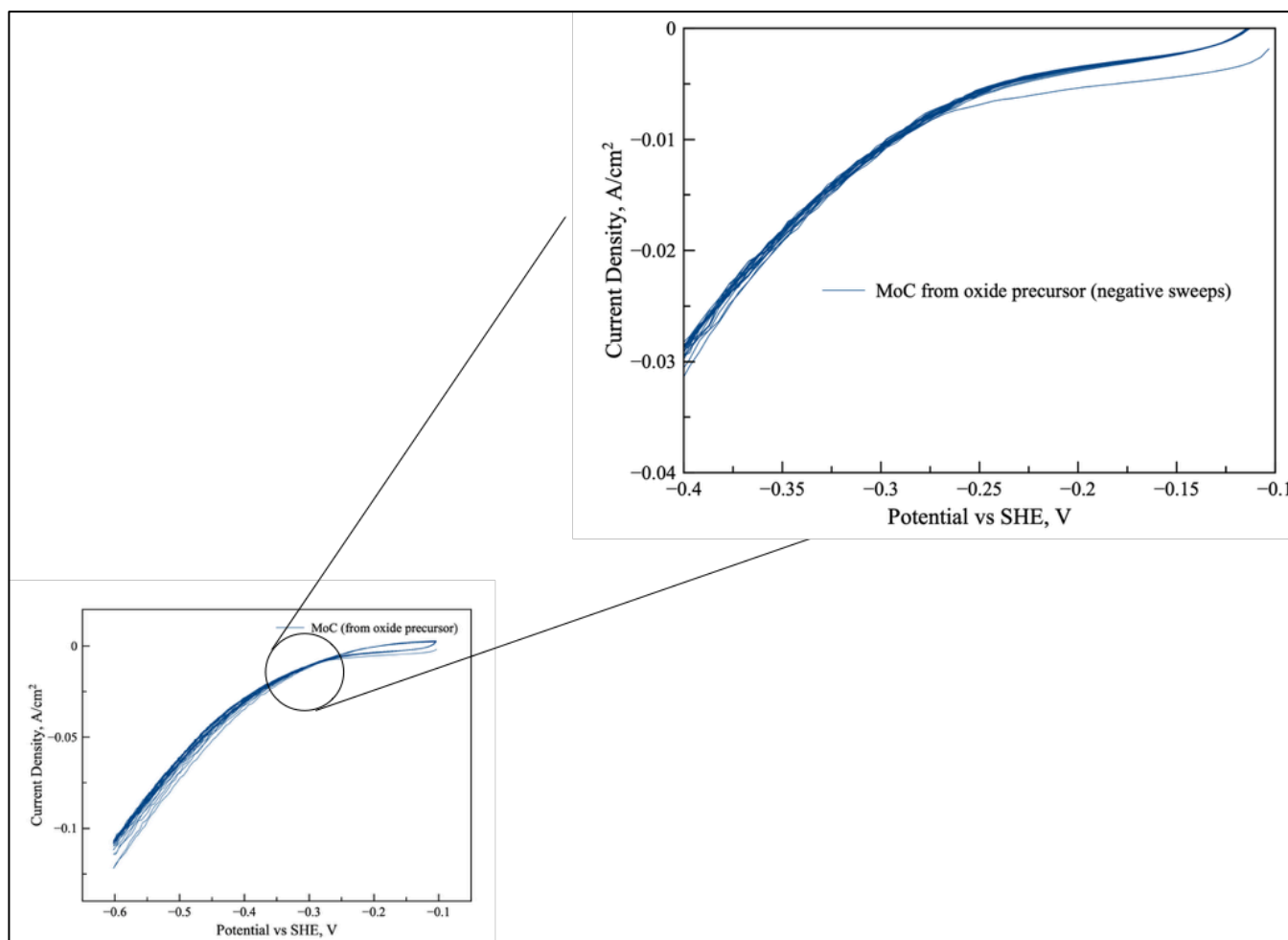


Figure 5-2. Cyclic Voltammetry scans (20 cycles) of Molybdenum carbide (from oxide precursor). Inset: Magnified figure of sweeps in negative direction.

Figure 5-2 also indicates that the carbide species is stable as the HER behavior does not vary with subsequent cycles.

In order to further test the stability of the molybdenum carbide samples, chronoamperometry experiments were carried out which involves holding the sample at a particular cell potential for a period of time. The cell potentials were chosen based on the theoretical stabilities reported earlier in this chapter. Figure 5-1 indicates that the molybdenum carbide 'MoC' species is stable at cell potential -0.1 V vs SHE (at pH = 0 and temperature of 25 °C). Similarly, a cell potential of 0.4 V is evidently in the instability region of the carbide. Therefore, the molybdenum carbide sample was held at -0.1 V and 0.4 V vs SHE for a period of sixty minutes prior to carrying out the cyclic voltammetry experiments (sweeps between the potentials of -0.1 V and -0.6 V vs SHE).

The CV obtained after holding the molybdenum carbide sample at -0.1 V is reported in Figure 5-3. At a current density of -0.01 A/cm², an overpotential of -0.29 V is observed. This is very similar to the overpotential observed in Figure 5-2 (MoC electrochemistry without any holds). Additionally, the cycles do not vary with subsequent samples which indicates that the carbide species is stable. These observations lead us to conclude that the electrocatalytic behavior of the carbide does not change when held at -0.1 V (vs SHE) for one hour.

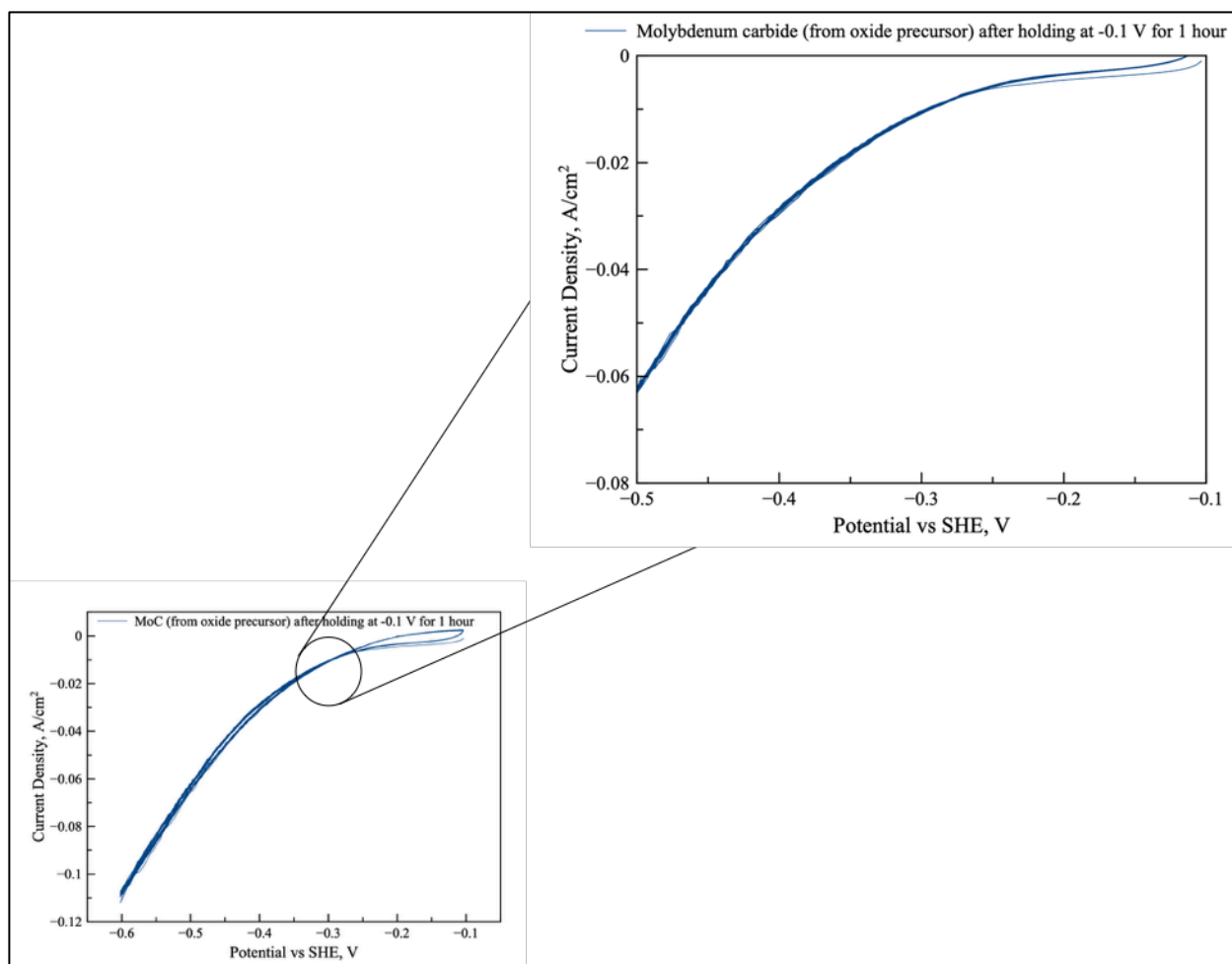


Figure 5-3. Cyclic Voltammetry scans (20 cycles) of Molybdenum carbide (from oxide precursor) after being held at -0.1 V for 1 hour. *Inset*: Magnified figure of sweeps in negative direction.

A similar hold was performed at 0.4 V, a thermodynamically deduced potential at which the molybdenum carbide species would be oxidized at ~ 0 pH. The results are shown in Figure 5-4.

At a current density of -0.01 A/cm^2 , an overpotential of -0.25 V is observed in the first cycle and -0.27 V in the later cycles. This is substantially different from that observed in Figures 5-2 and 5-3. Another key observation is that the first cycle looks different from the rest *i.e.* HER occurs at more negative potentials with subsequent cycles. This indicates that the chemistry of the carbide changed to an oxide when the carbide was held at 0.4 V for 1 hour. However, with constant

sweeping at negative potentials, the oxidized species was reduced leading to different HER potentials during subsequent cycles.

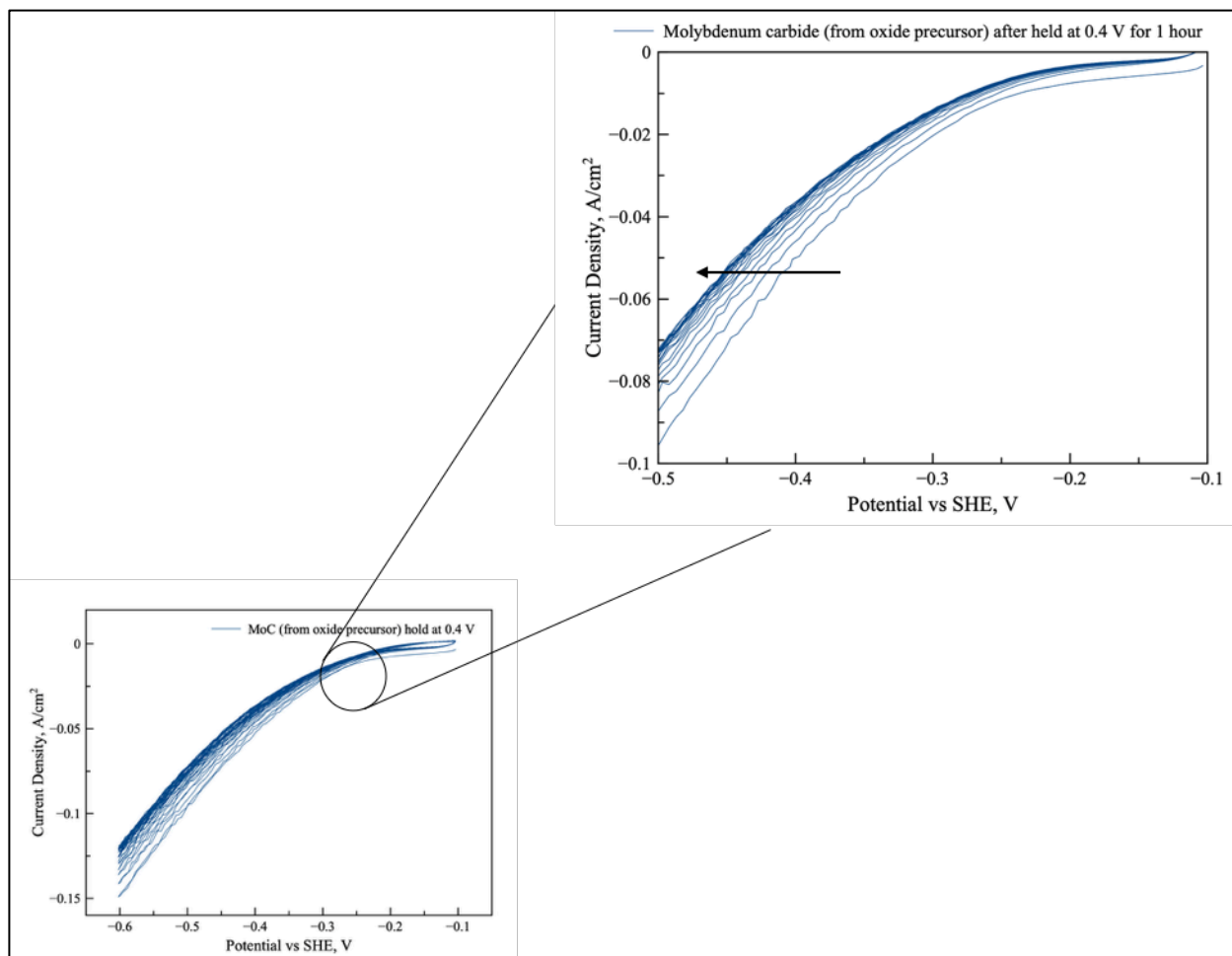


Figure 5-4. Cyclic Voltammetry scans (20 cycles) of Molybdenum carbide (from oxide precursor) after being held at 0.4 V for 1 hour. *Inset*: Magnified figure of sweeps in negative direction (arrow indicates direction of cycles from 1st to last).

The first cycles from CVs reported in Figures 5-2, 5-3 and 5-4 are shown in Figure 5-5. This further illustrates the fact that holding at -0.1 V does not change the chemistry of the carbide whereas a hold at 0.4 V oxidizes the carbide species. This again provides further proof to the theoretical calculations showing that positive potentials close to ~0.4 V are unstable conditions for the carbide to exist.

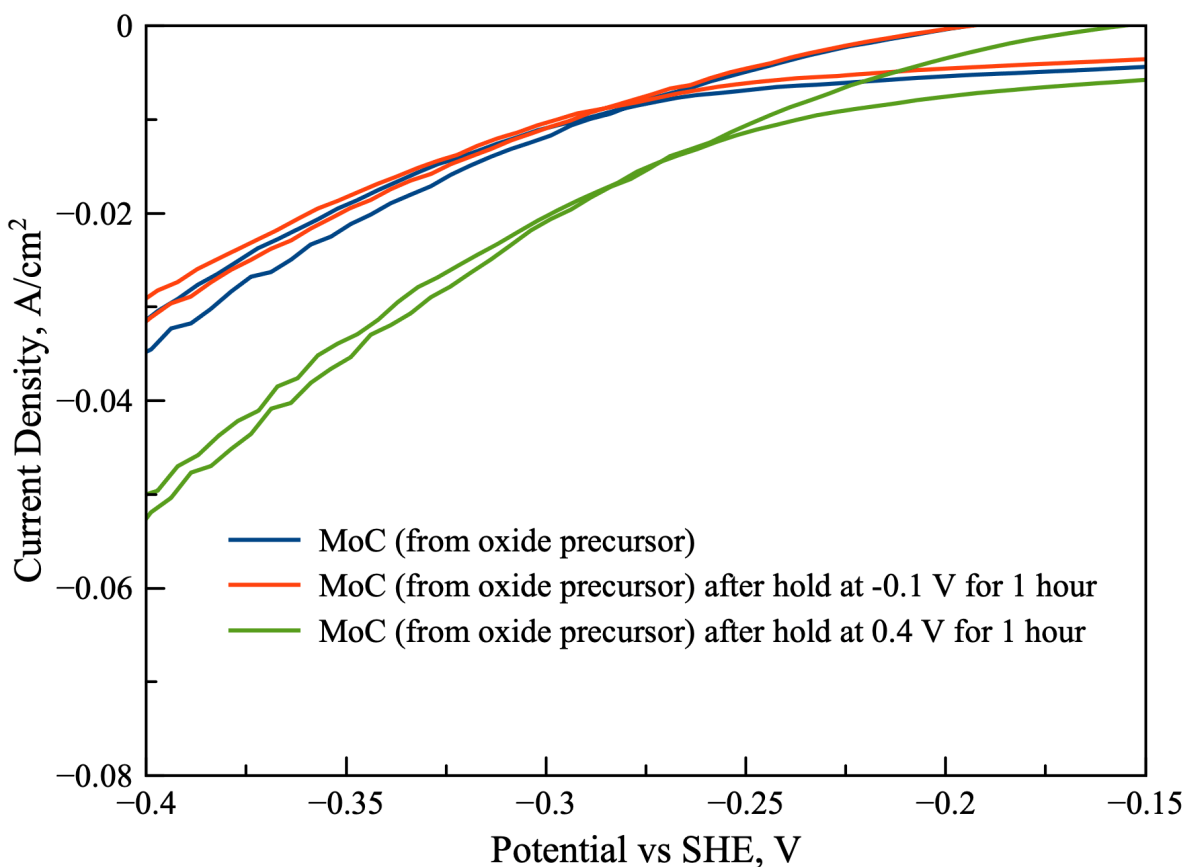


Figure 5-5. 1st cycles of CVs of MoC without any holds, MoC held at 0.1 V for 1 hour and MoC held at 0.4 V for 1 hour.

The surface chemistries of the carbide species were examined via XPS as well. The XPS studies were conducted post-mortem after holds at -0.1 V and 0.4 V for a period of 1 hour. The XPS studies like the CVs would examine only the first few layers of atoms (~5-10) of the carbide and therefore provide accurate information regarding the surface molybdenum, carbon and oxygen species.

The XPS results are shown in Figure 5-6. The analysis of the Mo 3d region was complicated by the presence of Nafion in the catalyst ink. Nafion contains sulfur which presents a 2s peak in the same energy region as Mo 3d. To account for this, a spectrum of Nafion was performed in the

same region as the catalyst samples. There is a broad peak at 234.1 eV that can be seen in Figure 5-7.

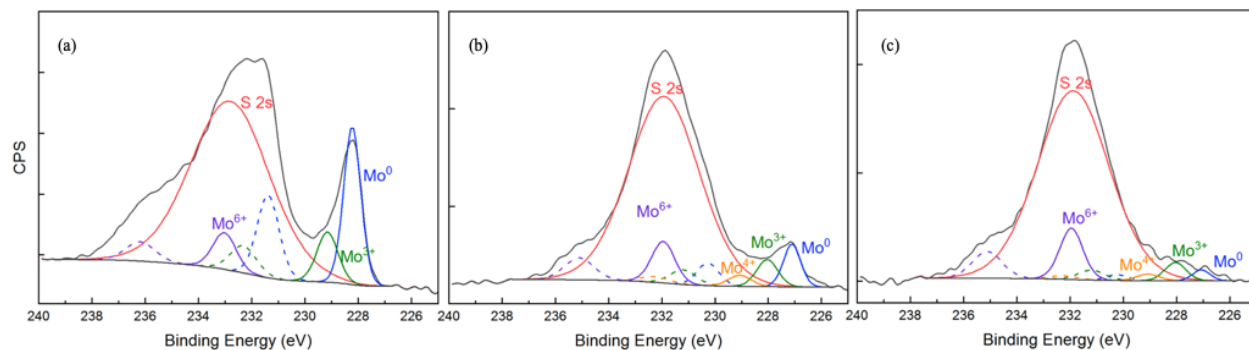


Figure 5-6. XPS analysis of (a) fresh molybdenum carbide sample mixed in Nafion before electrochemical measurements, (b) carbide sample post-mortem after being held at -0.1 V for 1 hour and (c) carbide sample post-mortem after being held at 0.4 V for 1 hour.

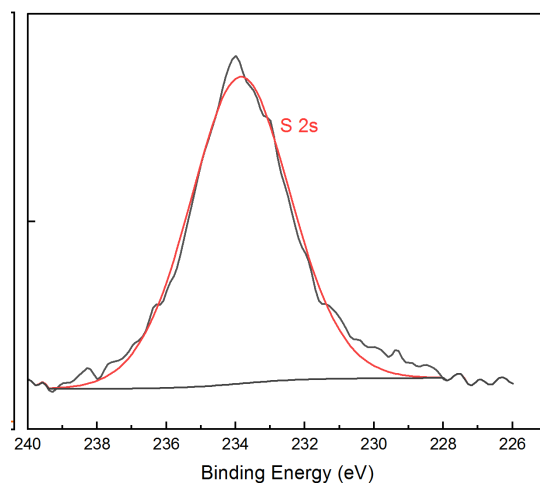


Figure 5-7. XPS analysis of Nafion.

This peak was used to account for the sulfur present in the catalyst samples and was used in the fitting of the spectra in Figure 5-6. The fresh catalyst sample shows a large amount of Mo^0 which we previously mentioned can be attributed to MoC . Figure 6-6c corresponds to molybdenum carbide sample after holding at 0.4 V (for 1 hour) and indicates that majority of the sample now

consists of Mo⁶⁺ which is attributed to the oxide species. This is further supported by quantification results from XPS shown in Table 5-3.

Sample	Mo ⁰ %	Mo ³⁺ %	Mo ⁴⁺ %	Mo ⁶⁺ %
MoC ink without any holds (a)	57.4	21.7	0.8	20.2
MoC after holding at -0.1 V for 1 hour (b)	30.4	25.2	11.8	32.5
MoC after holding at 0.4 V for 1 hour (c)	11.2	18.7	6.9	63.2

Table 5-3. Relative molybdenum compositions obtained from XPS analysis of fresh and post-mortem molybdenum carbide (from oxide precursor) sample.

The XPS results show that there is much more substantial oxidation of the carbide species when it is held at 0.4 V as compared to when held at -0.1 V. Thus, the XPS studies are in excellent agreement with the observations from the CVs.

5.2 Cyclic Voltammetry Experiments (Molybdenum Carbides from Ion Exchange Protocol)

Electrochemical measurements were carried out on the carbonized and methanized molybdenum carbide samples (sample codes M1 and M2 respectively from Table 5-1).

The CV scans for the carbonized sample are reported in Figure 5-8. The hydrogen onset sweeps to more negative values with each cycle. This is possibly due to the excess oxygen on the surface (as observed in XPS) which gets reduced when swept at negative potentials. This behavior is not observed in the molybdenum carbide from the oxide precursor. At a current density of -0.001 A/cm², an overpotential of -0.32 V is observed on the first cycle. On the later cycles when the molybdenum carbide species have stabilized, an overpotential of -0.35 V is observed at a current density of -0.001 A/cm². This variation is further illustrated in Figure 5-9 which shows the 1st and 20th (last) cycles of the CV scans shown in Figure 5-8.

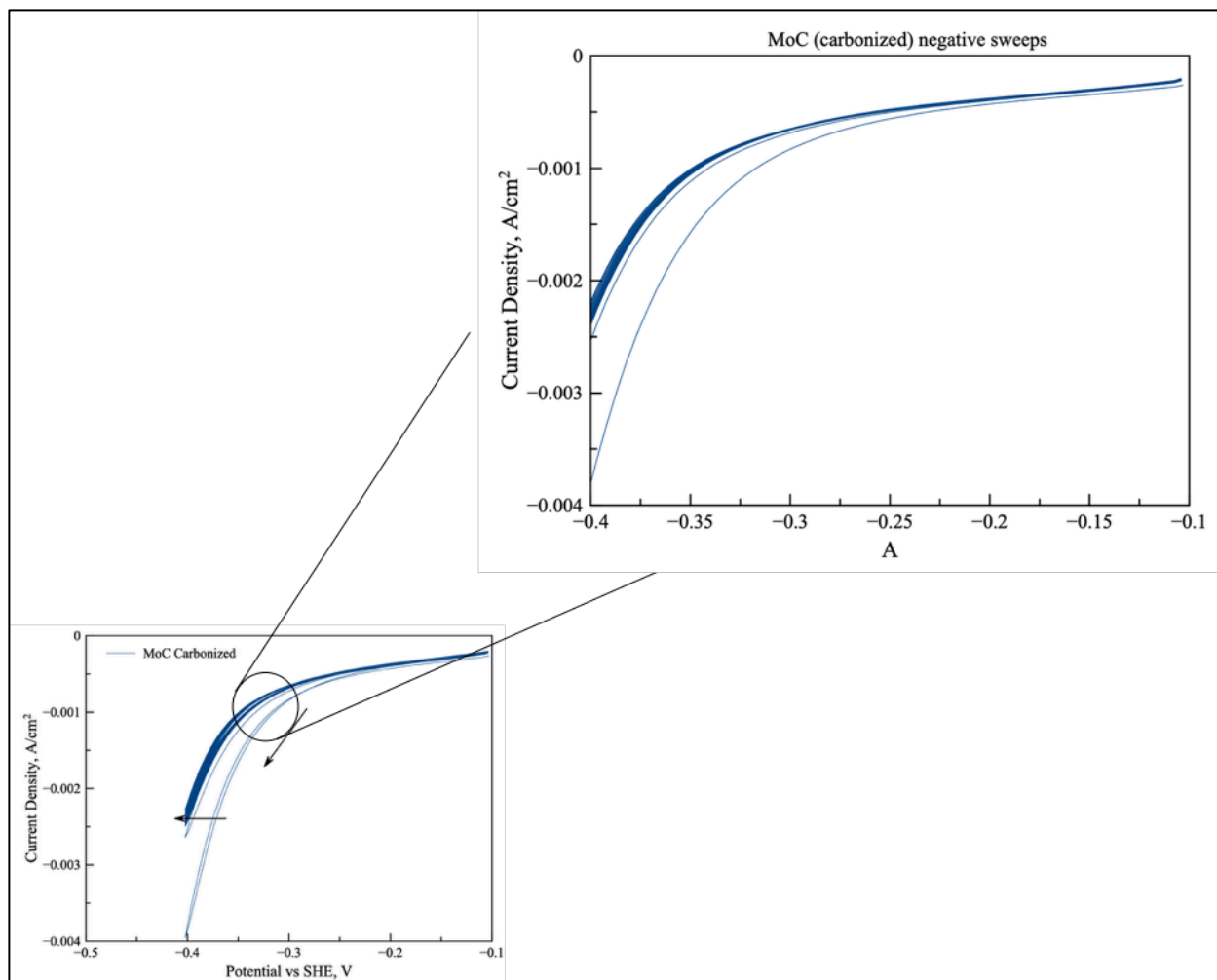


Figure 5-8. Cyclic Voltammetry scans (20 cycles) of Molybdenum carbide (carbonized) *Inset:*

Magnified figure of sweeps in negative direction.

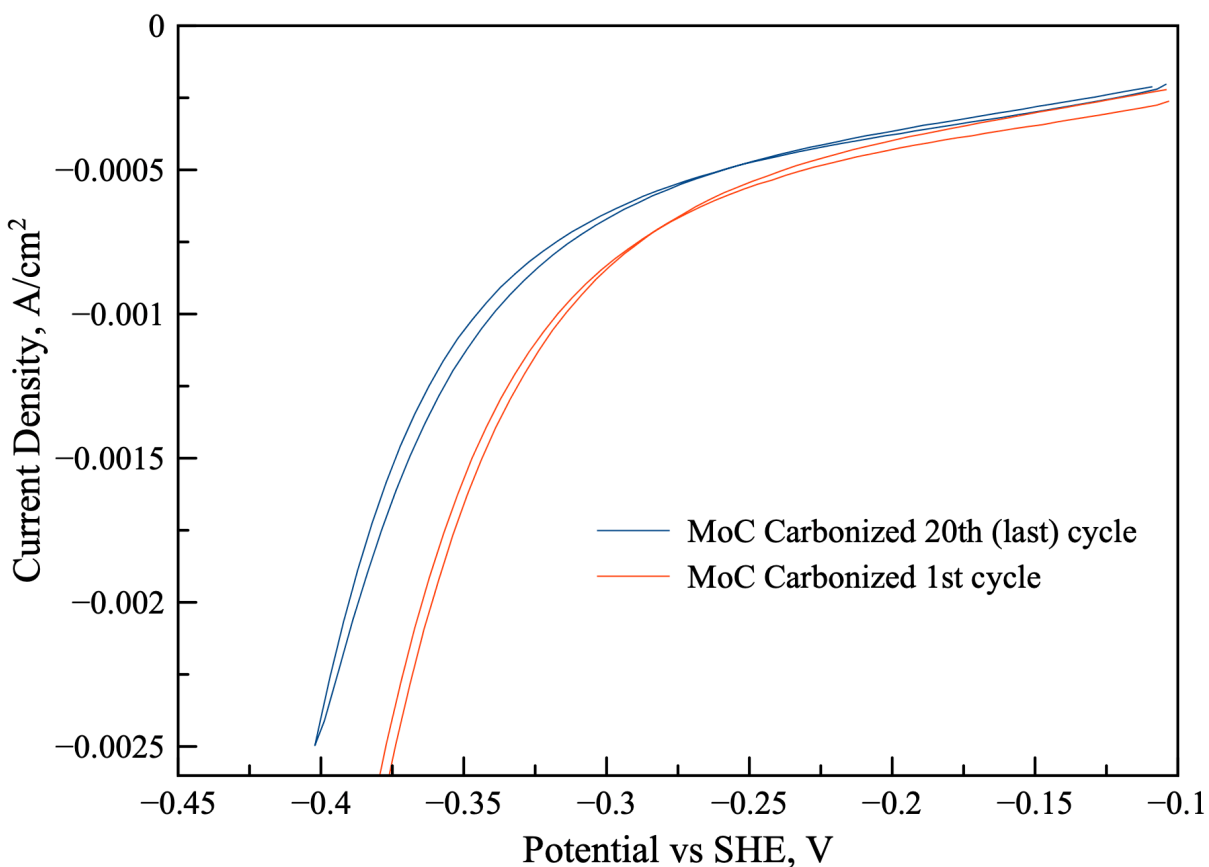


Figure 5-9. 1st and 20th cycles of CV done on molybdenum carbide (carbonized).

After the electrochemical behavior of the carbide species was stabilized, the potential was varied between 0.2 V and -0.4 V. This was done so as to compare the HER behavior of the 1st cycle of the CV (from Figure 5-8) and that obtained when swept at positive potentials. The results are shown in Figure 5-10.

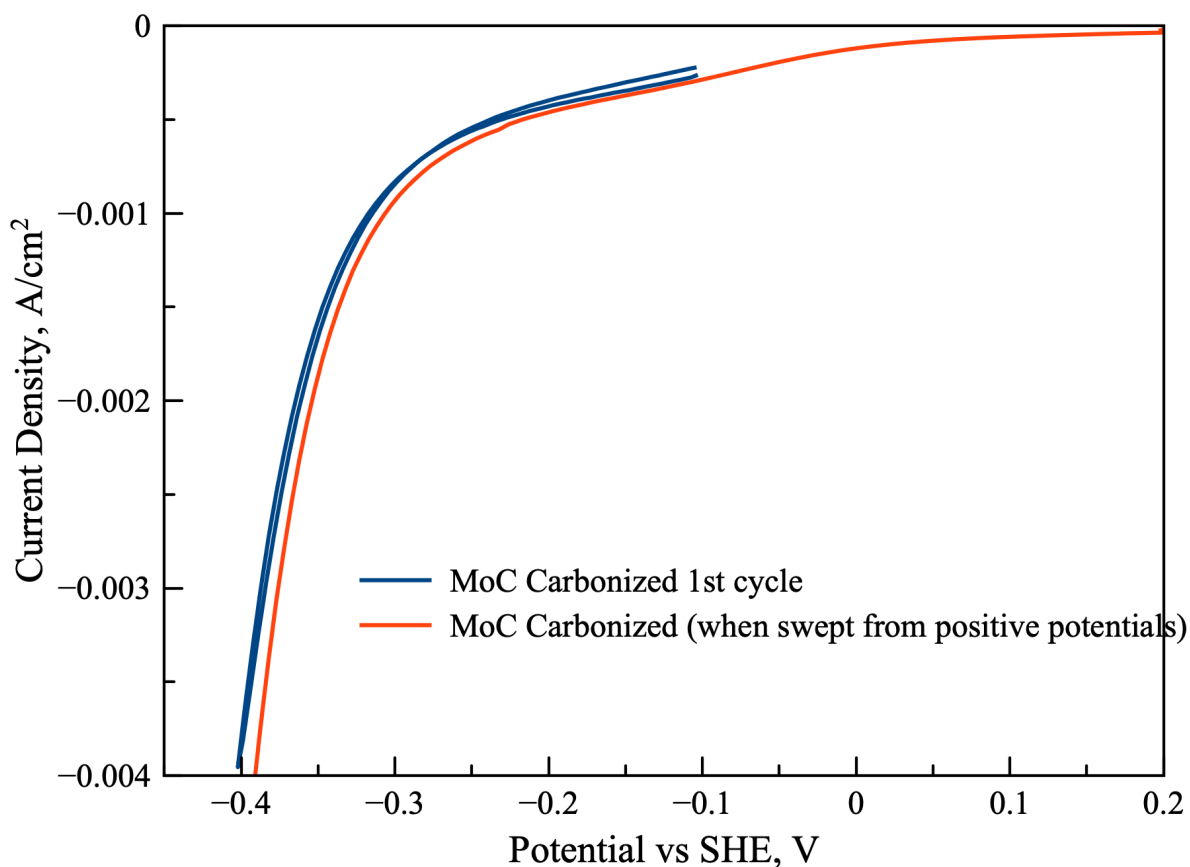


Figure 5-10. 1st cycle of CV scans of MoC (carbonized) and CV scan of MoC (carbonized) when swept from positive potentials.

The CV scan of the carbide species when swept from positive potentials show an overpotential of -0.31 V at a current density of -0.001 A/cm². The results indicate that when the carbide was taken to positive potentials, it was oxidized and therefore the hydrogen evolution onset is very similar to that observed in the first cycle in Figure 5-8.

The CV scans for the methanized molybdenum carbide sample are shown in Figure 5-11. At a current density of -0.005 A/cm², an overpotential of -0.39 V is observed on the first cycle. At the same current density, an overpotential of -0.44 V is observed on the last cycle. This variation is further highlighted in the comparison between the 1st and 20th (last) cycle shown in Figure 5-12.

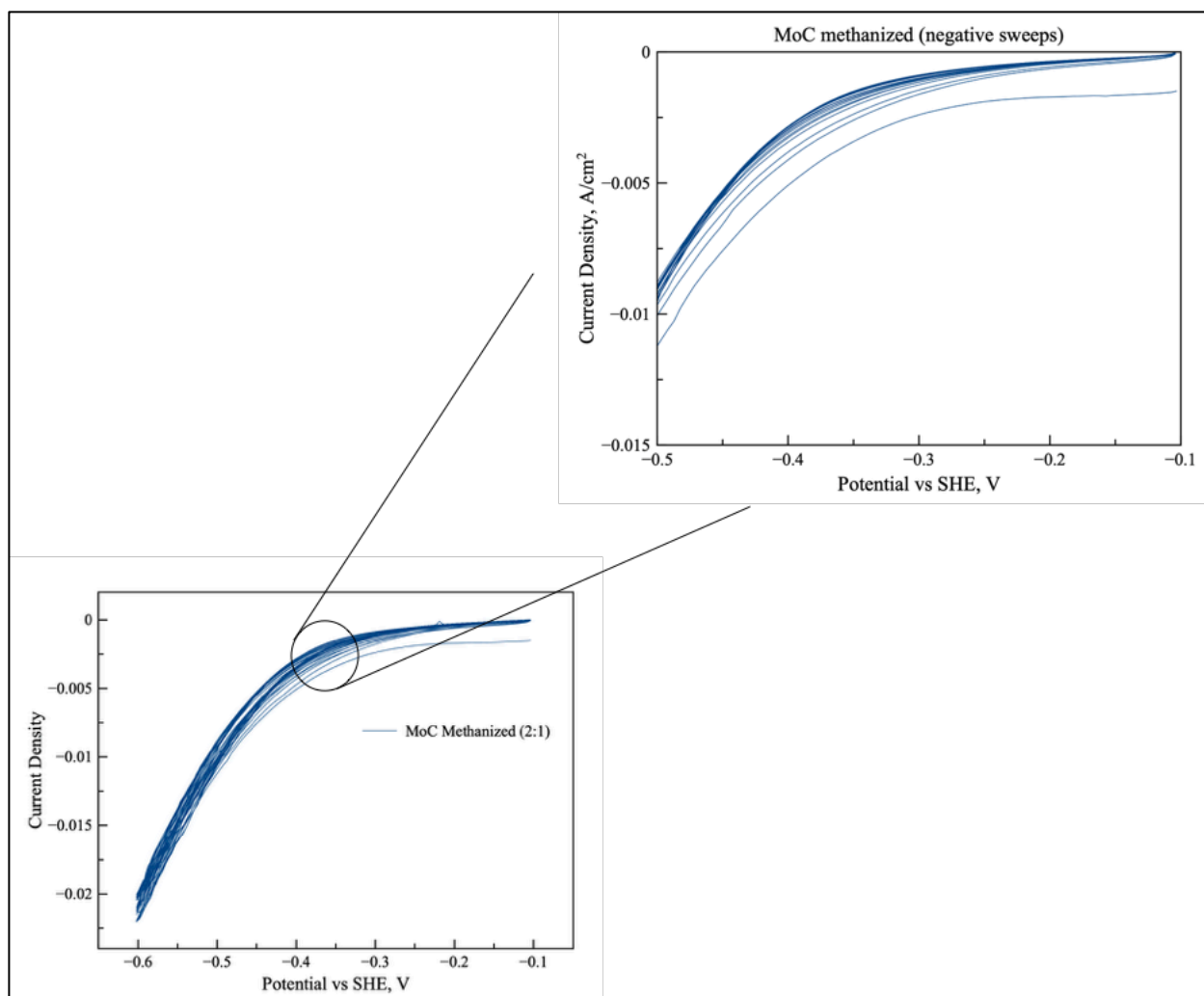


Figure 5-11. Cyclic Voltammetry scans (20 cycles) of Molybdenum carbide (methanized) *Inset:*

Magnified figure of sweeps in negative direction.

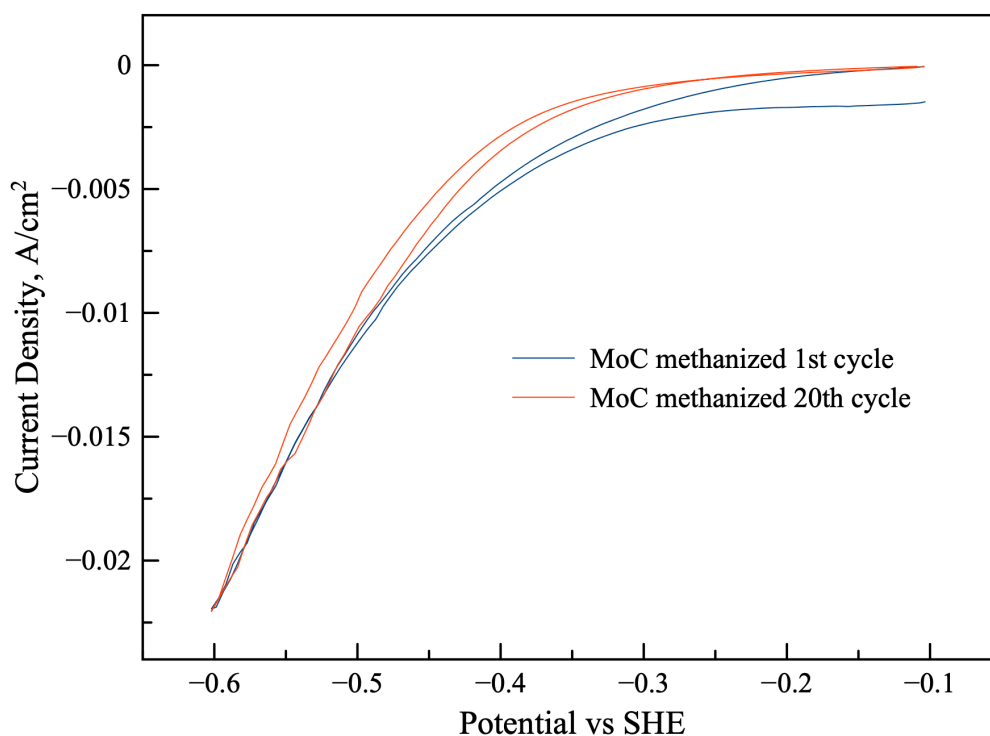


Figure 5-12. 1st and 20th (last) cycles of CV scans done on molybdenum carbide (methanized). The cyclic voltammetry experiments were carried out on carburized resin in order to assess the electrocatalytic behavior of the carbon from the ion exchange resin. Due to the excess carbon content in carbonized and methanized molybdenum carbide samples, it is essential to compare its activity to that of carburized resin. The results are shown in Figure 5-13. At a current density of -0.001A/cm^2 , the overpotential is observed to be -0.36 V . A key observation is that the HER behavior does not vary with subsequent cycles as is observed in the cases of the carbonized and methanized molybdenum carbides. This indicates that despite the excess carbon in the samples, there is active molybdenum carbide species on the surfaces of the carbonized and methanized carbides.

A comparison of the last cycles of the CVs of the carbonized and methanized molybdenum carbides and the carburized resin is also reported here. This shows the various HER behaviors of these materials in Figure 5-14.

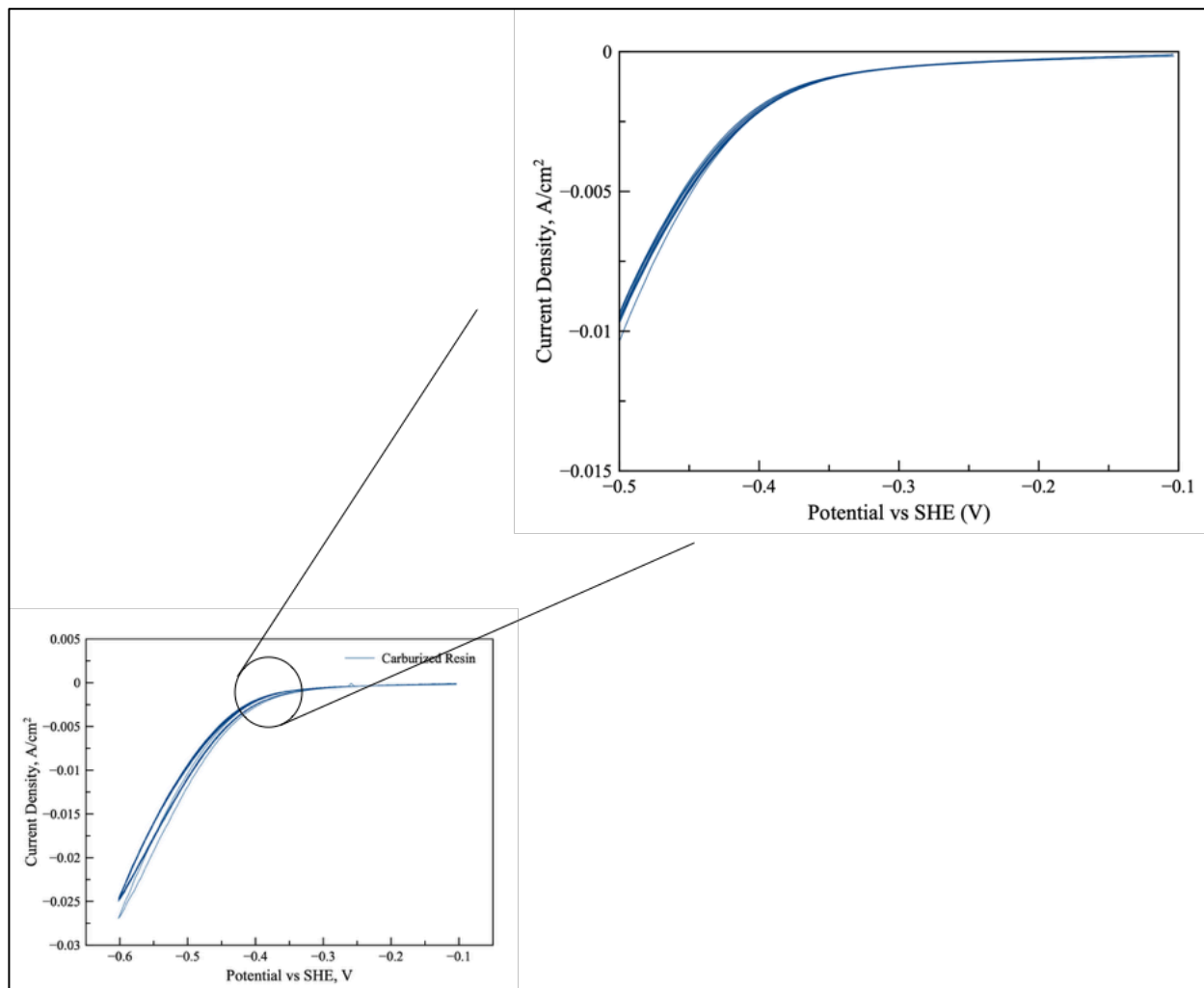


Figure 5-13. Cyclic voltammetry scans of carburized resin.

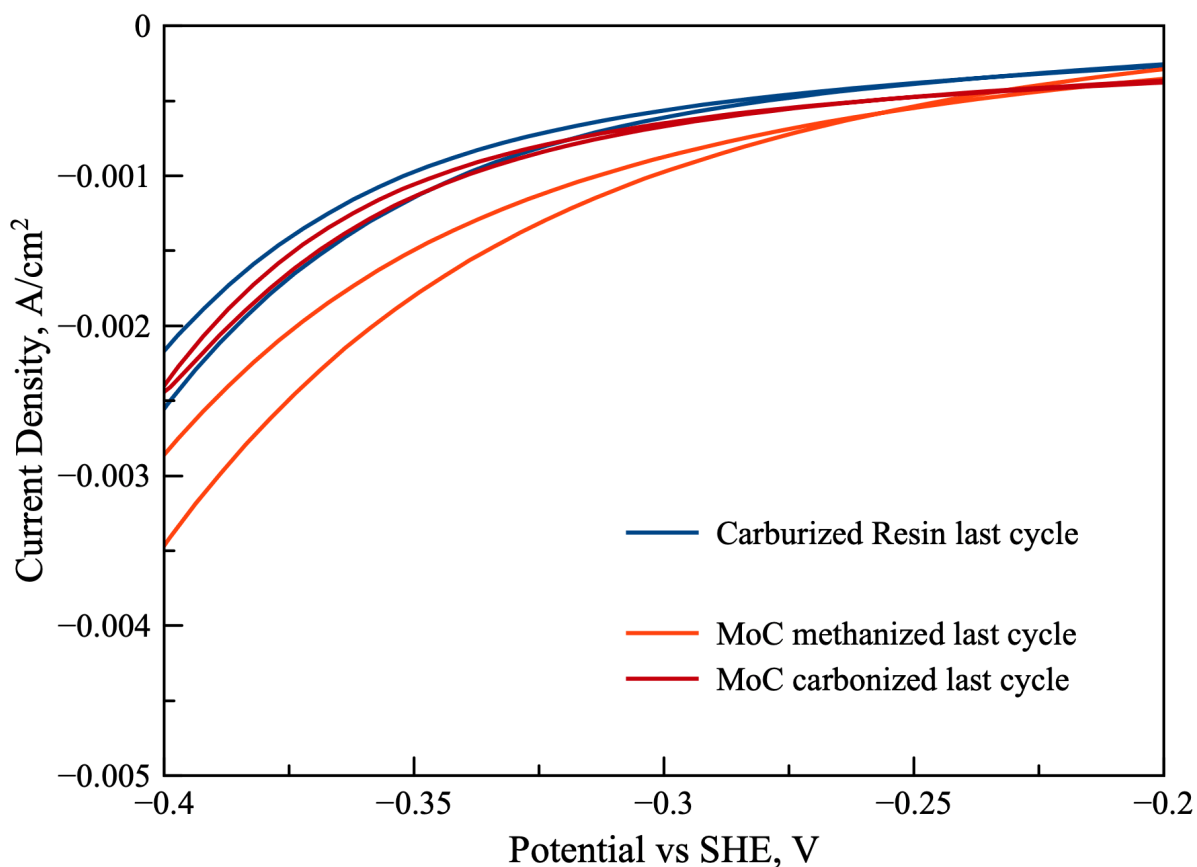


Figure 5-14. A comparison of last cycles of CV runs of the carburized resin, MoC methanized and MoC carbonized samples.

Figure 5-14 shows that at a current density of -0.001 A/cm^2 , an overpotential of -0.30 V is observed for the MoC (methanized sample). In comparison, the carburized resin and the carbonized sample both show an overpotential of -0.34 V at a current density of -0.001 A/cm^2 . The methanized molybdenum carbide sample is more active towards HER than the carbonized sample and the carburized resin. This corroborates the results reported in Chapter 3 where detailed characterization of the samples indicates that the carbonized sample has a substantially more amount of excess carbon as compared to that of the methanized molybdenum carbide.

5.3 Cyclic Voltammetry: Ru and Pt

Cyclic voltammetry experiments were also carried out on Ru/C synthesized using the incipient wetness method described in Chapter 4. The results are shown in Figure 5-9.

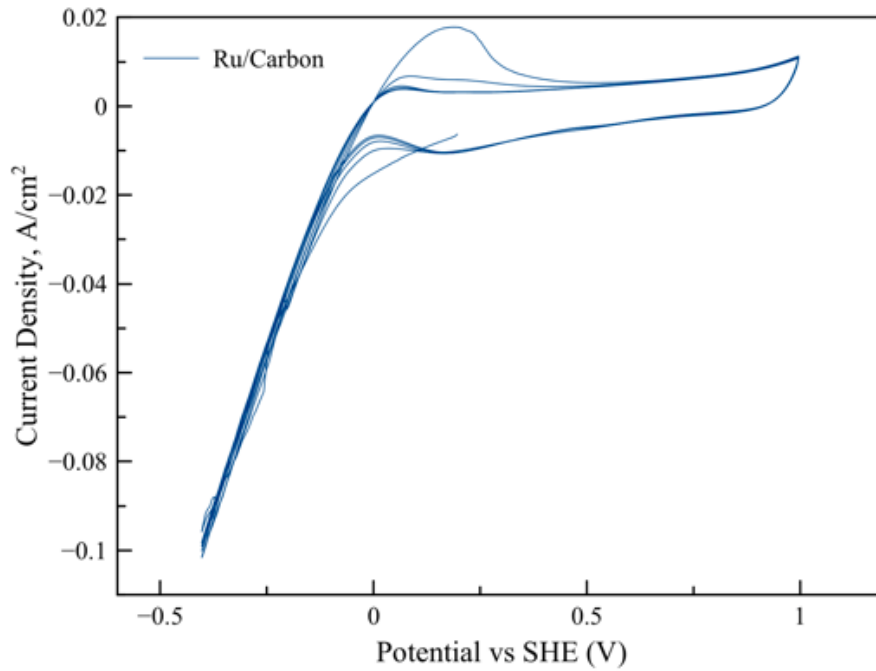


Figure 5-15. Cyclic Voltammetry on Ru/carbon in 0.5M H₂SO₄ electrolyte.

At a current density of -0.01 A/cm², an overpotential of -0.04 V is observed. The ruthenium is more active towards hydrogen evolution compared to any of the molybdenum carbide samples.

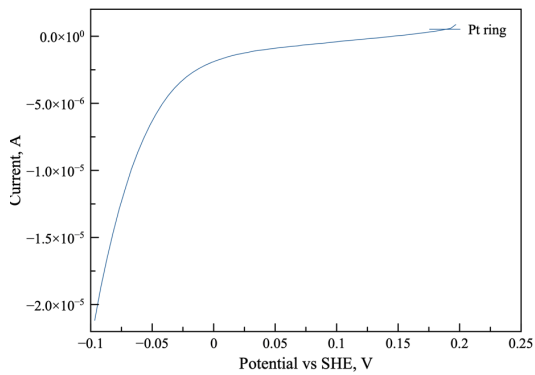


Figure 5-16. CV run of Pt ring in 0.5M H₂SO₄ electrolyte.

5.4 Summary

This investigation provides the much-needed information regarding the phase stabilities of molybdenum carbides in aqueous electrolytes. These results highlight the optimal reaction conditions where molybdenum carbide can be applied as a stable electrocatalyst. For instance, the theoretical stability tests show that the carbide is unstable at higher values of pH, which rules out its application in alkaline fuel cells. However, since the electrochemical behavior of the carbides shows little variation with respect to temperature, the material would be stable under acidic anodic conditions in a PEMFC setup. The carbide would also show a cathodic current in a reaction system such as carbon dioxide reduction (in acidic medium) and would be stable under conditions involving the reduction of CO₂ to carbon monoxide, formic acid, or oxalic acid. Similarly, it will also be stable under conditions involving the reduction of nitrogen to hydroxylammonium ion at the cathode under acidic conditions. These are only few examples of reaction systems and conditions for which the molybdenum carbide stability can be predicted using the thermo-calculations (without taking kinetics into account).

This chapter deals with the catalytic activity and stability of the carbide under potential reaction conditions. It shows the phase stability of molybdenum carbides in aqueous electrolytes. These are important takeaways from the study:

- The importance of developing and understanding stability regions of molybdenum carbide whose chemistry is susceptible to cell potential, pH and is smaller extent temperature, is highlighted.
- The synthesis processes developed in Chapter 4 has yielded a variety of molybdenum carbide samples with different particle sizes, surface areas, and carbon contents. Each of these samples has its unique electrochemical behavior as was established by the cyclic voltammetry measurements.

This investigation also highlights the inadequacy of conventional XRD methods for phase analysis and shows the importance of characterization tools such as XPS and TEM to truly understand the surface species of the material. We also show the profound role played by surface species such as carbon in determining electrocatalytic behavior.

It is therefore absolutely essential to understand the type of synthesis process (precursor, pathway, temperature and pressure) as well as the intricate properties of the material in order to apply it as an electrochemical catalyst or support.

The results of the study are being prepared for a publication:

Nayak, Benavidez, Matanovic, Garzon. A Theoretical and Experimental Investigation of Electrochemical Stability of Well-Characterized Molybdenum Carbides. To be submitted to *Electrochimica Acta*

REFERENCES

1. Nayak SK, Benavidez AD, Garzon FH. Facile Synthesis of High Surface Area Molybdenum Carbide Nanoparticles. *J Am Ceram Soc.* 2018;00(1–7).
2. Weidman MC, Esposito D V, Hsu Y, Chen JG. Comparison of electrochemical stability of transition metal carbides (WC , W 2 C , Mo 2 C) over a wide pH range. *Journal of Power Sources.* 2012;202:11–7.
3. Outotec HSC Chemistry Version 7.193
4. Nayak SK, Benavidez AD, Matanovic I, Garzon FH. Thermochemical analysis of Mo-C-H system for synthesis of molybdenum carbides. *Thermochimica Acta* 2019;676(January):27–32.
5. Kresse G, Hafner J. Ab initio molecular dynamics for liquid metals. *Phys Rev B* [Internet]. 1993 Jan;47(1):558–61. Available from: <https://link.aps.org/doi/10.1103/PhysRevB.47.558>
6. Kresse G, Hafner J. Ab initio molecular-dynamics simulation of the liquid-metal–amorphous-semiconductor transition in germanium. *Phys Rev B* [Internet]. 1994 May;49(20):14251–69. Available from: <https://link.aps.org/doi/10.1103/PhysRevB.49.14251>
7. Kresse G, Furthmüller J. Efficiency of ab-initio total energy calculations for metals and semiconductors using a plane-wave basis set. *Comput Mater Sci* [Internet]. 1996;6(1):15–50. Available from: <http://www.sciencedirect.com/science/article/pii/0927025696000080>
8. Kresse G, Furthmüller J. Efficient iterative schemes for ab initio total-energy calculations using a plane-wave basis set. *Phys Rev B* [Internet]. 1996 Oct;54(16):11169–86. Available from: <https://link.aps.org/doi/10.1103/PhysRevB.54.11169>

Chapter 6: Conclusion and Future Studies

This dissertation provides a much required in-depth investigation into the properties of molybdenum carbide. This systematic study provides information regarding the chemistry, thermodynamics and stability of as-synthesized molybdenum carbide surfaces. Various synthesis processes involving different precursors were employed to synthesize different types of carbide which were analyzed using a variety of techniques such as X-ray Diffraction, Electron Microscopy, Surface Area by Gas Adsorption and X-ray Photoelectron Spectroscopy. The electrochemical activity and stability of these different carbides were probed by investigating the hydrogen evolution reaction. These experimental studies were accompanied by thermochemical analyses which were conducted to understand the Mo-C-H system as well as the electrochemical stabilities of the carbide as a function of cell potential, pH and temperature.

The dissertation provides a detailed thermochemical analysis of the Mo-C-H system which has not existed previously in literature. We gained insight into the thermodynamics of carburizing reactions utilized in the synthesis of molybdenum carbides and found that methane and hydrogen mixtures at appropriate ratios is the optimal for synthesis. This is useful information for future researchers in search of appropriate carburizing agent for synthesis. In addition to being a comprehensive guide for the refinement of synthesis procedures of molybdenum carbide, this is also one of the very few studies involving the thermodynamics of the metastable cubic MoC phase. We developed a fast, facile and reproducible method to synthesize single carbide phase molybdenum carbide nanoparticles with the highest surface area reported in literature. The molybdenum carbide samples were well-characterized to especially understand the carbon content in the samples, a previously unexplored area in literature. We also found that nitrogen is not an appropriate adsorbate for analyzing surface areas of molybdenum carbide.

The investigation of electrochemical stabilities of molybdenum carbide provided an understanding of the influences of the surface species of as-synthesized molybdenum carbides on HER activity. We also established how pH, cell potentials and to a lesser extent temperature affect electrochemical behavior. We also show that the surface carbon profoundly affects the electrochemical activity.

This dissertation lays a foundation for future applications of molybdenum carbide and designing it as an efficient catalyst for a variety of reaction systems. It addresses the question of how different pathways affect the surface chemistries of the carbide and also, how these surfaces of as-synthesized molybdenum carbides affect the activity and stability of the material. The thermodynamic behavior of molybdenum is still unknown and only the chemistry of the Mo-C-H system has been established here. The oxide is a precursor for many synthesis processes reported in literature including one reported here. As a result, thermodynamics of Mo-O-C-N system also has to be examined in great detail. This would help refine synthesis pathways involving the oxide precursor and nitride intermediate to avoid the formation of contaminants. Moreover, it would shed light to the existence of a $\text{Mo}_a\text{O}_b\text{C}_c\text{N}_d$ and fill in the gaps in the phase analysis of Mo-O-C-N system as shown in Figure 6-1.

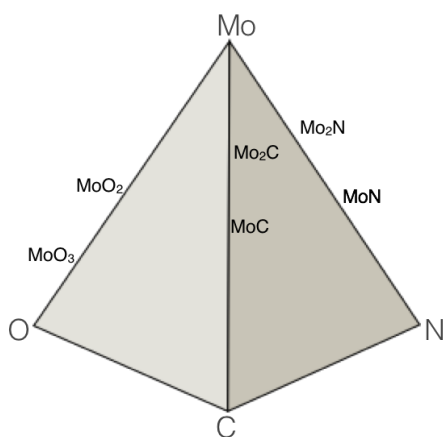


Figure 6-1. Known phases of Mo-O-C-N system.

It was observed that molybdenum carbides are not as active towards hydrogen evolution as Pt and Ru. This opens up possibilities of utilizing it in reaction systems such as electrochemical synthesis of ammonia where hydrogen evolution is an undesired competing reaction.

It was also observed that molybdenum carbide is stable under negative potentials and acidic conditions. In addition, this carbide material is resistant to poisoning, is mechanically durable and electronically conductive. Therefore, besides being used as a catalyst, molybdenum carbide can also serve as an excellent support for precious metal electrocatalysts, such as Pt.

Appendix A: List of Accomplishments

Publications:

Nayak SK, Benavidez AD, Garzon FH. Facile synthesis of high surface area molybdenum carbide nanoparticles. Journal of American Ceramic Society 2018;00:1–7.
<https://doi.org/10.1111/jace.16218>

Nayak SK, Benavidez AD, Matanovic I, Garzon FH, Thermochemical Analysis of Mo-C-H System for Synthesis of Molybdenum Carbides, Thermochemica Acta (2019),
<https://doi.org/10.1016/j.tca.2019.03.033>

Nayak, Benavidez, Matanovic, Garzon. A Theoretical and Experimental Investigation of Electrochemical Stability of Well-Characterized Molybdenum Carbides. To be Submitted to Electrochimica Acta.

A Critical Review Of Existing Studies Involving The Chemistry, Thermodynamics And Preparation Of Molybdenum Carbides. Publication in Preparation for Journal of Materials Chemistry A. Review Proposal ready.

Key Conferences

Nayak, Benavidez, Tsui and Garzon, “Additive Manufacturing of Ceramics for Electrochemical Oxidative Coupling of Methane” Materials Science & Technology Technical Meeting & Exhibition, September 29 - October 3, 2019, Portland, Oregon USA.

Nayak, Benavidez, Tsui and Garzon, “Tuning Catalyst Electronic Structure & O₂ Activity for OCM Reactions”, 12th Natural Gas Conversion Symposium, June 2-6 2019, San Antonio, Texas, USA. (Poster)

Nayak, Benavidez and Garzon, “Synthesis of High Surface Area Molybdenum Carbide as a Catalyst”, Electronic Materials & Applications 2017 Conference (American Ceramics Society), January 18-20 2017, Orlando, Florida, USA.

Awards

First place for poster presentation at 12th Natural Gas Conversion Symposium (June 2019).

Third place for poster presentation at Rocky Mountain Catalysis Society Annual Symposium (April 2019).